UNIVERSITÀ DI SALERNO

Dipartimento di Fisica E.R.Caianiello

Corso di Dottorato di Ricerca in Matematica, Fisica ed Applicazioni
XXXIII Ciclo

Tesi di Dottorato in Fisica

Out of equilibrium problems in classical spin models of statistical mechanics

Tutor

Prof. Federico Corberi

Candidate

Onofrio Mazzarisi

PhD Coordinator

Prof. Carmine Attanasio

Academic Year 2019/2020

Immaginavi tu forse che il mondo fosse fatto per causa vostra? Ora sappi che nelle fatture, negli ordini e nelle operazioni mie, trattone pochissime, sempre ebbi ed ho l'intenzione a tutt'altro, che alla felicità degli uomini o all'infelicità. Quando io vi offendo in qualunque modo e con qual si sia mezzo, io non me n'avveggo, se non rarissime volte: come, ordinariamente, se io vi diletto o vi benefico, io non lo so; e non ho fatto, come credete voi, quelle tali cose, o non fo quelle tali azioni, per dilettarvi o giovarvi. E finalmente, se anche mi avvenisse di estinguere tutta la vostra specie, io non me ne avvedrei.

— Giacomo Leopardi,
Dialogo della Natura e di un Islandese

Invitation

A deeper and more complete understanding of out of equilibrium systems is currently one of the main goal of theoretical physics. The theory is not mature as its equilibrium counterpart and it is not an obvious question whether it would be even possible to reach that level or not. The research efforts towards generalizations and improvements in the formulation of a unified framework for out of equilibrium phenomena should therefore go along with inquiries on specific problems. The latter have of course the primary goal of understanding particular instances but the methods developed and the knowledge accumulated in the process can contribute to the advance of the general theory. The research body presented in this thesis regards out of equilibrium properties of classical spin models.

Spin models are very attractive for theoretical physicists. The simplicity of their structures and their dynamical rules often allows for efficient numerical and analytical investigations and therefore provides a true fundamental understanding of the mechanisms at play. At the same time this simplicity does not imply triviality. The phenomenology these models display can be rich and complex and can mirror the behavior of realistic, more complicated, systems or can represent the starting point to approach their study.

The common thread running through the arguments considered in this thesis is their nonequilibrium nature. Apart from that the problems tackled may be sometimes loosely related to one another and this is partly due to the fragmented nature of the apparatus of out of equilibrium statistical mechanics. They regard aspects of the models which are diverse and the tools adopted for the inquiries vary as well. Therefore in Chapter 1 a context for the problems analyzed in the thesis is given but the introduction to the specific instances, along with a brief summary of the original results, is delineated at the beginning of each chapter for clarity. The rest of the thesis is dived in two parts. Part I is devoted to the Ising model. In Chapter 2 the dynamical properties of the fluctuations of observables of the model are studied. In particular a coarse grained field theoretical approach is used to describe the model and fluctuations properties are investigated through large deviation theory. Chapter 3 is inspired by the out of equilibrium properties of the distribution of cluster's sizes in the Ising model at criticality. The study of an observable relevant to this scenario, the heterogeneity, is reported in the context of a more general statistical system. PartII concerns the Potts model. In this case the material of the chapters is more homogeneous. Indeed the focus on both Chapter 4 and Chapter 5 is on the out of equilibrium dynamics of the Potts model due to temperature quenches that bring the system across a critical point. For given parameters of the model the phase transition is of first order and typical features like metastability and nucleation emerge. The first chapter of this part regards the description of the metastable states characteristic of this scenario and the second one focus on the escape from it through nucleation processes. As for the introductions also specific conclusions and comments can be found at the end of each chapter.

This thesis is based on the following publications

- [1] F. Corberi, **O. Mazzarisi**, and A. Gambassi.
  Dynamics of fluctuations in the Gaussian model with conserved dynamics. *Journal of Statistical Mechanics: Theory and Experiment*, 2019(10), 2019.

- [2] F. Corberi, **O. Mazzarisi**, and A. Gambassi.
  Dynamics of fluctuations in the Gaussian model with dissipative Langevin Dynamics. *Journal of Physics: Conference Series*, volume 1548, 2020.

- [3] **O. Mazzarisi**, F. Corberi, L. F. Cugliandolo, and M. Picco.
  Metastability in the Potts model: Exact results in the large q limit. *Journal of Statistical Mechanics: Theory and Experiment*, 2020(6), 2020.

and on these forthcoming ones

- [4] A. de Azevedo-Lopes, J. J. Arenzon, F. Corberi, and **O. Mazzarisi**.
  How heterogeneous a statistical system can be? *In preparation* (February 2021).

- [5] F. Corberi, L. F. Cugliandolo, M. Esposito, **O. Mazzarisi**, and M. Picco.
  How many phases nucleate in the bidimensional Potts model?. *In preparation* (January 2021).

Contents

Chapter 1

Introduction

In this chapter we provide a general context for the problems studied in Part I and II of this work. In the first section we discuss the absence of a unified framework in out of equilibrium statistical mechanics, comparable with the one of the equilibrium counterpart. Moreover we sketch some of the techniques used in the other chapters. In the second section we define the classical spin models which are both object and playground of this thesis: the Ising model and the Potts model.

1.1 Out of equilibrium problems

Out of equilibrium statistical mechanics lacks a well established framework which allows to analyze transversely the problems the theory is set to tackle. The apparatus of *equilibrium* statistical mechanics, on the other hand, allows to describe the *equilibrium* configurations of statistical systems by means of few thermodynamic variables and there are general principles that can be applied for this task. This general principles are related to the existence of *statistical ensembles*, which have no strict analogue in out of equilibrium problems. We elaborate on this point in this section and discuss some aspects of the out of equilibrium dynamics followed by statistical system in a relevant example: temperature quenches.

1.1.1 Statistical mechanics in and out of equilibrium

Physics thrives for the search of solid *theories* which can single-handedly account for the description of many and diverse phenomena, and allow for quantitative inquiries of those. The power of a working theory is well exemplified by the one which arguably decrees the beginning of theoretical physics: the apparatus of classical mechanics designed by Galilei and Newton. Newton writes in the preface of its *Philosophiae Naturalis Principia Mathematica* [6]

"... Rational Mechanics will be the sciences of motion resulting from any forces whatsoever, and of the forces required to produce any motion, accurately proposed and demonstrated ... And therefore we offer this work as mathematical principles of his philosophy. For all the difficulty of philosophy seems to consist in this from the phenomenas of motions to investigate the forces of Nature, and then from these forces to demonstrate the other phenomena ..."

A perspective on these lines is that Newton is proposing *framework*, a concise set of *principles* to use systematically in the quest to understand physical reality. Classical mechanics finds its more powerful and versatile formulation in the Hamiltonian

formalism [7]. The *state* of a hamiltonian dynamical system with N degrees of freedom is defined by the set of its generalized coordinate $\{q_1, \ldots, q_N, p_1, \ldots, p_N\}$ which identifies a point on the $2N$-dimensional phase space. The evolution in the phase space is given by Hamilton's equations

$$\dot{q}_i = \frac{\partial \mathcal{H}}{\partial p_i}, \qquad \dot{p}_i = -\frac{\partial \mathcal{H}}{\partial q_i} \tag{1.1}$$

where $\mathcal{H} = \mathcal{H}(q_1, \ldots, q_N, p_1 \ldots, p_N)$ is the hamiltonian of the system. Hamiltonian dynamics is the usual starting point to construct yet another theory, namely *statistical mechanics* which deals with systems composed by a large number of degrees of freedom, and aim to the understanding of macroscopic objects and phenomena on the base of their microscopic constituents.

Equilibrium

In particular equilibrium statistical mechanics lays its basis in the *ergodic hypothesis* first introduced by Boltzmann [8], which state that Eqs. (1.1) evolve a phase space point of a confined Hamiltonian system in such a way that for a diverging time $t \to \infty$ it explore all the submanifold with equal energy. There are of course cases when this is not satisfied, e.g., in the presence of other integrals of motion and even in less trivial scenarios, see Fermi-Pasta-Ulam-Tsingou problem [9]. If the hypothesis is assumed, it is possible to equate time averages of observables to averages over a measure on the equal energy submanifold of the phase space and this measure is constant. An *Excusatio non petita* is due: ergodicity is one of the cornerstones of both classical and quantum equilibrium statistical mechanics and the importance of a rigorous mathematical and physically sound description of this concept should not be overlooked, see, e.g., Ref. [10]. Moreover for an interesting historical review of the idea of the ergodic hypothesis, and some insights to its relevance even for nonequilibrium scenarios see Ref. [11]. For a philosophical perspective on the foundations of statistical mechanics see Ref. [12]. In this work however we do not delve into the details of ergodicity, we just adopt the *equiprobability principle* that it brings.

Classical spin models are at the core of this work, therefore we phrase the discussion on basic ideas of equilibrium statistical mechanics in this context. Consider a d-dimensional lattice with a spin variable φ_i at each vertex i which can assume a *discrete* number of values. This implies that the space of all the possible microstates of the system Γ is discrete, and we denote a generic microstate with $\varphi = \{\varphi_1, \ldots, \varphi_N\}$ where N is the total number of spins. The nature of the interactions among the spins and between the spins and external fields is codified by an hamiltonian $\mathcal{H}[\varphi]$. A caveat: spin systems can be defined through an hamiltonian but this does not necessarily equip them with a "natural" dynamics. Therefore to study dynamical properties of a spin model it should be completed with some rules, we elaborate below on this point. For the present discussion, related to equilibrium properties, we do not actually need that. The only fact we require to make contact with the statistical mechanics of hamiltonian systems is again ergodicity, which in this context purely[1] amounts to the request that the *a priori equiprobability principle holds*. If such is the case the equilibrium probability for a system at fixed energy E to be in a specific microstate φ is given by

$$P_E([\varphi]) = \frac{\delta_{\mathcal{H}[\varphi],E}}{\Omega(E)}, \tag{1.2}$$

[1] By *purely* here we mean that there are no arguments related to time averages, although when a dynamics is defined such a connection can be made.

where the Kronecker delta enforces the energy constraint and $\Omega(E)$ is the number of microstates which satisfy it

$$\Omega(E) = \sum_{\varphi \in \Gamma} \delta_{\mathcal{H}[\varphi],E}. \tag{1.3}$$

This last quantity is also called the *microcanonical partition function* and the probability distribution in Eq. (1.2) is the *microcanonical ensemble*. From Eq. (1.3) is possible to define the *entropy* $\mathcal{S}(E) = k_B \ln \Omega(E)$ associated to a macrostate with given energy (k_B is the Boltzmann constant), the concept of *temperature* $1/T = \partial \mathcal{S}/\partial E$ and in general begin to build connections between the microscopic realm and the laws of thermodynamics. From this point is also possible to build the *canonical ensemble*, which is more tractable but equivalent to the microcanonical in the thermodynamic limit. We rely on the same assumptions about equiprobability used above which characterize equilibrium statistical mechanics. In the canonical setting we allow energy fluctuations, to achieve this we focus only on a part of the system of total energy E, say a large portion n of the spins which is nonetheless small compared to the total $n \ll N/2$. We denote now with $\varphi \in \Gamma$ the microstates of just the small portion and with $\varphi_r \in \Gamma_r$ the microstates of the rest of the spins which we consider as a *reservoir* at fixed temperature T. This means that we are allowing the reservoir to absorb energy form the small system without letting the temperature change. Denoting the total space of the microsates with $\Gamma_t = \Gamma \times \Gamma_r$ we can understand this approximation acknowledging that the energy $\mathcal{H}[\varphi] \ll E$ $\forall \varphi \in \Gamma$. We can formally write the microcanonical partition function of the total system as

$$\Omega(E) = \sum_{\varphi \in \Gamma} \sum_{\varphi_r \in \Gamma_r} \delta_{\mathcal{H}[\varphi]+\mathcal{H}[\varphi_r],E} = \sum_{\varphi \in \Gamma} \Omega_r(E - \mathcal{H}[\varphi]) = \sum_{\varphi \in \Gamma} e^{\mathcal{S}_r(E-\mathcal{H}[\varphi])/k_B}. \tag{1.4}$$

Taylor expanding now the entropy of the reservoir due to our consideration above we can write

$$\Omega(E) \approx \sum_{\varphi \in \Gamma} e^{\mathcal{S}_r(E)/k_B - \partial \mathcal{S}_r/\partial \mathcal{H}[\varphi_r]\Big|_{\mathcal{H}[\varphi_r]=E} \mathcal{H}[\varphi]/k_B} = e^{\mathcal{S}_r(E)/k_B} \sum_{\varphi \in \Gamma} e^{-\beta \mathcal{H}[\varphi]}, \tag{1.5}$$

where $\beta = 1/k_B T$ and from this last equation is clear that we coarse grained the degrees of freedom of the reservoir. At this point we employ again the equiprobability principle and note that the probability of each microstate of the total system is $1/\Omega(E)$ and the number of those state for which the partition of the system has microstate φ is $e^{\mathcal{S}_r(E)/k_B} e^{-\beta \mathcal{H}[\varphi]}$. Therefore the probability for the system of interest of being in the microstate φ, given that the reservoir is at inverse temperature β, is

$$P_\beta([\varphi]) = \frac{e^{-\beta \mathcal{H}[\varphi]}}{Z(\beta)}, \tag{1.6}$$

where

$$Z(\beta) = \sum_{\varphi \in \Gamma} e^{-\beta \mathcal{H}[\varphi]}. \tag{1.7}$$

The probability distribution above is the *canonical ensemble* and the *partition function* $Z(\beta)$ is of course the most important object of equilibrium statistical mechanics. The theory allows a broad and deep comprehension of a vast spectrum of macroscopic phenomena, among which *phase transitions*, i.e., sharp changes in the structure of matter, or in more abstract contexts in the collective behavior of the constituents of a system, at critical values of external control parameters such as temperature (Ref. [13] is a beautiful textbook on the subject). This success is due

to the existence of the statistical ensembles which assign measures on the space of possible microstates of a system at equilibrium requiring only the knowledge of the nature of the microscopic interactions and of external control parameters. This is not achievable in *out of equilibrium* regimes, the dynamical details and boundary conditions are relevant and the theory does not provide a model-independent form for the measures.

Out of equilibrium

Out of equilibrium situations are more common in nature then equilibrium ones, this is true in physical settings but also in other areas such as biology for example. Consider, e.g., *homeostasis*, one of the most characteristic features which allows to distinguish living organisms from inert matter, it is precisely the effort to avoid equilibration of the system with the environment (thermal, chemical and so on). As we anticipated above the lack of a framework as solid as the one of equilibrium problems is due to the relevance of the *dynamics* in this context, time enters the game. Therefore we have a measure for the microstates which has no universal form and it is either time dependent $P([\varphi], t)$ or, in the case of nonequilibrium stationary states (NESS), a time independent one $P_{NESS}([\varphi])$ which nonetheless depends on the details of the dynamics. There are diverse situations where out of equilibrium tools have to be employed. For example when an open system, say in a canonical setting, has a very *slow* equilibration dynamics such that it never really achieve equilibrium. A prominent instance of this scenario is the description of *glassy systems* [14], one of the most interesting (and hard) open problems in condensed matter and out of equilibrium statistical mechanics. An other typical subject of out of equilibrium statistical mechanics is represented by *externally driven* systems, in this case one is mostly interested in NESS but not necessarily. Examples are driven lattice gasses [15], reaction-diffusion processes [16] and active matter [17] to list just a few. The last situation we want to mention, which is the most relevant for this thesis regard the relaxational dynamics (not necessarily slow in reaching equilibrium) of systems which cross a phase transition and undergo *phase ordering kinetics* [18]. For a nice overview of (classical and quantum) out of equilibrium dynamics in statistical systems see, e.g., Ref. [19].

Let us express again basic concepts of the theory by means of classical spin models and consider the generic one defined above to discuss equilibrium. Once the model dependent properties of the dynamical scenario under analysis are set, we need to give a rule, a dynamic conditions, for the evolution of the spin variables. There are different ways to do this which target specific goals and serve for different scopes, but are all related and in some sense equivalent. Two possible choices are the following. To approach out of equilibrium problems from a computational point of view the usual strategy is to simulate the system evolution via *Monte Carlo methods*. Concretely, one design a Markov chain in which at each microscopic time step one site i is chosen at random and changes the value of the local spin φ_i according to a probabilistic rule which may depend on both the initial and final microstates of the system. An approach more versatile for analytical inquiries is that of *Langevin*, or *time dependent Ginzburg-Landau*, equations. In this case a coarse graining of the spin lattice is performed and the spin variables are describe by a field, the dynamics of which is regulated by a specific stochastic partial differential equation. We sketch below the problem of temperature quenches for classical spin system, an instance relevant for the body of this thesis, to elucidate some of these ideas.

1.1.2 Temperature quenches

Consider a canonical setting, in the sense that the system is coupled with a reservoir and energy can be exchanged. The problem consist in preparing the system at equilibrium with the bath at a given temperature T_i and then abruptly change the temperature of the bath to T_f. We are interested in the relaxation dynamics which leads the system to the new thermal equilibrium. We specialize for this discussion the generic spin model introduced above to the d-dimensional Ising model with nearest neighbor ferromagnetic interaction without external fields. The hamiltonian of the model is given in the section below, for the purpose of the discussion it suffice to say that the spin are binary variables $\varphi_i \in \{-1, 1\} \quad \forall i \in N$ and use the well known fact that a finite critical temperature T_c separates, through a continuous phase transition, a disordered (paramagnetic) high temperature phase to an ordered (ferromagnetic) low temperature one.

One way to explore the dynamics is by means of Monte Carlo methods. Consider a microstate φ^a, select with uniform probability distribution a spin φ_k from the lattice and then propose the following move

$$\varphi^a = \{\varphi_1, \ldots, \varphi_i, \ldots, \varphi_N\} \quad \rightarrow \quad \varphi^b = \{\varphi_1, \ldots, -\varphi_i, \ldots, \varphi_N\}, \tag{1.8}$$

turning, say, $\varphi_i = 1$ in $\varphi_i = -1$ resulting in the new microstate φ^b. The move is accepted with probability, or *transition rate*, $T_{a\to b}$. For relaxational problems we require a dynamics which does not lead to a generic NESS, but the stationary solution for $t \to \infty$ should be an equilibrium one. This is achieved if the transition rates respect *detailed balance* [20]

$$\frac{T_{a\to b}}{T_{b\to a}} = e^{-\beta_f(\mathcal{H}[\varphi^b]-\mathcal{H}[\varphi^a])}, \tag{1.9}$$

where β_f is the inverse temperature of the bath after the quench. This ensure that the probability for the system to be found in a given microstate and change to another is the same as the inverse process, it has to do with reversibility and its a distinctive feature of equilibrium states. For a system with N spins, conventionally, N update attempts correspond to one Monte Carlo step (MCs). There is some freedom in the choice of the transition rates as it is clear by an inspection of Eq. (1.9), one of the most common is

$$T_{a\to b} = \min\Big\{1, e^{-\beta_f(\mathcal{H}[\varphi^b]-\mathcal{H}[\varphi^a])}\Big\} \tag{1.10}$$

which defines the Metropolis algorithm [21]. In Fig. 1.1 we display the relaxation dynamics of the Ising model (see caption for details) as captured by snapshot at various time obtained by means of Monte Carlo simulations.

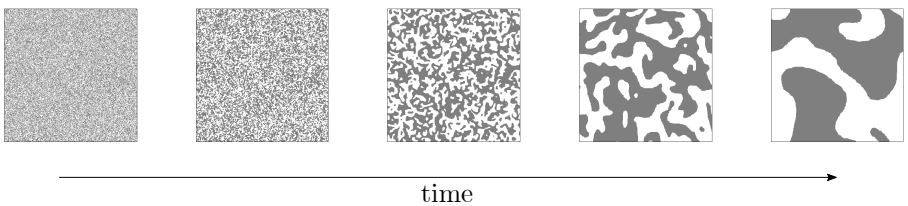

Figure 1.1: Snapshots capturing the relaxation dynamics up to 10^5 MCs of the nearest neighbor $2d$ Ising model on a square lattice of linear size $L = 1000$ with periodic boundary conditions (p.b.c.). The system is prepared in a completely disordered state ($T_i \to \infty$) and then quenched to $T_f = 0$.

Another way to analyze the dynamics in the effort to grasp some understanding of the process from an analytical point of view is through Langevin equations. To describe the Langevin approach to the dynamics we define a coarse graining field for the spin variables

$$\phi(\vec{x}) \equiv \frac{\sum_{i \in C} \varphi_i}{N l^d}, \tag{1.11}$$

which is the average of the values of the spin included in a d-dimensional cube C of side l and centered in $\vec{x}$ normalized to have $\phi = \int d\vec{x}\phi(x) \in [-1, 1]$. The Ginzburg-Landau free energy for the ordered phase of the model has the form (see section below for the derivation)

$$\mathcal{F}[\phi] = \int d\vec{x}\Big[\frac{1}{2}(\nabla\phi)^2 + f(\phi)\Big] \tag{1.12}$$

where the gradient term takes into account the energy cost of interfaces between areas of different values (gray and white in Fig. 1.1) and

$$f(\phi) = (1 - \phi^2)^2 \tag{1.13}$$

is the characteristic double-well potential with minima in $\phi = \pm 1$. The stochastic dynamics of the system is built on the fact that the thermal bath induces fluctuations in the systems and allows for dissipation of its energy. From the coupling of the system with the bath is possible to derive (see, e.g., Ref. [13]) the overdamped[2] Langevin equation

$$\frac{\partial\phi(\vec{x}, t)}{\partial t} = -\frac{\delta\mathcal{F}[\phi]}{\delta\phi(\vec{x}, t)} + \eta(\vec{x}, t), \tag{1.14}$$

where on the left hand there is the dissipative term, then a deterministic force is represented by the functional derivative of the Ginzburg-landau free energy and $\eta(\vec{x}, t)$ is a zero mean Gaussian noise with correlation defined through averages over realizations give by

$$\langle\eta(\vec{x}, t)\eta(\vec{x}', t')\rangle = 2\beta^{-1}\delta(\vec{x} - \vec{x}')\delta(t - t'). \tag{1.15}$$

This equation can be heuristically understood considering that the deterministic part evolves the field towards configurations which minimize the free energy functional and the noise allows for exploration of the landscape to avoid local minima. As for the Monte Carlo methods the stationary solution of this evolution rule should be an equilibrium one, i.e. the probability distribution $P([\phi])$ for a global configuration of the field ϕ at stationarity should be a Gibbs measure. This is achieved by the amplitude of the noise being proportional to the temperature of the bath, as well as friction constants that we tacitly absorbed here simply rescaling time. With this choice passing to from the stochastic Langevin equation for the field to the equivalent deterministic Fokker-Planck equation for the evolution of the probability distribution of the field $P([\phi], t)$ (see, e.g., Ref. [13] for details) one obtains

$$\frac{\partial P([\phi], t)}{\partial t} = \int d\vec{x}\frac{\delta}{\delta\phi}\Big(\frac{\delta\mathcal{F}[\phi]}{\delta\phi}P([\phi], t) + \beta^{-1}\frac{\delta P([\phi], t)}{\delta\phi}\Big), \tag{1.16}$$

which is satisfied at stationarity by $P_{eq}([\phi]) \sim e^{-\beta\mathcal{F}[\phi]}$ by direct inspection. The Langevin approach is fruitful to study the phase ordering kinetics, namely the details *how* the systems reach an ordered phase. In the scenario at hand is possible, as an example, to provide in few lines quantitative insights on the time dependence of the

[2] In the sense that it does not contain an acceleration term which is dropped because the time scales associated are short and not relevant for the dynamics.

size of the ordering clusters with extremely simplified arguments. In the case of a quench at $T_f = 0$, as in Fig. 1.1, Eq. 1.15 reduce to a gradient descent

$$\frac{\partial \phi(\vec{x}, t)}{\partial t} = -\frac{\delta \mathcal{F}[\phi]}{\delta \phi(\vec{x}, t)}. \tag{1.17}$$

We consider now the faith of an ideal spherical domain with bulk value of the field, e.g., $\phi = -1$ in a large portion of the space where $\phi = 1$. How the radius $R(t)$ of the domain changes with time? We can place our reference frame at the center of the domain and due to the spherical symmetry of the problem expect the field to be of the form $\phi(r, t) = g(r - R(t))$, where $g(\xi)$ equals -1 for negative arguments, 1 for positive argument and varies from one to the other in a small region around $\xi = 0$, the interface. The evolution equation can be cast in spherical coordinates

$$\frac{\partial \phi}{\partial t} = \frac{\partial^2 \phi}{\partial r^2} + \frac{d-1}{r}\frac{\partial \phi}{\partial r} - \frac{df}{d\phi}, \tag{1.18}$$

which, substituting the expected form for the field, reads

$$\frac{d^2 g}{d\xi^2} + \Big(\frac{dR}{dt} + \frac{d-1}{r}\Big)\frac{dg}{d\xi} - \frac{df}{dg} = 0. \tag{1.19}$$

If we consider a thin enough interface, $dg/d\xi$ is a function sharply picked around zero, where $d^2g/d\xi^2 = 0$, and zero everywhere else. Thus if we multiply the last equation for $dg/d\xi$, and keep in mind that f is equal on both side of the interface, an integration in ξ leads to

$$\frac{dR}{dt} + \frac{d-1}{R} = 0. \tag{1.20}$$

Solving for the radius this last equation gives $R(t) = \sqrt{R^2(0) - 2(d-1)t}$, which means that a cluster of size R disappear after a time $t \sim R^2$. This quite naive calculation allows to deduce something deep, indeed if there are no domains smaller in linear size then $t^{1/2}$ at time t, the typical length of the domains R_{typ} can be roughly estimated as

$$R_{typ}(t) \sim t^{-1/2}. \tag{1.21}$$

There are of course more refined methods to land to this result and confirm that it is sound (see, e.g., Ref. [18]), but it is striking that this simple calculation allows to understand something this general. Equation (1.21) is the Lifshitz-Allen-Cahn (LAC) law [22,23], an example of *growth law* shared by many systems which are very different but nonetheless display the same coarsening behavior. Indeed we used a free energy functional form which only depends on symmetries and dimensionality of the system and general dynamical equations which just have to lead equilibrium and, in this specific case, do not conserve the order parameter (see Chapter 2), no detailed microscopic features were invoked. This concluding remark is a way to state that even though it is true that the theory of out of equilibrium statistical mechanics does not share the unity of its equilibrium counterpart, there are nonetheless general results like this one and many more in several other branches of the theory that we (somehow guiltily) did not mention in this brief introduction.

1.2 Classical spin models of statistical mechanics

In this section we introduce the classical spin models which constitute the backbone of this thesis, the Ising model and one of its best known generalizations: the Potts model. This will not be an overview of the subject; the reason is twofold. The topic is so wide and deep that an effort of giving a comprehensive overview of all

the properties and applications of these models will result, in the best case, in an enormous amount of information which would drive our focus away form the scope of this work and in the worst case in a unsatisfactory result. The second motivation is that the literature is already rich in beautiful reviews (see, e.g., Ref. [24, 25]) and adding a new one (possibly not as complete and clear) would be of no use. Therefore we just define the models and describe facts which turn out useful for the discussion below.

1.2.1 The Ising model

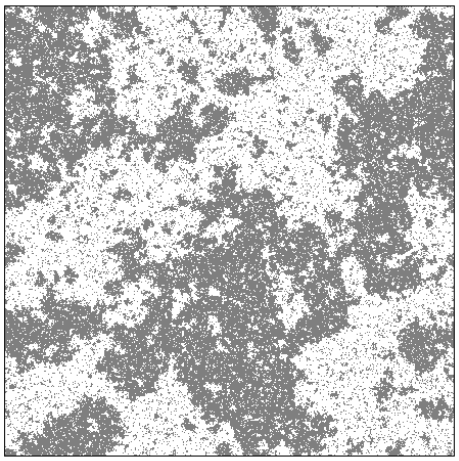

Figure 1.2: Snapshot of the n.n. Ising model on a two dimensional square lattice of linear size $L = 1000$ with p.b.c. in equilibrium at criticality.

This is arguably the most studied model of statistical mechanics, and its relevance percolated throughout the maze of several other branches of physics and mathematics. Introduced in 1925 by Lenz and Ising [26], in a rather general version it is defined by the hamiltonian on a d-dimensional lattice

$$\mathcal{H}[\varphi] = -\sum_{i,j} J_{ij}\varphi_i\varphi_j + \sum_i h_i\varphi_i \tag{1.22}$$

where J_{ij} is regulates the strength and the kind of the interaction among the spins, h_i stands for the coupling of the spins with external fields and $i, j \in \{1, \dots, N\}$ runs over all the N spins of the lattice. This can of course be further generalized, e.g. with terms accounting to interactions between more then two spins (see p-spin models [27]), or general graph instead of geometric lattices. We instead, for the scopes of this work, reduce to the ferromagnetic Ising model, meaning $J_{ij} > 0 \quad \forall i, j$, without external magnetic fields. The partition function of the model on a $2d$ square lattice with nearest neighbor (n.n.) interaction was exactly solved by Onsager [28] in 1944. This allowed to rigorously prove the existence of a second order phase transition at finite temperature T_c for the model which well justify its relevance in statistical mechanics. In Fig. 1.2 we report a snapshot of the Ising model at its critical point. Below we derive the Ginzburg-Landau free energy functional for the model which is relevant in the body of this work.

Ginzburg-Landau free energy

The form of the Ginzburg-Landau free energy for a system can be determined from few crucial properties, the most important are the symmetries of the system. Then the parameters that appear in the equation should be evaluated phenomenologically. As mentioned in the section above this formalism is indeed also useful for analytical explorations of out of equilibrium properties of statistical systems, we make use of it to study in Chapter 2 some dynamical properties of the fluctuations of observables of the model. Therefore we give below a direct derivation from the microscopic hamiltonian which is feasible in the case of the Ising model.

We consider the coarse grained field $\phi(\vec{x})$ defined in Eq. (1.11) and promote the J_{ij} in Eq. (1.22) to a continuous version $J(|\vec{x}-\vec{x}'|)$ which depends only on the distance of two points in space. The microscopic hamiltonian can then be cast as

$$\begin{aligned}\mathcal{H}[\phi] &= -N\int d\vec{x}d\vec{x}'J(|\vec{x}-\vec{x}'|)\phi(\vec{x})\phi(\vec{x}') \\ &= \frac{N}{2}\int d\vec{x}d\vec{x}'J(|\vec{x}-\vec{x}'|)\Big[\Big(\phi(\vec{x})-\phi(\vec{x}')\Big)^2-\Big(\phi^2(\vec{x})+\phi^2(\vec{x}')\Big)\Big] \qquad (1.23)\\ &\approx \frac{N}{2}\int d\vec{x}d\vec{r}J(r)(\nabla\phi\cdot\vec{r})^2 - N\int d\vec{x}d\vec{r}J(r)\phi^2(\vec{x}), \qquad (1.24)\end{aligned}$$

where $\vec{r}=\vec{x}-\vec{x}'$. The first term of the last line can be explicitly written as

$$\frac{1}{2}\int d\vec{x}d\vec{r}J(r)(\nabla\phi\cdot\vec{r})^2 = \frac{1}{2}\sum_{i=1}^{d}\int d\vec{r}J(r)r_i^2\int d\vec{x}\Big(\frac{\partial\phi}{\partial r_i}\Big)^2, \qquad (1.25)$$

and acknowledging that the integral $\int d\vec{r}J(r)r_i^2$ is independent from the direction i one can define $a\equiv\int d\vec{r}J(r)r_i^2/2=\int d\vec{r}J(r)r^2/2d$. Moreover defining $b\equiv\int d\vec{r}J(r)$ the hamiltonian reads

$$\mathcal{H}[\phi] = aN\int d\vec{x}(\nabla\phi)^2 - bN\int d\vec{x}\phi^2(\vec{x}). \qquad (1.26)$$

To construct the free energy functional $\mathcal{F}[\phi]=\mathcal{H}[\phi]-T\mathcal{S}[\phi]$ we need the the total entropy

$$\mathcal{S}[\phi] = N\int d\vec{x}\Big[\ln 2-\frac{1-\phi(\vec{x})}{2}\ln(1-\phi(\vec{x}))-\frac{1+\phi(\vec{x})}{2}\ln(1+\phi(\vec{x}))\Big]. \qquad (1.27)$$

The derivation of the integrand, which correspond to the entropy, relative to the magnetization of the small cube C considered in the coarse graining process, is showed in an unusual context in the introduction of Chapter 2. Taylor expanding to the fourth order the integrand of the entropy for small ϕ, which is justified in the vicinity of T_c we end up with the Ginzburg-Landau free energy

$$\mathcal{F}[\phi] = N\int d\vec{x}\Big[a(\nabla\phi)^2+\frac{T-2b}{2}\phi^2+\frac{T}{12}\phi^4\Big], \qquad (1.28)$$

where we dropped uninfluential constants from the integrand.

1.2.2 The Potts model

The Potts model was introduced in 1951 by Domb and its student at the time Potts [29] and it is a generalization of the Ising model in which the spin variables take q integer values. As an historical note we mention that a version of the model

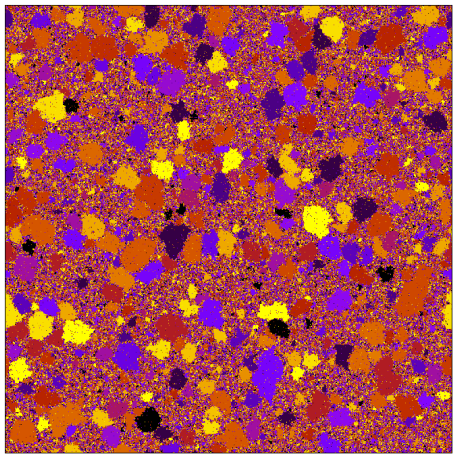

Figure 1.3: Snapshot of a 2d Potts model on a square lattice of linear size $L = 1000$ with a number $q = 14$ of possible values for the spin variables. Specifically, in this picture the system is following a relaxation dynamic towards a thermal equilibrium at subcritical temperature after a quench from a completely disordered state, the details though are not relevant at this point.

with $q = 4$ was already studied by Ashkin and Teller [30] in 1943. In a version specialized for the interests of this thesis the model is defined by the hamiltonian

$$\mathcal{H}[\varphi] = -J \sum_{\langle ij \rangle} \delta_{\varphi_i \varphi_j}, \tag{1.29}$$

where $J > 0$ is a coupling constant, the sum is restricted to nearest-neighbors on a $2d$ square lattice lattice, δ_{ab} is the Kronecker delta and φ_i take integer values from 1 to $q \geq 2$. In the sum one counts each bond once and for this geometry the energy is bounded between $-2JN$, with N the number of spins in the sample, and 0. For $q = 2$ it reduces to the Ising model, indeed

$$\begin{aligned} \mathcal{H}[\varphi] &= -J \sum_{\langle ij \rangle} \delta_{\varphi_i \varphi_j} = -2J \sum_{\langle ij \rangle} (\delta_{\varphi_i \varphi_j} - \frac{1}{2}) \\ &= -J \sum_{\langle ij \rangle} \varphi_i \varphi_j, \end{aligned} \tag{1.30}$$

where the last equality holds if we chose $\varphi_i \in \{-1, 1\}$ instead of $\varphi_i \in \{1, 2\}$.

The model attracted attention at the early ages of phase transition studies since the order of the phase transition changes when the number of states of the spins is tuned: in two dimensions, for $2 \leq q \leq 4$ it is of second-order, while for $q > 4$ it is of first-order [25, 31]. Beyond the fundamental interest that it produced, the Potts model found applications in many areas of physics, and even beyond the physical domain. For instance, the large q limit is used to describe soap foams and metallic grain systems [32–34]. In its anti-ferromagnetic version ($J < 0$), the Potts model represents the coloring problem of computer science [35, 36]. Another application in this realm is to community detection in complex networks [37–39]. Furthermore, weakly disordered Potts ferromagnets are the paradigmatic models in which the effects of randomness on phase transitions were studied [40, 41], and disordered and frustrated mean-field Potts models [42,43] realize the random first-order phase transitions scenario for the glassy arrest [44–46].

Although the problem is not fully solvable for $q > 2$, some exact results are known. Duality allows one to prove that the critical temperature is [29]

$$k_B T_c(q) = \frac{J}{\ln\left(1+\sqrt{q}\right)} \ . \tag{1.31}$$

We set $k_B = J = 1$, if not otherwise stated, in the body of the thesis. An exact solution on the square lattice was provided in 1973: by exploiting a mapping to the ice-rule six-vertex model Baxter gave an exact expression for the model's free-energy *at the critical point*. He thus showed that the transition is second order for $q \leq 4$ and first order for $q > 4$, and he calculated the latent heat in the latter case [31]. A proof that the simplest possible mean-field approach yields, in the thermodynamic limit, the exact free-energy at criticality for $q \geq q_c(d)$ (with $q_c(2) = 4$) to leading order in q, in the large q limit, was soon after given by Mittal and Stephen [47], see also [48]. Many numerical studies put these ideas to the test since then. For example, Binder in Ref. [49] and much more recently the authors of Refs. [50–53] focused on the analysis of the critical properties, both in the second order and first order cases, using different numerical methods. In this work our focus is on the out of equilibrium dynamics of the Potts model after quenches to subcritical temperature for the case where $q > 4$, i.e. in presence of a first order transition.

First order transition: behavior of the model after sudden quenches

We summarize here how the phenomenology displayed by the model during the relaxation dynamics varies with respect to the temperature of the quench. We point out that there is a lack of understanding for shallow quenches, i.e. final temperatures *close* to the critical one, where dynamical phenomena like metastability and nucleation are relevant. In Chapters 4 and 5 we approach this problems.

A scheme of the dynamical regimes of the system was given in Ref. [54] and is portrayed in Fig. 1.4. All the characteristic temperatures which enter the game are in general dependent on the parameters and are not always properly defined or precisely known, nonetheless this picture offers a true partition of the possible relaxational regimes. Consider very low temperature quenches with $0 \leq T_f \leq T_g$, the system approaches a glassy state [55–57] which relaxes really slow and perdures for all the (long) observed evolution time in the simulations portrayed in Fig. 1.4. It is known that the system finally reaches blocked state of the same kind of those encountered even for higher temperature when glassy behavior is absent. Indeed for quenches to temperatures in the range $T_g \leq T_f \leq T_b$ the system undergoes curvature driven coarsening which satisfies LAC law until get trapped in blocked states (see Fig. 1.4). These are highly symmetrical configurations, which have stripes or honeycomb like [22] shapes, and are escaped only through activated processes (see, e.g., Ref. [54, 58]). If the temperature is high enough the system relaxes through simple coarsening in agreement with LAC law, see e.g. Ref. [59,60]. But in the case of quenches close enough, in a way that we quantify more in the last chapters of this work, to the critical temperature the behavior is different. Shallow quenches are accompanied by metastability properties (with finite life-time in finite dimensions) and in general, quantifying metastability and the dynamic escape from it through nucleation is a hard and longstanding problem [61–63]. With respect to the other regimes less numerical inquiries and analytical arguments exist and it remains the less understood one. In Chapter 4 we describe the properties of the metastable states, in particular in the large q limit where we can provide some exact results and where it is also possible to give a more precise meaning to the *metastable* temperature T_m. In Chapter 5 instead we focus on the complicated nucleation process that brings the system from the metastable state to a coarsening regime.

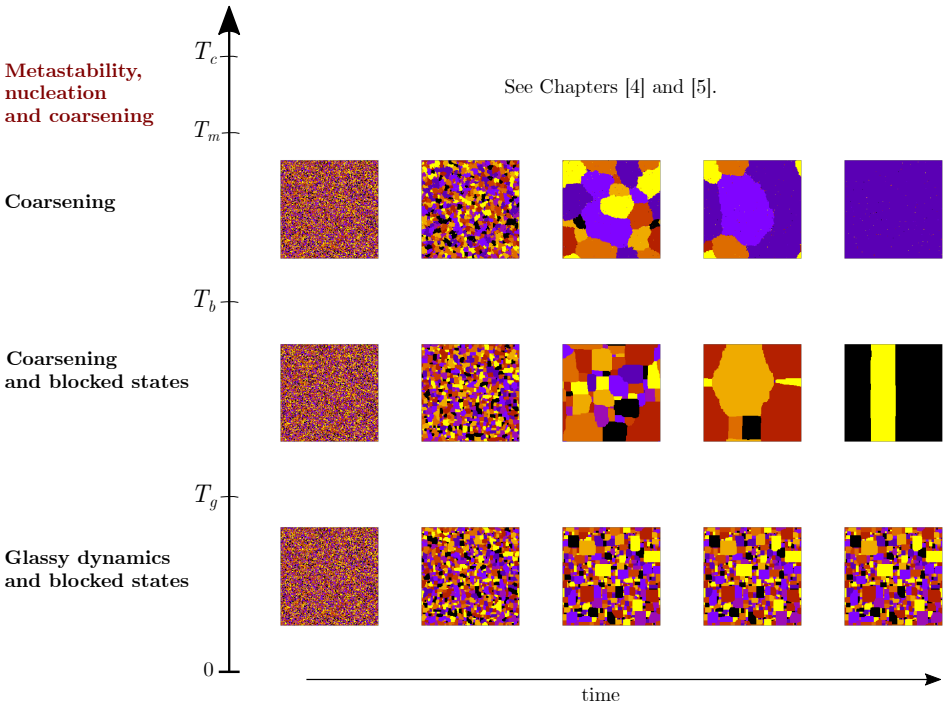

Figure 1.4: Dynamical regimes in the long term relaxation of the model, with $q > 4$, after a quench from infinite temperature down to subcritical ones. The Snapshots are instances of the relaxation dynamics up to 10^6 MCs of the $q = 9$ Potts model on a squared lattice of linear size $L = 200$ with p.b.c. for a quench starting from initial temperature $T_i \to \infty$. The final temperature are $T_f = 0.7T_c$ for the simple coarsening, $T_f = 0.4T_c$ for coarsening with blocked states and $T_f = 0.01T_c$ for the glassy dynamics.

Part I

Ising Model

Chapter 2

Fluctuations and their dynamics

In the first section of this chapter we introduce the problem of rare fluctuations and of the description of their dynamics, motivating the theoretical and practical interest in their study. We give a brief summary of the results contained in the chapter in the second one and in the third one we tackle the problem of the dynamics of the fluctuations of collective variables, i.e. observables, in the Gaussian model of statistical mechanics, based on our works in Ref. [1, 2].

2.1 Introduction: Rare fluctuations

The law of large numbers is a probability concept familiar even to the layman. Toss a fair coin several times and, in the long run, the number of heads and tails will be comparable. To be more precise we can say that it is a very strong approximation for the probability of the outcome of a collective variable (the number of heads in the previous scenario for example) , i.e. it is one if the random variable equals its mean and zero otherwise. The higher the number of tosses the better is this approximation in predicting the outcome, being exact (in a sense that would deserve some precisations) in the limit of infinite tosses. But we can of course do better then considering just the mean value and even if we don't have access to the complete distribution we may be able to approximate it to a Gaussian distribution centered around the average by means of the central limit theorem (see, e.g., [64]), when it holds. Loosely speaking in this case we are taking into account the average of the distribution and the fluctuations around it. What about *rare* fluctuations though? A way to define what we mean by *rarity* here is indeed to consider rare such fluctuations which are poorly, if not at all, described by the central limit theorem. Therefore in other terms we are referring to events associated to the tails of the distribution describing the process, which are not captured by the Gaussian approximation about the mean.

2.1.1 Large deviation theory, an example with spin statistics

Large deviations theory (LDT) is the perfect language in which to phrase this problem. To be brutally synthetic LDT consists of exponential approximations for probability distributions which generalizes the central limit theorem. But it is more then a useful tool to deal with rare events, it has been argued [65, 66] that it represents the very mathematical language of statistical mechanics, in the same way in which differential geometry relates to general relativity. Fundamental results in

this branch of probability theory bear important consequences in several fields of science [67–69] and are successfully applied to various practical situations [70, 71].

Under conditions provided by general theorems (or sometimes to be checked for the specific problem), the probability $P(S)$ to observe a certain value S of a collective variable $\mathcal{S}[\varphi]$ of the microstates φ of the system obeys a large deviation principle (LDP) [66]. This amount to say that $P(S) \sim e^{-NI(s)}$, where N is a measure of the number of degrees of freedom contributing to S, assumed to be large, $s = S/N$ is the intensive variable associated with S, and $I(s)$ the so-called *rate function* which is non-negative and it generically vanishes at the average and most probable value of s. The above holds in the large N limit. Consider to illustrate these concepts a system composed by a number N of *uncorrelated* spins φ_i, with $i \in \{1, \dots, N\}$. Each spin is with equal probability found in state 1 or -1, i.e.

$$P(\varphi_i) = \begin{cases} 1/2 & \text{for} \quad \varphi_i \in \{-1, 1\} \\ 0 & \text{otherwise} \end{cases} \quad , \quad \forall\, i \in \{1, \dots, N\}. \tag{2.1}$$

A collective variable we may study is the sum of all the spin values, i.e. the total magnetization

$$\mathcal{M}[\varphi] = \sum_{i=1}^{N} \varphi_i \,, \tag{2.2}$$

where $\varphi = \{\varphi_1, \dots, \varphi_N\}$ denotes a microstate of the system. The probability of a fluctuation M of the magnetization can be formally expressed as

$$P(M) = \sum_{\varphi \in \Gamma} P([\varphi]) \delta_{\mathcal{M}[\varphi], M} \,, \tag{2.3}$$

where Γ stands for the space of all the possible microstates each having a probability $P([\varphi])$ and the Knronecker delta, δ, constraints the sum to the subspace of configurations associated to the macrostate with magnetization M. Equation (2.1) tells us that $P([\varphi]) = 2^{-N}\ \forall\, \varphi \in \Gamma$ therefore to evaluate Eq. (2.3) we just need to count the microstates with magnetization M. The number of negative spins has to be $(N - M)/2$ and consistently the positive spins are $(N + M)/2$, considering all the permutations we end up with the exact expression for the probability

$$P(M) = \frac{2^{-N} N!}{(\frac{N-M}{2})!(\frac{N+M}{2})!} \,. \tag{2.4}$$

If we consider the *large N limit*, the factorials present in the expression above can be estimated through Stirling approximation ($n! \sim n^n e^{-n}$) and we can write after some manipulations

$$P(M) \sim \frac{2^{-N} N^N}{(\frac{N-M}{2})^{(\frac{N-M}{2})} (\frac{N+M}{2})^{(\frac{N+M}{2})}} \,. \tag{2.5}$$

By taking the logarithm, exponentiating, collecting N and using the notation $m = M/N$ we are finally able to write the a large deviation principle $P(M) \sim e^{-NI(m)}$ for the probability of the total magnetization, with rate function

$$I(m) = \frac{1-m}{2} \ln(1-m) + \frac{1+m}{2} \ln(1+m) \,, \tag{2.6}$$

which is depicted in Fig. (2.1). This rate function has all the properties we mentioned above, in particular it vanishes at the average value ($\langle m \rangle = 0$ specifically) which is also the minimum. It is straightforward from here to recover the central limit theorem (dashed line in Fig. 2.1), indeed expanding the rate function around

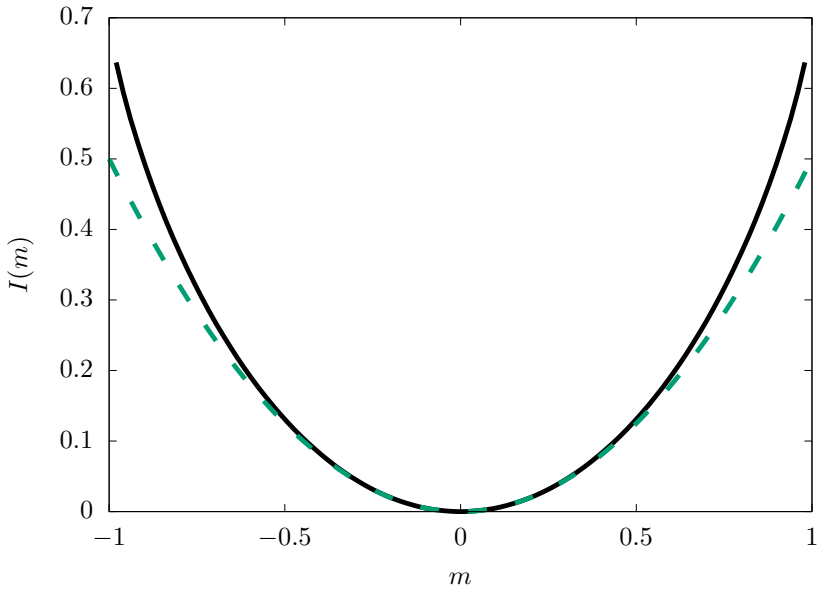

Figure 2.1: Rate function defined in Eq. (2.6), the dashed line represents the quadratic exponent characteristic of the Gaussian approximation obtained expanding to the second order the rate function and recovering the central limit theorem.

the average to the second order we get $I(m) \approx m^2/2$. The law of large numbers is finally recovered when N goes to infinity and the only value of m which does not let $P(M)$ vanish is the mean one. As a remark we mention that, in this case, $-I(m)$ is nothing but the *entropy* of the macrostate associated to a given magnetization[1] rescaled by the number of total spins N.

In this simple example we have access to the complete probability distribution and we then show that it obeys a LDP, often though this is not the case and the derivation of a LDP is our best chance to understand the process.

2.1.2 Singular rate functions

Considering again the case of a generic observable $\mathcal{S}[\varphi]$, the rate function, and thus $P(S)$, can exhibit singular points [69, 72–84, 84–86] at which some derivatives are discontinuous. This fact is usually interpreted as a phase transition occurring at the level of fluctuating configurations. Namely, if s_c is one of these singular points, the configurations of the system corresponding to $s < s_c$ or to $s > s_c$ are qualitatively different. This is exactly what occurs when an ordinary phase transition is present in a statistical system. The difference is that in the latter case the typical and statistical properties of the system change qualitatively when a control parameter (the role of which is played here by s) crosses a critical value (the analogous of s_c), whereas here there is no need to change any external parameter, because rare fluctuation spontaneously occurring with $s < s_c$ or $s > s_c$ naturally correspond to radically different system properties.

In spite of the fact that large deviation theory has been widely used for studying the stationary properties of both equilibrium and non-equilibrium stochastic processes [69], the topic of the dynamics of large fluctuations is largely unexplored. The

[1] shifted by $\ln 2$ which is the logarithm of phase-space volume for a single variable, therefore 2 in this case for binary spins.

most general problem consists in understanding how an atypical state which realizes a rare fluctuation can be reached by the system starting from a certain, specified condition where such large fluctuations are absent. In literature [87], this issue was addressed in a solvable model where $S = \sum_{k=1}^{N} s_k$ is the sum of a large number N of independent and identically distributed variables s_k, which evolve in time according to a certain stochastic dynamics. Depending on the actual distribution of the s_k, the probability $P(S)$ can exhibit a singular point S_c. Starting from a typical state with $S = \langle S \rangle$, the probability $P(S,t)$ of finding any value S was determined. It was observed that the evolution of $P(S,t)$ is radically different if a critical point S_c for the variable S is present or not. In its absence, $P(S,t)$ evolves quite smoothly and, in a relatively short time, rare fluctuations with $S - \langle S \rangle \sim \mathcal{O}(N)$ are developed such that the probability to observe them quickly attain its stationary value. If, instead, a critical point S_c is present, the evolution occurs as described above only on one side of the value S_c (in that concrete example for $S < S_c$), whereas on the other side, the evolution of $P(S,t)$ is slow and characterized by a never-ending algebraic relaxation which strongly resembles the one observed in thermodynamic systems brought across a phase transition [18, 88, 89]. This fact reinforces the interpretation of a singular point in $P(S,t)$ as a sort of a phase transition.

We conclude this section noticing that when LDT does not apply one is not completely spoiled of systematic approaches to study rare events. For example when the underlying statistics is characterized by fat-tailed distributions the mathematical framework of the big-jump principle can be in some cases fruitfully employed, see e.g. [90, 91] .

2.2 Summary of the results

The main results presented in this chapter regards the dynamical properties of the fluctiations of a collective variable in a paradigmatic model of statistical mechanics, the Gaussian model. This field theory can be used to describe the local coarse-grained order parameter of a d-dimensional Ising model in the disordered phase. Specifically we focus on the probability distribution of the variance of the order parameter whose deviations are characterised by a critical point both in and out of equilibrium [72, 89, 92–97], where the model experiences a condensation transition at the level of fluctuations, a phenomenon which has been dubbed *condensation of fluctuations*. Accordingly, this is a natural candidate to study how the presence of such a singularity affects the dynamical properties of large deviations. The dynamical settings consist of a quench of the temperature of a thermal bath the system is in contact with and the subsequent relaxation of the system in the cases of conserved (COP) and not conserved order parameter (NCOP). We find that the fluctuations of the variance s behave differently depending on weather they are affected by condensation or not. Specifically non-condensed values converge in an adiabatic-like way to stationarity while fluctuation affected by condensation display a comlplex evolution, corroborating an interesting interpretation of the phenomenon in terms of ordinary theory of phase transitions. This is evinced from the dynamical evolution of the rate function $I(s,t)$, which we evaluate analitically for both COP and NCOP regimes, reported in Fig. 2.2. The main difference between the two cases consists in the fact that in the absence of a conserved quantity the system relaxes again to a true equilibrium configuration while the structure of the fluctuations in the COP case is not the one expected for the system in equilibrium at the final temperature. This is related to the fact that precisely the zero mode of the field, i.e. the conserved quantity, has a special role in the condensation transition.

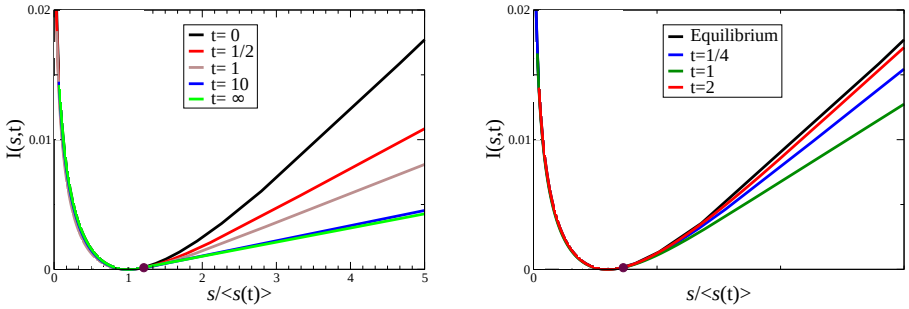

Figure 2.2: Rate function $I(s,t)$ for the COP (left) and NCOP (right) dynamics as a function of the rescaled variable $s/\langle s(t)\rangle$ where $\langle s(t)\rangle$ is the average value of s at time t, for various fixed values of the time t after a quench from inverse temperature β_i to β_f, see Fig. 2.4, Fig. 2.6 and body of the chapter for details. The critical value $s_c^{(eq,\beta_f)}/\langle s\rangle^{(eq,\beta_f)}$ is marked by a thick dot.

2.3 Fluctuations in the Gaussian Model

We discuss in this section some new and interesting features of the dynamics of fluctuations of observables in the Gaussian model.

2.3.1 The model

The Gaussian model [13, 98], describes a real scalar field $\varphi(\vec{x})$ (with $\vec{x}$ a vector in a d-dimensional space) which is characterized at equilibrium by the Hamiltonian

$$\mathcal{H}[\varphi] = \frac{1}{2}\int_V d\vec{x}\left[(\nabla\varphi)^2 + r\varphi^2(\vec{x})\right]. \tag{2.7}$$

Here r is the non-negative parameter, often called *the mass* of the model, which determines the equilibrium spatial correlation length of the system $\xi = r^{-1/2}$ [13] while the divergence term accounts for the energetic cost of the inhomgeneities of the field.

It is useful to consider the expression of the hamiltonian in terms of the Fourier components $\varphi_{\vec{k}}$ of the field

$$\mathcal{H}[\varphi] = \sum_{\vec{k}} \mathcal{H}_{\vec{k}} = \sum_{\vec{k}} \frac{1}{2V}\omega_k \varphi_{\vec{k}}\varphi_{-\vec{k}}, \tag{2.8}$$

with $\omega_k = k^2 + r$ and V the volume if the system. A finite volume implies the quantization of the modes, note the sum in Eq.(2.8), moreover we assign periodic boundary conditions, even if this choice does not affect the results of the analysis presented here. An other assumption we use is that an ultraviolet cut-off Λ is present and accounts for a microscopic length scale, arising, e.g., in the Ising interpretation from the spacing of the lattice. Only modes with wave vectors of smaller magnitude than Λ are therefore allowed. A consequence of $\varphi(\vec{x})$ being a real field is that $\varphi_{-\vec{k}} = \varphi^*_{\vec{k}}$, i.e. half of its Fourier components are actually independent. We keep track of this by changing the notation and indicating now with $\sum_{\vec{k}}$ the summation on only half the $\vec{k}$ space and consistently weighting with a factor 2 the addends. $\mathcal{H}_{\vec{k}}$ in Eq. (2) now reads

$$\mathcal{H}_{\vec{k}} = \frac{1}{V}\chi_k\omega_k\varphi_{\vec{k}}\varphi_{-\vec{k}}, \tag{2.9}$$

where we defined the function χ_k as

$$\chi_k = \begin{cases} 1/2 & \text{for} \quad k = 0 \\ 1 & \text{otherwise,} \end{cases} \tag{2.10}$$

to properly take care of the zero modes which is to be counted once.

We consider in the following two paradigmatic dynamics for relaxational models, the NCOP (Non Conserved Order Parameter) dynamics, often dubbed Model A in literature, and the COP (Conserved Order Parameter) dynamics, the so-called Model B [99]. These two different dynamics represent two common scenarios, back to the underlying Ising model the first one would be the appropriate description if we are modeling a ferromagnet the second one instead would be the correct one if we are dealing with mixtures, e.g. a binary alloy, where the mass of the two components is conserved in time. The evolution of the field is governed respectively by the overdamped Langevin equations [13, 99]

$$\frac{\partial \varphi(\vec{x},t)}{\partial t} = \left(\nabla^2 - r\right)\varphi(\vec{x},t) + \eta(\vec{x},t), \tag{2.11}$$

and

$$\frac{\partial \varphi(\vec{x},t)}{\partial t} = -\nabla^2\left[\left(\nabla^2 - r\right)\varphi(\vec{x},t) + \eta(\vec{x},t)\right], \tag{2.12}$$

where $\eta(\vec{x},t)$ is an uncorrelated, zero mean, Gaussian noise associated to a thermal bath at temperature $\beta^{-1} = k_B T$ (k_B is the Boltzmann constant), with

$$\langle \eta(\vec{x},t)\eta(\vec{x}',t')\rangle = 2\beta^{-1}\delta(\vec{x}-\vec{x}')\delta(t-t'). \tag{2.13}$$

In both cases, the probability distribution function at stationarity for the field is in general an equilibrium one, given therefore by $P_{eq}[\varphi] \propto \mathrm{e}^{-\beta\mathcal{H}[\varphi]}$. To keep the discussion as clear as possible we only focus here on Model B, stressing that the same arguments are valid *mutatis mutandis* for the dynamics in absence of conservation laws. We recover Model A below discussing the results. The dynamical process we consider is the relaxation of the system, prepared at equilibrium with a bath at initial inverse temperature β_i, after an instant quench to $\beta_f > \beta_i$ at $t = 0$. Casting Eq.(2.12) in Fourier space gives

$$\frac{\partial \varphi_{\vec{k}}(t)}{\partial t} = -\widetilde{\omega}_k \varphi_{\vec{k}}(t) + \zeta_{\vec{k}}(t), \tag{2.14}$$

where $\widetilde{\omega}_k = k^2(k^2 + r)$ and we absorbed the laplacian in the definition of the noise, now indicated by ζ, so that the correlator of its Fourier transform reads

$$\langle \zeta_{\vec{k}}(t)\zeta_{\vec{k}'}(t')\rangle = \frac{V}{\chi_k}\beta^{-1}k^2\delta_{\vec{k},-\vec{k}'}\delta(t-t'). \tag{2.15}$$

The solution for $t > 0$ of Eq.(2.14) for the generic k mode is

$$\varphi_{\vec{k}}(t) = \varphi_{\vec{k}}(0)e^{-\tilde{\omega}_k t} + \int_0^t dt'\ e^{-\tilde{\omega}_k(t-t')}\zeta_{\vec{k}}(t'). \tag{2.16}$$

This implies the autocorrelation at a given time t is

$$\langle \varphi_{\vec{k}}(t)\varphi_{-\vec{k}}(t)\rangle = \langle \varphi_{\vec{k}}(0)\varphi_{-\vec{k}}(0)\rangle_0 e^{-2\tilde{\omega}_k t} + \frac{\beta_f^{-1}V}{2\chi_k\omega_k}(1 - e^{-2\tilde{\omega}_k t}), \tag{2.17}$$

with $\langle\cdot\rangle_0$ indicating the average over initial conditions. Therefore the expectation value of the Hamiltonian at time t can be expressed

$$2\langle \mathcal{H}_{\vec{k}}\rangle = \beta_k^{-1}(t) = \left(\beta_i^{-1} - \beta_f^{-1}\right)e^{-2\widetilde{\omega}_k t} + \beta_f^{-1}. \tag{2.18}$$

The function $\beta_k(t)$ introduced above can be heuristically interpreted as an instantaneous non-equilibrium mode-dependent inverse temperature. At equilibrium the equipartition theorem holds therefore we have the same value for all the modes, $\beta_k(0) = \beta_i$ at the beginning and $\beta_{k\neq 0}(t \to \infty) = \beta_f$ at the end of the dynamics. When the system is relaxing the equipartition theorem breaks down and the expectation value $\langle \mathcal{H}_{\vec{k}} \rangle$ cannot be related to any temperature and it depends by the specific k mode. We stress that the effective inverse temperature of the zero mode $\beta_0^{-1}(t) = \beta_0^{-1}$ does not evolve during the evolution and its value is determined by the initial conditions because of the conservation laws encoded in the dynamics, this is not the case for the Model A and this difference is clear in the discussion of the dynamics of the fluctuations below.

2.3.2 Condensation of fluctuations

The collective variable we consider in our analysis is the order parameter variance

$$\mathcal{S}[\varphi] = \int_V d\vec{x}\, \varphi^2(\vec{x}, t) = \frac{2}{V} \sum_{\vec{k}} \chi_k \varphi_{\vec{k}}(t) \varphi_{-\vec{k}}(t). \tag{2.19}$$

The choice of a quadratic observable allows for an analytical treatment of the problem, the energy of the system (2.8) could be another proper candidate to analyze [100]. We are interested in the properties of the fluctuations of this quantity and the chances that $\mathcal{S}[\varphi]$ takes the value S at time t are given by the formal probability distribution

$$P(S, t) = \int_\Gamma D\varphi\, P([\varphi], t)\, \delta(S - \mathcal{S}[\varphi]), \tag{2.20}$$

where Γ is the space of configurations of the field φ, $P([\varphi], t)$ is the probability of one of such configurations at time t, and δ is the Dirac delta function. Because the problem is diagonalized in Fourier components, the phase-space measure $P([\varphi], t) = \Pi_{\vec{k}} P_{\vec{k}}(\varphi_{\vec{k}}, t)$ is factorized at all times. On the basis of the explicit solution for the field at a certain time given in Eq. (2.16), it follows that the distribution of the single $\varphi_{\vec{k}}$ are Gaussian and therefore they are completely characterized by their (vanishing) average and variance, the latter being essentially encoded in $\mathcal{H}_{\vec{k}}$, the expectation value of which is reported in Eq. (2.18). Thus

$$P_{\vec{k}}(\varphi_{\vec{k}}, t) = Z_{\vec{k}}^{-1}(t) e^{-\beta_k(t) \mathcal{H}_{\vec{k}}(\varphi_{\vec{k}})}, \tag{2.21}$$

where $Z_{\vec{k}}^{-1}(t) = \left[\frac{\chi_k \beta_k(t) \omega_k}{\pi V} \right]^{\frac{1}{2}}$.

In equilibrium conditions at inverse temperature β one has $P([\varphi], t) = P_{eq}([\varphi]) = Z^{-1} e^{-\beta \mathcal{H}[\varphi]}$, where Z is the normalization constant. It is easy to show that, considering equilibrium states at different temperatures, we have

$$P_{eq}(S) = f\left(\frac{S}{\langle S \rangle} \right), \tag{2.22}$$

where $\langle S \rangle = \int_0^\infty dS\, S\, P(S) = \beta^{-1} \sum_{\vec{k}} \omega_k^{-1}$, is the average value of S. Indeed if we start from Eq. (2.20) and we change variable as $\psi_{\vec{k}} = (\langle S(t) \rangle / V)^{-1/2} \varphi_{\vec{k}}$ we have

$$\begin{aligned} P(S, t) = \quad & Z^{-1}(t) \int_\Gamma D\psi\, \exp\left\{ -\tfrac{1}{2V} \textstyle\sum_{\vec{k}} \omega_k \frac{\psi_{\vec{k}} \psi_{-\vec{k}}}{\langle \psi_{\vec{k}}(t) \psi_{-\vec{k}}(t) \rangle} \right\} \times \\ & \delta\left(\tfrac{1}{V} \textstyle\sum_{\vec{k}} \psi_{\vec{k}} \psi_{-\vec{k}} - \frac{S}{\langle S(t) \rangle} \right). \end{aligned} \tag{2.23}$$

In equilibrium all the time dependencies drop out, and $\langle \psi_{\vec{k}} \psi_{-\vec{k}} \rangle$ is independent of the temperature (and of $\vec{k}$), due to the equipartition theorem, hence one has

Eq. (2.22). The scaling property (2.22) means that the only effect on $P_{eq}(S)$ of considering different temperatures is to set a different scale $\langle S\rangle$ of S. Accordingly, by measuring S in units of $\langle S\rangle$ one recovers the same universal behavior described by the function f reported in Eq. (2.22).

Expressing the δ function constraint in Eq. (2.20) via the representation $\delta(y) = \frac{1}{2\pi i}\int_{a-i\infty}^{a+i\infty} dz\, e^{-zy}$ one arrives at

$$P(S,t) = \frac{1}{2\pi i}\int_{a-i\infty}^{a+i\infty} dz\, e^{-V[zs+\lambda(z,t)]}, \tag{2.24}$$

where $s = S/V$ is the intensive variable associated with S, and

$$\lambda(z,t) = -\frac{1}{V}\ln\int D\varphi P([\varphi],t)e^{z\mathcal{S}[\varphi]} = -\frac{1}{V}\sum_{\vec{k}}\ln\frac{1}{\sqrt{1-\frac{2z}{\beta_k(t)\omega_k}}} \tag{2.25}$$

is the so called scaled cumulant generating function. In Eq. (15), a is any real number such that $\lambda(z,t)$ is analytic for $\mathrm{R}e\, z > a$. Using Gärtner-Ellis theorem [69], for a large volume $V \to \infty$ one arrives at the large deviation form

$$P(S,t) \sim e^{-VI(s,t)}, \tag{2.26}$$

where the rate function $I(s,t)$ is given by

$$I(s,t) = z^*(s,t)s + \lambda(z^*(s,t),t), \tag{2.27}$$

where $z^*(s,t)$ is determined by the extremization condition

$$\left.\frac{\partial\lambda(z,t)}{\partial z}\right|_{z=z^*(s,t)} + s = 0. \tag{2.28}$$

In the large volume limit, if the sums over the wavevector $\vec{k}$ can be transformed into an integral according to $\frac{1}{V}\sum_{\vec{k}}\cdots \to \int\frac{d\vec{k}}{(2\pi)^d}\ldots$, where d is the number of spatial dimensions, the extremal condition (2.28) reads

$$s = \Omega_d\int_0^\Lambda \frac{dk}{(2\pi)^d}\,\frac{k^{d-1}}{\beta_k(t)\omega_k - 2z^*}, \tag{2.29}$$

where $\Omega_d = 2\pi^{d/2}/\Gamma(d/2)$ is the d-dimensional solid angle, $\beta_k(t)$ is given in Eq. (2.18), and $\Gamma(\cdot)$ the Euler function. This equation has to be solved in order to determine $z^* = z^*(s,t)$. Since s is positive by definition, z must be smaller than $\beta_0(t)\omega_0/2$, because, given Eq. (2.18), β_0 is the smallest among the $\beta_k(t)$ upon varying k. The integral on the r.h.s. of Eq. (2.29) diverges in the limit $z \to \beta_0\omega_0/2$ if $d \le 2$, while it is finite for $d > 2$. In the latter case the solution of Eq. (2.29) exists only for values of s smaller than $s_c(t)$ defined by the condition

$$s_c(t) = \Omega_d\int_0^\Lambda \frac{dk}{(2\pi)^d}\,\frac{k^{d-1}}{\beta_k(t)\omega_k - \beta_0\omega_0}. \tag{2.30}$$

For $s > s_c(t)$, the solution requires a careful mathematical treatment [93]. Alternatively, the solution can also be found within an approach motivated and inspired by what is known for the Bose-Einsten condensation: One singles out the mode $k = 0$ from the momentum sum, transforming the rest into an integral as before, thus arriving at

$$s = \frac{1}{V}\,s_0(s,t) + \Omega_d\int_0^\Lambda \frac{dk}{(2\pi)^d}\,\frac{k^{d-1}}{\beta_k(t)\omega_k - 2z^*}, \tag{2.31}$$

instead of Eq. (2.29), with

$$s_0(s,t) = \frac{1}{\beta_0\omega_0 - 2z^*(s,t)}. \tag{2.32}$$

For $s < s_c(t)$,b one has $z^*(s,t) \leq \beta_0\omega_0/2$ and hence the first term is negligible for large V. For $s \geq s_c(t)$, instead, one has $z^* \equiv \beta_0\omega_0/2$ and, for $s > s_c(t)$ this term becomes macroscopically large and takes the value $s - s_c(t)$. As a consequence, the large deviation form (2.26) holds with

$$I(s,t) = \begin{cases} z^*(s,t)s + \lambda(z^*(s,t),t) & \text{for} \quad s \leq s_c(t), \\ \beta_0\omega_0(s-s_c)/2 + I(s_c,t) & \text{for} \quad s > s_c(t), \end{cases} \tag{2.33}$$

instead of Eq. (2.28). Because $I(s,t)$ is linear for $s \geq s_c(t)$ while it is not for $s \leq s_c(t)$, the left and right derivatives with respect to s at $s = s_c(t)$ differ at a certain order, lager than the first one [93]. Notice also that $\lim_{s\to 0} I(s,t) = \infty$[2], hence $P(S = 0, t) = 0$, because $S = 0$ can be realized by the sole configuration $\varphi \equiv 0$.

2.3.3 Dynamics of fluctuations

We analyze both the COP and NCOP dynamics of the fluctuations of the order parameter variance after the quench of the inverse temperature β of the stochastic noise from β_i to β_f.

COP dynamics

We discuss here the phenomenology of the fluctuations dynamics for the Model B derived solving the model equations in the previous section. The evolution of $I(s,t)$, in the sample case $d = 3$, is shown in Fig. 2.3 for three different values of times, i.e., the initial state $t = 0$, $t = 0.5$ and $t = \infty$ corresponding to the eventual stationary state. According to the large deviation form (2.26), the average value $\langle s(t)\rangle$ corresponds to the minimum, which is also the zero, of $I(s,t)$ and its expression derives from Eq. (2.29) taking in account the fact that, for the average, z^* in (2.27)vanish at all times

$$\langle s(t)\rangle = \frac{\Omega_d}{(2\pi)^d}\int_0^\Lambda dk\, \frac{k^{d-1}}{\beta_k(t)\omega_k}. \tag{2.34}$$

Since the fluctuations of the order parameter are due to thermal fluctuations, their typical value $\langle s(t)\rangle$ moves from the initial to the final equilibrium values $\langle s\rangle^{(eq,\beta_i)}$, $\langle s\rangle^{(eq,\beta_f)}$, obtained taking respectively $t = 0$ and $t \to \infty$ in (2.34), decreasing in time being $\beta_f > \beta_i$. Using the model equation we shown in Appendix A that the evolution of the average variance for sufficiently long times is

$$\langle s(t)\rangle = \langle s\rangle^{(eq,\beta_f)} + A\; t^{-d/2}, \tag{2.35}$$

with

$$A = \frac{\Omega_d(\beta_i^{-1} - \beta_f^{-1})\Gamma(d/2)}{r(2\pi)^d(2r)^{d/2+1}}, \tag{2.36}$$

where Γ is the Gamma function. Because of the Gaussian nature of the problem the critical point $s_c(t)$, above which condensation occurs, must also decrease proportionally to what $\langle s\rangle$ does. Solving the model equations (see Appendix A) one

[2]Indeed it can be easily checked from Eq. (2.29) that $z^*(s,t) \to -\infty$ with $z^*(s,t)s \to$ const. and that $\lim_{s\to 0}\lambda(z^*(s,t),t) = \infty$, after Eq. (2.25).

finds that during the non-equilibrium evolution $s_c(t)$ decreases monotonically and, at long times, one has

$$s_c(t) = s_c^{(eq,\beta_f)} + a\ t^{-d/2}, \tag{2.37}$$

with

$$a = \frac{\Omega_d \beta_f \Gamma(d/2)\zeta(d/2)}{(2\pi)^d (2r)^{d/2+1} \beta_i(\beta_f - \beta_i)}, \tag{2.38}$$

where ζ is the Riemann zeta function.

During the process, the slope $\beta_0\omega_0/2$ of the linear branch of $I(s,t)$ corresponding to condensation (see Eq. (2.33)) is fixed because, as already observed, β_0 is time-independent. This means that, in the condensed region for $s > s_c(\infty)$, the rate function $I(s,\infty)$ at $t = \infty$ cannot be superimposed on the initial one $I(s,0)$ using the equilibrium relation (2.22). The reason of this apparent incongruence is that the two equilibrium states are different not only because of β, as implicit in Eq. (2.22), but also because of the reduction of the set of possible final states that can be reached, starting from an assigned initial one, by the conserved dynamics.

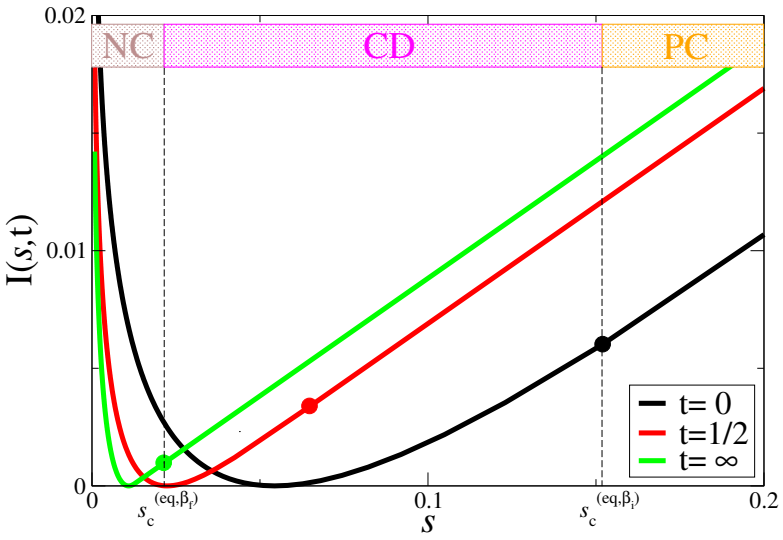

Figure 2.3: Rate function $I(s,t)$ as a function of s for three different values of the time $t = 0$, 0.5, and ∞ elapsed from the quench with $\beta_i = 1/5$ and $\beta_f = 1$, in the case $d = 3$ (the same qualitative features are observed for other values of $d > 2$), with $r = 1$, while the value of the ultraviolet cut-off Λ is set to 1. The critical value $s_c(t)$ of the variable s is marked by a thick dot. The three regions NC, CD, and PC, discussed in the main text, are highlighted at the top of the figure. [1]

Given this phenomenology, it is clear that the evolution of $I(s,t)$ displays different features depending on whether condensation occurs or not. Indeed we argue below that the dynamical process accompanying condensation, namely the building up of a macroscopic $s_0(t)$ out of a microscopic initial value $s_0(t = 0)$, is much slower

and collective than the easier rearrangement of fluctuations occurring at values of s for which this does not occur. On the basis of these considerations we can divide the range of values of s into three different sectors within which fluctuations have markedly different character, as also indicated in Fig. 2.3.

Non-condensed (NC) region - This region corresponds to $s < s_c^{(eq,\beta_f)} = s_c(t = \infty)$ and is characterized by the fact that condensation never occurs during the dynamics and all the fluctuating modes s_k contribute to the final value $s = \sum_{\vec{k}} s_k$ of the variance with "microscopic" contributions of order $1/V$. Accordingly, during the dynamics, one simply observes the redistribution of their contributions in order for the fluctuations to pass smoothly from the initial to the final equilibrium behaviors. Give that such a redistribution involves only modes which provide microscopic contributions – contrary to what happens when condensation occurs – we expect the dynamics within this NC region to be fast.

We rationalize this hypothesis as follows: in a system at equilibrium, the scaling in Eq. (2.22) holds true. Clearly, the same does not hold *a priori* out of equilibrium and, indeed, there is no way to show it as one does in the case of equilibrium discussed above. However, if the process of rearrangement occurs *quasi adiabatically*, we would expect the only effect of the quench on $I(s,t)$ to be the shift of $\langle s(t)\rangle$, according to Eq. (2.35), without affecting the form of $f(y)$ reported in Eq. (2.22). In this case, plotting $I(s,t)$ for a fixed time t as a function of $s/\langle s(t)\rangle$, one should observe superposition of the curves at different times on the mastercurve $f(y)$, formally corresponding to the case $t = \infty$. This scenario is tested in Fig. 2.4, where one clearly sees that in the NC region (namely to the left of the thick dot in the figure) curves corresponding to different times superimpose almost perfectly at all times, implying an adiabatic evolution.

Clearly, the scaling encoded in Eq. (2.22) and observed in the NC region is not expected to be exact, as in equilibrium, but it anyhow turns out to be an excellent approximation. In particular, Eq. (2.22) does not hold out of equilibrium because now in Eq. (2.23) there is an explicit time dependence in $\langle \psi_{\vec{k}}(t)\psi_{-\vec{k}}(t)\rangle$, where $\psi_{\vec{k}} = \langle s(t)\rangle^{-\frac{1}{2}}\varphi_{\vec{k}}$ is the rescaled field. The observed approximate scaling behavior might be possibly due to the fact that the domain of integration in Eq. (2.23), given by the part of Γ where the argument of the δ-function vanishes, for $s < s_c$ constrains the integration variables $\psi_{\vec{k}}$ in regions much smaller than their variances $\omega_k^{-1}\langle\psi_{\vec{k}}(t)\psi_{\vec{k}}(t)\rangle$, thereby making the time-dependence induced by the dynamics largely irrelevant. Clearly this is not possible in the presence of condensation since the variance of the mode with $k = 0$ grows macroscopic.

Condensation-developing (CD) region - Any fixed value of s within the CD region $s_c^{(eq,\beta_f)} < s < s_c^{(eq,\beta_i)}$ is crossed by $s_c(t)$ at a certain time $t^*(s)$. Note that $s_c^{(eq,\beta_f)} < s_c^{(eq,\beta_i)}$ holds due to Eq. (2.30). This implies that for $t < t^*(s)$, the contribution to the average variance of the zero mode $s_0(s,t)$ is a finite quantity in the thermodynamic limit, with $s_0 \sim \mathcal{O}(V^0)$. Instead, for $t > t^*(s)$, $s_0(s,t)$ diverges in the same limit, with $s_0 \sim \mathcal{O}(V)$. This is pictorially sketched in Fig. 2.5, where in the lower panel the time behavior of $s_0(s,t)$ for various values $(s_1, s_2, s_3, s_4, s_5)$ of s within the CD region is shown; in the upper panel of the same figure the position of these values is shown in relationship with the rate functions at $t = 0$ and at $t = \infty$, the critical values of which (indicated by the dots) define the boundaries of the CD region. For times $t \lesssim t^*(s)$ the divergence of $s_0(s,t)$ occurs as (see Appendix A)

$$\lim_{V\to\infty} s_0(s,t) \simeq \begin{cases} [t^*(s) - t]^{-1} & \text{for} \quad s > s_c^{(eq,\beta_f)}, \\ t^{d/2} & \text{for} \quad s = s_c^{(eq,\beta_f)}, \end{cases} \tag{2.39}$$

i.e., $s_0(s,t)$ with $s > s_c^{(eq,\beta_f)}$ diverges linearly while $s_0(s_c^{(eq,\beta_f)}, t)$ algebraically.

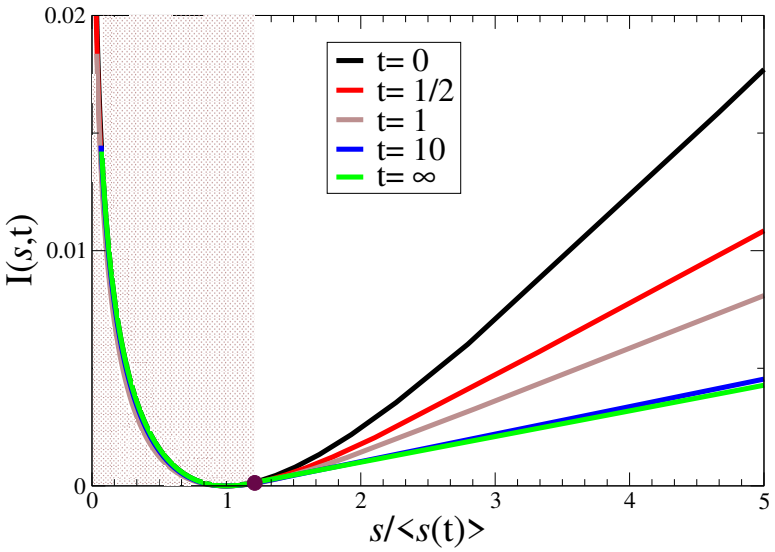

Figure 2.4: Rate function $I(s,t)$ as a function of the rescaled variable $s/\langle s(t)\rangle$ for various fixed values of the time t after a quench from $\beta_i = 1/5$ to $\beta_f = 1$, with $r = 1$, $\Lambda = 1$, in the case $d = 3$. The critical value $s_c^{(eq,\beta_f)}/\langle s\rangle^{(eq,\beta_f)}$ is marked by a thick dot and the NC region is highlighted by a brown background. [1]

Figure 2.4 shows that the relaxation of the rate function in the CD region is much slower than that in the NC region. Indeed, while for the times reported in the figure fluctuations are adiabatically in equilibrium in the NC region (corresponding to the values of s on the left of the thick dot), in the CD and in the further region denoted as PC (discussed below) where condensation is present from the beginning (on the right of the dot) a significant change is observed and convergence occurs only at much longer times ($t \gtrsim 10$ on the scale of the present figure).

Permanent-condensation (PC) region - For $s > s_c^{(eq,\beta_i)}$, $s_0(s,t)/V$ increases monotonically in time from $s - s_c^{(eq,\beta_i)}$ to $s - s_c^{(eq,\beta_f)}$. Also in this case $s_0(s,t)$ changes by an infinite amount in the thermodynamic limit $V \to \infty$. This is similar to what happens when the value of s is within the CD region described above, apart from the fact that in the latter case $s_0(s,0)$ is finite. Accordingly, we observe also in this case that fluctuations do not relax adiabatically. Notice also that, no matter how large t is, for sufficiently large values of s the rate function $I(s,t)$ differs significantly from its asymptotic form. A similar behavior was observed in Ref. [87].

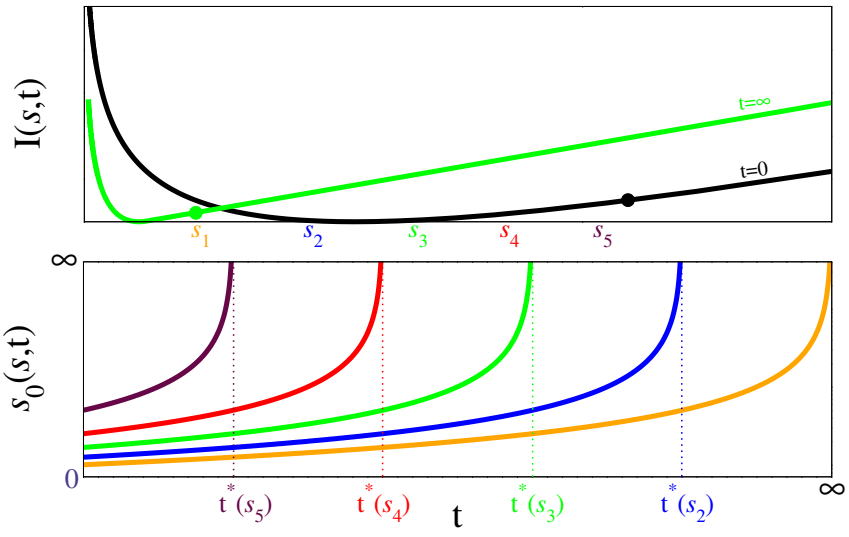

Figure 2.5: Upper panel: Rate function $I(s,t)$ as a function of s the initial equilibrium state , i.e., immediately before the quench (black line, $t = 0$) and in the final one ($t = \infty$). In both cases, the corresponding critical value of s are indicated by dots. Lower panel: time dependence of $s_0(s,t)$, for various values $(s_1, s_2, s_3, s_4, s_5)$ of s which, for comparison, are located in the upper panel with respect to the rate functions at $t = 0$ and $t = \infty$. Both panels refer to the case $d = 3$, $r = 1$ and $\Lambda = 1$ for a quench from $\beta_i = 1/5$ to $\beta_f = 1$. [1]

NCOP dynamics

If we solve the Langevin equation in the absence of conservation laws, Eq. (2.11), we obtain

$$\varphi_{\vec{k}}(t) = \varphi_{\vec{k}}(0)e^{-\omega_k t} + \int_0^t dt' \; e^{-\omega_k (t-t')}\eta_{\vec{k}}(t'), \tag{2.40}$$

where we recall that $\omega_k = k^2 + r$ and the correlator of the Fourier transform of the noise is

$$\langle \eta_{\vec{k}}(t)\eta_{\vec{k}'}(t')\rangle = \frac{V}{\chi_k}\beta^{-1}\delta_{\vec{k},-\vec{k}'}\delta(t-t'). \tag{2.41}$$

Following the same line of reasoning we developed for the Model B scenario, it is possible form the solution of the model to construct the time-dependent form of the rate function which describes the fluctuations of the field variance. In Figure 2.6 the rate function, I, is plotted versus $s/\langle s(t)\rangle$ for the initial equilibrium state, for intermediates times of the quench dynamics and for the final state reached by the system at the end of the equilibration process, in spatial dimension $d = 3$. Due to the scaling law (2.22) the profile of the rate function for the system equilibrated at the initial inverse temperature β_i and at the final one β_f is the same. The solution of the model shows that the singular point $s_c(t)$, starting from its initial value $s_c(0)$,

decreases after the quench, reaches a minimum $s_{inf} = \inf_t[s_c(t)]$ at some time (the dot in Fig. 2.6), and then increases up to the final value $s_c(\infty) < s_c(0)$.

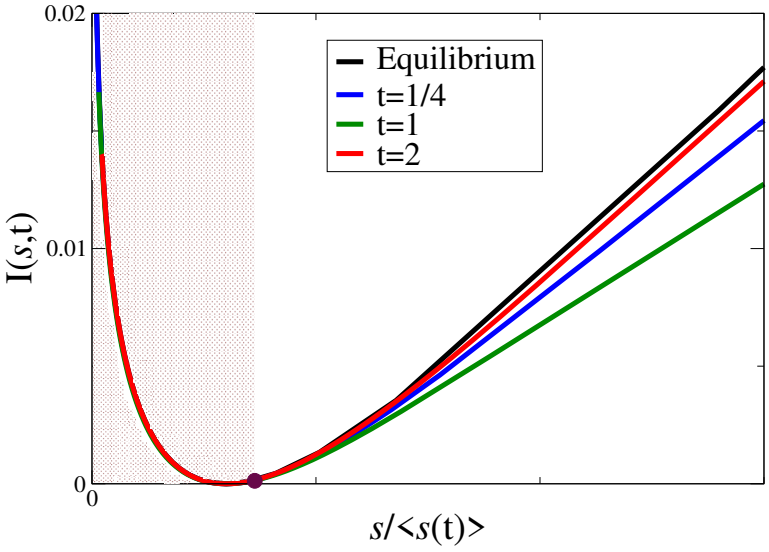

Figure 2.6: Rate function $I(s,t)$ for $r = 1$ and $d = 3$ plotted versus the rescaled variable $s/\langle s(t)\rangle$, for various times t after a quench from $\beta_i = 1/5$ to $\beta_f = 1$. The plots for $t = 0$ and $t = \infty$ are represented by the same black line. The value $s_{inf}/\langle s(t)\rangle$ is marked by a thick dot while the brown background highlights the region where condensation never occurs. [2]

In order to discuss the non-equilibrium behavior of the rate function, it is useful again to separate the region that is never interested by condensation $0 \leq s \leq s_{inf}$, from the one with $s > s_{inf}$, where condensation plays a role. In fact, it is clearly seen in Fig. 2.6, that the evolution of the rate function is markedly different within these two regions. In the range of s where condensation does not occur, the rate function overlaps with the equilibrium expression at all times. Like in the Model B scenario fluctuations in this case behave as adiabatically in equilibrium at some time-dependent temperature corresponding to the actual value of $\langle s(t)\rangle$. The evolution of the fluctuations associated to condensed configurations for $s > s_{inf}$ is, instead, more complex. Here the rate function deviates appreciably from the equilibrium form, from the very beginning of the non-equilibrium evolution. The branch of $I(s,t)$ with $s > s_c(t)$ is linear at all times, due to the condensation, but with a slope which depends on time. Specifically, its behavior follows that of $s_c(t)$, i.e., it initially decreases and then, when $s_c(t)$ reaches s_{inf}, increases until it attains the slope of the equilibrium state. Note that, since smaller values of I correspond to a larger probability of the corresponding fluctuations, this signals that out of equilibrium the chances for the system to reach a configuration affected by condensation increase and have a peak, as already pointed out in Ref. [100].

The qualitatively different behavior occurring to the left and to the right of s_{inf} can be heuristically explained as for the COP dynamics. The system stays adiabatically close to the equilibrium state characterized by the actual value of $\langle s(t)\rangle$ if its own relaxation time is comparable to the time associated with the evolution of $\langle s(t)\rangle$. In the non-condensed phase the sample variance takes comparable contribu-

tions from all the k-modes. Then the relaxation time of the system is comparable to the average relaxation time of all these modes. Solving the model it can be shown that this latter time is also comparable to the time associated with the displacement of $\langle s(t)\rangle$. This explains why the equilibrium collapse of Eq. (2.22) is observed also out of equilibrium for $s \leq s_{inf}$. For $s > s_{inf}$, however, the contribution of the mode with $k = 0$ becomes macroscopic and dominates the relaxation process. Since this is also the slowest mode (see Eq. (2.40)), the overall evolution is much slower than that of $\langle s(t)\rangle$ and therefore the condition of adiabaticity is not fulfilled.

2.4 Comments

In the last part of this Chapter we analysed some aspects of the dynamics of fluctuations of the variance s, of the order parameter in the Gaussian model with a COP and NCOP stochastic dynamics, in which large deviations may display the phenomenon of condensation. After a quench of the temperature of the thermal bath the model is in contact with, we have shown that the non-equilibrium behavior of fluctuations is radically different depending on whether the selected value of s is affected or not by the condensation as time goes by. In particular, fluctuations which do not condense converge almost adiabatically to a stationary, equilibrium-like form. Those affected by the condensation, instead, display a slow and complex evolution determined by the slow contribution $s_0(s,t)$ of the $k = 0$ wavevector.

The emergence of these two qualitatively different behaviors, which was already observed in another solvable model [94] of statistical mechanics, has a nice interpretation in the framework of what is known for ordinary phase transitions. It must be recalled, in fact, that the expression (2.19) of the probability we consider is formally equivalent [69, 92] to the partition function of a Gaussian model on a reduced phase space where the order-parameter variance is fixed to take the value S. This correspondence is usually referred to as *duality*. A well-known model with such a constraint is the spherical model of Berlin and Kac [101]. This model has a ferromagnetic to paramagnetic phase transition located at $s_c(\beta)$. Crossing a critical point in magnetic models induces a slow, never-ending (in the thermodynamic limit) coarsening phenomenon characterized by an algebraic growth of a quantity that sets the scale of spatial fluctuations. Indeed, the zero wavevector mode of the structure factor diverges because of the formation of the Bragg peak, $\lim_{t\to\infty}\langle\varphi(\vec{k},t)\varphi(-\vec{k},t)\rangle \sim \delta(\vec{k})$. If we consider the COP dynamics studied above for example, the values of s within the CD region are crossed, at a certain time, by $s_c(t)$ and therefore they are expected to share some of the properties of the slow kinetics observed in quenched ferromagnets. In fact, we have shown that this is actually the case, and the quantity $s_0(s_c^{(eq,\beta_f)},t)$ diverges algebraically. In the purely relaxational dynamics (Model A), behave analogously Clearly, relaxation in the NC region is much faster, corresponding — according to the analogy drawn above — to quenching a ferromagnetic system without crossing the critical point.

While we studied here the case of a quench of the temperature of the thermal bath, one might consider different kind of quenches, e.g., those in which other parameters are varied, such as r or, equivalently, the coefficient of the square gradient term in Eq. (2.7) (which we fixed here to be one for simplicity). Similarly, other observables beyond the order-parameter variance could be considered, e.g. the energy of the system as pointed out above. Apart from quantitative specific differences, we expect to observe in all these cases phenomena similar to those described here, with markedly different behavior of fluctuations depending on whether they cross or not a critical point. An analogous behavior is expected in the Gaussian model with purely relaxational dynamics, with the notable difference that, in this case, the relaxation occurs exponentially fast in time, in contrast to the algebraic one

observed in Model B.

The model considered here, and the related cases discussed above, as well as the model considered in Ref. [94] are characterized by independently fluctuating modes. However, there are examples of probability distributions which display a behavior similar to the one discussed in this work also in more complex systems in which these modes interact, for instance in intrinsically non-equilibrium states of models of active matter [95, 102]. The dynamics of fluctuations in these cases is largely unexplored and represents an interesting topic for further investigations.

Chapter 3

Heterogeneity

This chapter is somehow different from the others in this thesis in that its core is not strictly about out of equilibrium problems nor the Ising model. That being said, precisely the two dimensional Ising model and some of its out of equilibrium properties inspired the discussion below and, as it is clear going through the sections, its relevance to this subject is considerable. In the first section we introduce the concept of *heterogeneity* in the context of the 2d Ising model. In the second we study a general model of independent and identically distributed (*i.i.d.*) random variables focusing on the evaluation of the heterogeneity and study a particular case relevant for interacting classical spin systems. Finally we shortly add some complication to the model to enhance the similarities with the Ising model at criticality in a last, quite speculative, section.

3.1 Introduction: Cluster heterogeneity in the Ising model

Close to its critical temperature, the spin configurations of the ferromagnetic Ising model are quite heterogeneous, with domains of neighboring parallel spins (geometric domains) having a very broad size distribution. Such richness of domain sizes is produced by the unbounded fluctuations associated with the continuous phase transition. The geometrical understanding of phase transitions and the connection with the percolation transition has been proved very useful, paving the way, for example, to the introduction of powerful cluster algorithms to probe equilibrium properties. In addition, the geometric approach has helped to unveil many dynamical properties of these systems. For example, it was recently shown that at the early stages of the coarsening dynamics following a sudden temperature quench into the ordered phase [103–106], the system approaches the percolative critical point. This property has an important role, allowing not only to demonstrate that dynamical scaling is obeyed [103, 104] but also in determining whether the asymptotic state will have spanning stripes [105, 107–113].

Among the many single observables that have been proposed to geometrically characterize a domain configuration, the equilibrium cluster size *heterogeneity* $H(T)$ [114–118] and its dynamical counterpart [119] have some interesting properties that are not yet fully understood. Differently from the mean cluster size [120] that considers both the sizes of the domains and their frequency, the heterogeneity H only counts the number of different clusters sizes that are present in a single configuration. Nonetheless, the number of domains with the same size are indirectly accounted for by the space filling constraint. Consider, to illustrate the point, the cluster size distribution at the critical temperature. Although in the thermody-

namical limit this distribution is a dense, fully developed power-law, for finite-size systems the space constraints impose both a size cutoff and the impossibility of all possible sizes (those smaller than the system size) being present in a single configuration. To give an impression, we draw here a possible microstate for a system of linear size $L = 5$

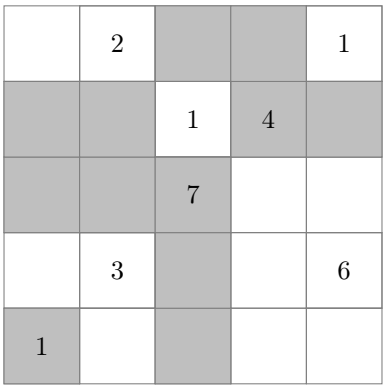

which has clusters of dimensions from 1 to 7 but a cluster of size 5 is missing. Thus, H is measured for each sample and takes into account those holes in the size distribution. Of course, once averaged, the distribution becomes dense. For the 2d Ising model, the geometric domains percolate at the same critical temperature T_c. Very close to this temperature (say, T_1), $H(T)$ presents a peak [116, 118] that grows as $H(T_1) \sim L^{d/\tau}$ where $\tau = 379/187 \simeq 2.027$ is the Fisher exponent associated with the cluster size distribution $n(a) \sim a^{-\tau}$ at T_c [121, 122]. There is, remarkably, a second and larger peak of $H(T)$ at a temperature T_2 well above T_c that seems related with the percolation transition [118]. Indeed, the value of τ that well collapses this second peak is closer to the percolation value, albeit not equal. This unexpected second peak is a finite-size feature as, for increasing system sizes, both peaks merge and converge to T_c. Moreover, the equilibrium cluster size heterogeneity was recently extended [119] to out-of-equilibrium conditions and studied for the coarsening dynamics of the 2d Ising model after the temperature is suddenly quenched from very high temperatures into the ferromagnetic phase. The dynamical measure of H also shows pronounced peak related with the first appearance of a percolating cluster during the dynamics, whose height is, interestingly, very close to the equilibrium peak of H at T_2.

3.2 Summary of the results

An interesting question is how do we compare different long tailed distributions? How different values of the exponent τ change the behavior of the heterogeneity in a finite system? For large values of τ, most of the chosen sizes are small and similar, resulting in a small heterogeneity H. In the other limit, small τ, large clusters do get more probable and although it is more likely that all clusters have different sizes, the total number of clusters necessary to fill S is smaller. Consequently, their diversity will also be small. We thus expect that, for intermediate values of τ, there will be a maximum value of the heterogeneity. The main result of this chapter is the comlete determination of the average heterogeneity $\langle H \rangle_S$ as a function of the exponent τ and the size of the system S and consequently the solution of the maximization problem with respect to the exponent which is $\tau = 2$. In the left panel of Fig. 3.1 the average heterogeneity is displayed and compared with numerical simulations. In the right panel it is portrayed the behaviour with respect to τ of the exponent α which characterize the size dependence of the heterogeneity: $\langle H \rangle_S \sim S^{\alpha(\tau)}$.

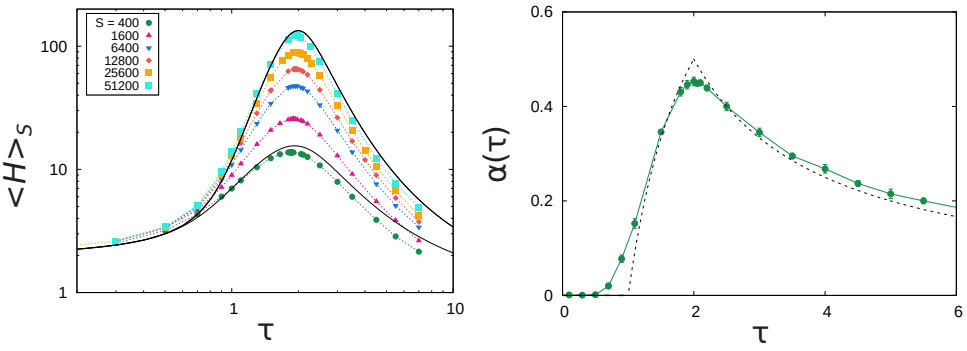

Figure 3.1: Left pane: average heterogeneity vs τ for several system sizes S, analytical results (reported for the smaller and the bigger size) corresponds to black solid lines while numerical simulations are the colored ones. Right panel: exponent α vs τ. See Fig. 3.4, Fig. 3.5 and main text for details.

3.3 Heterogeneity in statistical systems

In this section we introduce a general, albeit simple model that generate independent domains whose only constraint is to fill the system area S. We describe the model, show that is solvable, evaluate the heterogeneity and compare the results with numerical simulations.

3.3.1 A general model with *i.i.d.* random variables

We consider a model where independent and identically distributed (*i.i.d.*) random variables $\{s_d\}$, are extracted from a probability distribution $p(s)$. In the analogy with a domains problem, s_d represents the size, i.e. the volume, of the i-th domain. $p(s)$ is a generic probability distribution that will be denoted as *bare* since the effective distribution of the s_d is shaped by the presence of the global constraint

$$\sum_{d=1}^{D} s_d = S, \tag{3.1}$$

where S is a parameter playing the role of the system's size. Here D is the fluctuating number of domains that, according to the particular extraction of the $\{s_d\}$, is needed to fulfill the constraint (3.1). As it is, this approach is rather general. However, it can be adapted to describe specific models (e.g. random percolation or the Ising model) by using the appropriate domains size distribution $p(s)$.

The probability of a configuration $\mathcal{C} \equiv [s_1, s_2, \ \dots\ , s_D; D] \equiv [\{s_d\}; D]$ is given by

$$p_S(\{s_d\}; D) = \frac{1}{Z_S} \prod_{d=1}^{D} p(s_d) \delta_{\sum_{d=1}^{D} s_d, S} \ , \tag{3.2}$$

where the constraint given by Eq. (3.1) is enforced by the Kronecker delta. The quantities

$$Z_S(D) \equiv \sum_{s_1=1}^{S} \sum_{s_2=1}^{S} \dots \sum_{s_D=1}^{S} \prod_{d=1}^{D} p(s_d) \delta_{\sum_{d=1}^{D} s_d, S} \ , \tag{3.3}$$

and

$$Z_S = \sum_{D=1}^{\infty} Z_S(D), \tag{3.4}$$

play the role of *partition functions* respectively in ensembles with a fixed number of domains D and in another where D fluctuates. From this simple observation one immediately obtains the probability to have a number D of domains as

$$p_S(D) = \frac{Z_S(D)}{Z_S}, \tag{3.5}$$

and the average number of domains reads

$$\langle D \rangle_S = \sum_{D=1}^{S} D p_S(D) \tag{3.6}$$

As already discussed, because of the constraint (3.1), the *dressed* probability distribution of finding a domain of size s is different from the bare one, and can be obtained from Eq. (3.2) by marginalization as

$$\begin{aligned} p_S(s) &= \frac{p(s)}{\sum_{D=1}^{\infty} D\ Z_S(D)} \sum_{D=1}^{\infty} D \sum_{s_1=1}^{S} \sum_{s_2=1}^{S} \cdots \sum_{s_{D-1}=1}^{S} \prod_{d=1}^{D-1} p(s_d) \delta_{\sum_{d=1}^{D-1} s_d, S-s} \\ &= \frac{p(s)}{\sum_{D=1}^{\infty} D\ Z_S(D)} \sum_{D=1}^{\infty} D\ Z_{S-s}(D-1)\ , \end{aligned} \tag{3.7}$$

where the extra factor D comes in the game if we do not care about which domain takes the specific size s.

The average domain size therefore reads

$$\langle s \rangle_S = \sum_{s=1}^{S} s p_S(s). \tag{3.8}$$

At this point we can consider the heterogeneity. Given a configuration $\mathcal{C}$, this is defined, using the notation where $\sum_n^{1,S} \equiv \sum_{n=1}^{S}$, as

$$H = \sum_{n_1}^{1,S} \delta_{n_1,s_1} + \sum_{n_2 \neq s_1}^{1,S} \delta_{n_2,s_2} + \sum_{n_3 \neq s_1,s_2}^{1,S} \delta_{n_3,s_3} + \cdots \sum_{n_D \neq s_1,s_2 \cdots,s_{D-1}}^{1,S} \delta_{n_D,s_D}\ , \tag{3.9}$$

namely as the number different values assumed by the random variables $\{s_d\}$.

The probability to observe a certain value of H is given by

$$\begin{aligned} p_S(H) = \frac{1}{H!} \sum_{D=H}^{S} D! \sum_{s_1}^{1,S} \sum_{s_2 \neq s_1}^{1,S} \sum_{s_3 \neq s_1,s_2}^{1,S} \cdots \\ \cdots \sum_{s_H \neq s_1,s_2 \cdots,s_{H-1}}^{1,S} \sum_{\substack{k_i=1,D-H+1 \\ k_1,k_2,\cdots,k_H \\ \sum_i k_i = D}} \left[\frac{1}{\prod_{j=1}^{H} k_j!} \prod_{m=1}^{H} p(s_m)^{k_m} \delta_{\sum_{n=1}^{H} k_n s_n,\, S} \right]. \end{aligned} \tag{3.10}$$

We can rationalize the equation above as follows. i) The product $\prod_{m=1}^{H} p(s_m)^{k_m}$ is the probability of a configuration where there are $\{k_m\}$ domains of sizes $\{s_m\}$. ii) One can run over all such configurations by summing over all the k_m, provided that $\sum_{i=1}^{H} k_i = D$, the total number of domains. Furthermore, each k_i goes from 1, because each of the H different sizes must be represented by at least one domain, up to $D - H - 1$, which is the situation in which all the other sizes, except s_i, are represented by a single domain. iii) The factor $D!/\prod_{j=1}^{H} k_j!$ ($D!$ has been moved

to the beginning of the expression since it is the last to be summed) is the number of ways to have a realization of $\{k_m\}$. The extra factor $H!$ comes from the fact that we don't want to over count configurations that have the same realization of the domains due to the symmetry upon re-labeling of the sizes. iv) The δ function fixes the system total size S. v) The sums over $s_1, \cdots, s_H$ are constrained not to overlap because, given H, there must be H domains of different areas, no matter what these areas are. vi) The sum over D starts from H is because while it is true that there can be a different number of domains, given H, at least H of them are needed.

From Eq. (3.10) the average heterogeneity is obtained as

$$\langle H \rangle_S = \sum_{H=1}^{S} H p_S(H). \tag{3.11}$$

3.3.2 Formal solution

In principle all the probabilities can be computed using the formulas provided above. This approach, however, becomes rapidly unfeasible already for moderate values of S, unless some clever way to handle such expression is adopted. Let us consider, to fix the ideas, the computation of quantities like $p_S(s)$ or $p_S(D)$ (Eqs. (3.7,3.5)), which involve the functions Z_S defined in Eq. (3.4). The sums in its definitions contain, *a priori*, a number S^S of terms, which cannot be enumerated by a fast computer already for relatively small values of S. However, due to the constraint imposed by the δ function, only a small fraction of such terms doesn't vanish. This suggests that the algorithmic complexity involved in the determination of Z_S can be tamed by resorting to some clever summation scheme. This can be done using the recurrency relation

$$Z_S(D) = \sum_{s=1}^{\infty} p(s) Z_{S-s}(D-1), \tag{3.12}$$

that can be easily proved upon writing $\delta_{\sum_{d=1}^{D} s_d, S} = \delta_{\sum_{d=2}^{D} s_d, S-s_1}$ in Eq. (3.3). It was shown in [94] that using the recurrency relation above the algorithmic complexity is lowered to polynomial.

Employing this tool is possible to obtain an exact solution of the model up to relatively large values of S. We start discussing the dressed size probability $p_S(s)$. This quantity is plotted in Fig. 3.2 using an algebraic bare probability $p(s) \sim s^{-\tau}$. The exact determination of this quantity, obtained from Eq. (3.7), is compared with the outcome of a numerical simulations where, after extracting the random variables s_d, only the configurations respecting the constraint (3.1) are kept. One sees a perfect agreement. As expected, the dressed and the bare distribution coincide, $p_S(s) \simeq p(s)$, up to values $s \lesssim S$. This suggests that the bare distribution $p(s)$ can be used, in place of $p_S(s)$, in the calculation of different quantities, thus simplifying the task. We will use this fact in the next section.

Let us now move to the computation of the heterogeneity $\langle H \rangle_S$, which requires the evaluation of Eq. (3.10). Clearly, also in this case a huge number of terms in the summations happen to vanish due to the δ function, but here, at variance with Z_S, a recurrency technique could not be found, because of the further requirements $s_2 \neq s_1,\ s_3 \neq s_1, s_2, \cdots, s_H \neq s_1, s_2 \cdots, s_{H-1}$. Hence we resort to a different approach, which provides us directly the value of $\langle H \rangle_S$.

Following [119], we argue that

$$\langle H \rangle_S \simeq s^* + \langle D \rangle_S \sum_{s=s^*}^{S} p_S(s), \tag{3.13}$$

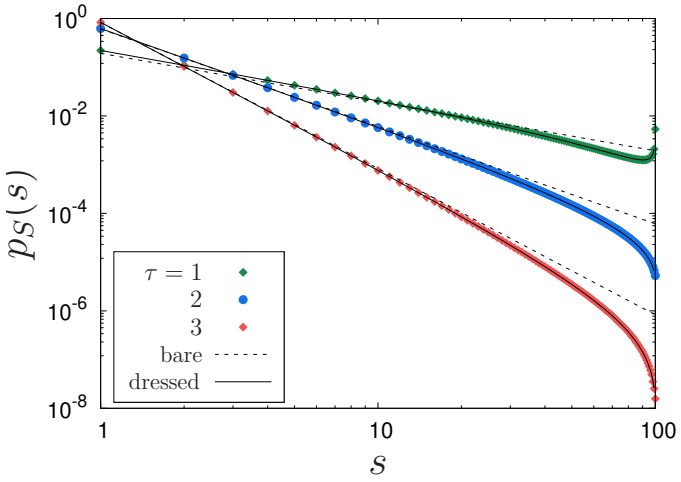

Figure 3.2: The exact dressed probability distribution $p_S(s)$ obtained from Eq. (3.7) is compared with numerical simulations (see main text) for a system of size $S = 100$, using a bare size distribution $p(s) \sim s^{-\tau}$ and several values of τ. [4]

where s^* is defined by

$$\langle D \rangle_S \; p_S(s^*) = 1. \tag{3.14}$$

Indeed, it follows from the definition of s^* that there is at least one domain of each size $s \leq s^*$ in the system, and such domains contribute the quantity s^* on the r.h.s. of Eq. (3.13). For $s > s^*$ a domain of size s is found only with probability p_S, which provides the further contribution on the r.h.s. of Eq. (3.13).

With Eq. (3.13), the computation of $\langle H \rangle_S$ is reconducted to the that of $\langle D \rangle_S$ and $p_S(s)$, both of which can be done with the recurrency method discussed above.

3.3.3 Algebraic bare distribution: analysis for power laws

Here we discuss a case which is particularly relevant in view of application to critical models: algebraic bare distributions. The proper definition for the bare probability distribution, given a total size S of the system is

$$p(s) = \begin{cases} N^{-1}(\tau, S) s^{-\tau} & ; \quad \text{for} \quad s \leq S \\ 0 & ; \quad \text{for} \quad s > S, \end{cases} \tag{3.15}$$

where the normalisation is a generalized harmonic number and can written in terms of the Riemann and Hurwitz zeta functions, respectively $\zeta(x)$ and $\zeta(x, y)$

$$\begin{aligned} N(\tau, S) &= \sum_{s=1}^{S} p(s) = \zeta(\tau) - \zeta(\tau, S+1), \\ &\simeq \zeta(\tau) - \frac{1}{1-\tau} S^{1-\tau}, \end{aligned} \tag{3.16}$$

with the last line valid for large S.

The quantity $\langle D \rangle_S$, computed by means of Eqs. (3.5,3.6), is plotted in Fig. 3.3 against S for three values of τ.

In this figure, this exact determination is compared with an analytical approximation which can be obtained by writing

$$\langle D \rangle_S \simeq \frac{S}{\langle s \rangle_S}. \tag{3.17}$$

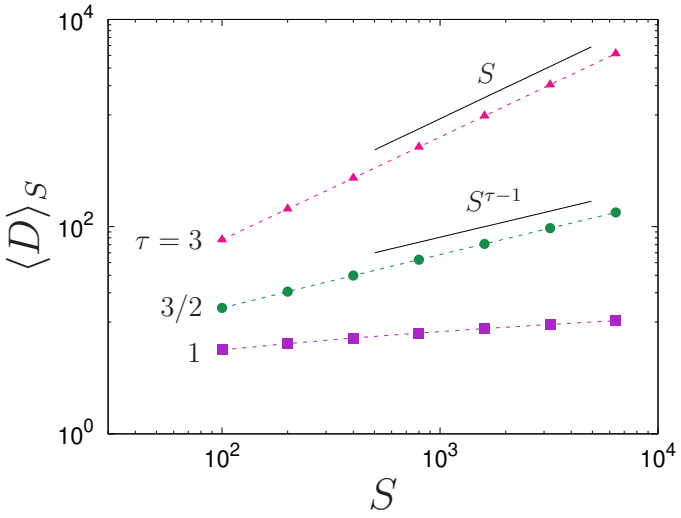

Figure 3.3: Average number of domains as a function of the size of the system for different values of τ evaluated through Eq. (3.6). The solid lines represent the predicted asymptotic behavior given by Eq. (3.18), while for $\tau = 1$, $\langle D \rangle_S \simeq \ln S$. [4]

In this expression $\langle s \rangle_S$ can be evaluated through Eq. (3.8) with the approximation $p_S(s) \simeq p(s)$. One obtains using Eq. (3.16), for large S

$$\langle D \rangle_S \simeq \begin{cases} \frac{2-\tau}{1-\tau} & ; \text{for} \quad \tau < 1 \\ \ln S & ; \text{for} \quad \tau = 1 \\ \zeta(\tau)(2-\tau)S^{\tau-1} & ; \text{for} \quad 1 < \tau < 2 \\ \zeta(2)S/\ln S & ; \text{for} \quad \tau = 2 \\ \frac{\zeta(\tau)}{\zeta(\tau-1)}S & ; \text{for} \quad \tau > 2 \ . \end{cases} \tag{3.18}$$

Fig. 3.3 shows that this results agrees very well with the exact determination even in $\tau = 1$ and $\tau = 2$ where the leading term is not a simple power law.

From Eq. (3.14) and approximating the Riemann zeta function by $\zeta(x) \simeq (x-1)^{-1} + \gamma$ we can estimate s^* as

$$s^*(\tau, S) \simeq S^{1/\tau} \left(\gamma + \frac{S^{2-\tau} - 1}{2-\tau} \right)^{-1/\tau} \tag{3.19}$$

where $\gamma \simeq 0.577$ is the Euler constant. substituting in Eq. (3.13), one arrives at the sought after result for the heterogeneity:

$$\langle H \rangle_S \simeq \frac{\tau s^* - (s^*)^\tau S^{1-\tau}}{\tau - 1}. \tag{3.20}$$

This determination of $\langle H \rangle_S$ is portrayed in Fig. 3.4 and compared with the outcome of numerical simulations. In both cases $\langle H \rangle_S$ presents a peak at $\tau \simeq 2$ that becomes

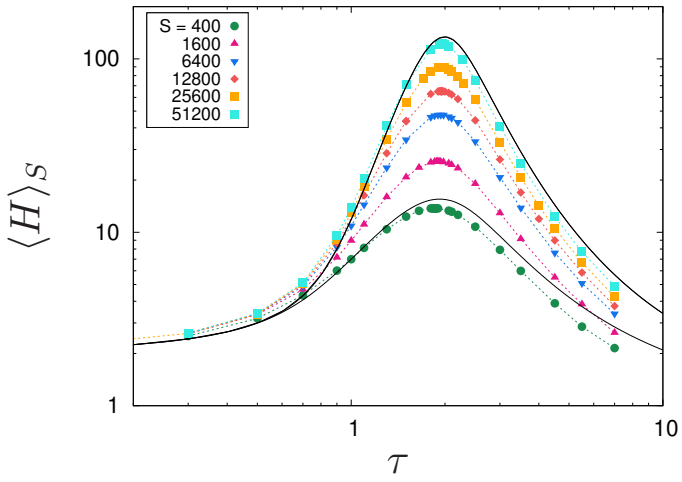

Figure 3.4: The cluster size heterogeneity, $\langle H \rangle_S$, obtained through numerical simulations for various sizes S. The results presents averages over a large number of samples (10^6 for the smallest size and 10^4 for the largest). The solid line, whose agreement with the numerical results is very good (shown for the smallest and largest size), is the approximate analytical solution given by Eq. (3.20). [4]

more pronounced as S increases. For large S,

$$\langle H \rangle_S \simeq \begin{cases} \dfrac{2-\tau}{1-\tau} & ;\text{ for } \quad \tau < 1 \\ \ln S & ;\text{ for } \quad \tau = 1 \\ \dfrac{\tau(2-\tau)^{1/\tau}}{\tau - 1} S^{1-1/\tau} & ;\text{ for } \quad 1 < \tau < 2 \\ 2\left(\dfrac{S}{\ln S}\right)^{1/2} & ;\text{ for } \quad \tau = 2 \\ \dfrac{\tau}{\tau-1}\left[\dfrac{S}{\zeta(\tau-1)}\right]^{1/\tau} & ;\text{ for } \quad \tau > 2\ . \end{cases} \tag{3.21}$$

From the above equation one has $\langle H \rangle_S \sim S^{\alpha(\tau)}$ with

$$\alpha(\tau) = \begin{cases} 0 & ;\text{ for } \quad \tau < 1 \\ 1 - 1/\tau & ;\text{for } \quad 1 < \tau < 2 \\ 1/\tau & ;\text{ for } \quad \tau > 2. \end{cases} \tag{3.22}$$

The exponent $\alpha(\tau)$ is plotted in Fig. 3.5 and compared with its determination obtained by means of numerical simulations.

From the form of $\alpha(\tau)$ one concludes that, with an algebraic bare distribution $p(s)$, there is a maximum value of the heterogeneity corresponding to $\tau = 2$. The physical motivation of this fact is clear: For a given number of domains D, it is intuitive that the steeper the bare distribution is, i.e. the larger τ is, the smaller $\langle H \rangle_S$ is. This is because small domains are repeatedly extracted, whereas larger ones have little chances to be selected. The above is true for any value of τ, however the dependence of $\langle D \rangle_S$ on S makes a difference between the two cases $\tau > 2$ and $\tau \leq 2$. Indeed, in the former case, fixing S implies a fixed (independent of τ) $\langle D \rangle_S$ as well, in view of Eq. (3.18), and this explains the decay of $\langle H \rangle_S$ with increasing τ (for fixed S). Instead, for $1 < \tau \leq 2$, upon fixing S, $\langle D \rangle$ still depends on τ. Hence

increasing τ in this range produces, next to the general result of lowering H at fixed D, a competing effect due to the average increase of D. The second result globally prevails, so that H increases for $1 < \tau \leq 2$ and displays a pronounced maximum right at $\tau = 2$. Notice also the singular form of $\alpha(\tau)$, signaling an abrupt change of behavior around $\tau = 1$ and $\tau = 2$.

3.3.4 Algebraic with large-s cutoff

In this subsection we present some arguments which are still quite speculative in nature and require more work to be soundly tested. We think nonetheless that they are worth mentioning to elucidate the connection of the results above with interacting spin models, *praesertim*, the Ising model.

In the neighborhood of a critical point, the probability distributions of observable quantities, such as the domains size, usually behave as at criticality, namely algebraically, up to a certain value Σ of s, playing the role of a coherence size, and then rapidly fall off for $s > \Sigma$. Hence one has, in this case

$$p(s) = \begin{cases} N^{-1}(\tau, S) s^{-\tau} f\left(\frac{s}{\Sigma}\right) & ; \quad \text{for} \quad s \leq S \\ 0 & ; \quad \text{for} \quad s > S, \end{cases} \tag{3.23}$$

with the following properties of the cutoff function

$$f(x) \simeq \begin{cases} 1 & ; \quad \text{for} \quad x \ll 1 \\ 0 & ; \quad \text{for} \quad x \gg 1. \end{cases} \tag{3.24}$$

Criticality corresponds to $\Sigma = \infty$. Comparing with the expression (3.15) one sees that for $\Sigma \ll S$ one basically recovers the situation with $p(s)$ purely algebraic but with the replacement $S \to \Sigma$. In other words, the correlation size Σ plays the role played by the total system size in a system at criticality. Instead, for $\Sigma \gg S$, the presence of the cutoff is irrelevant and one recovers the same results of the previous section. In a physical system which becomes critical for a certain value T_c of a control parameter T, the two situations above represent the two cases in which the thermodynamic limit $S \to \infty$ and $T \to T_c$ are taken in the two orders $\lim_{T \to T_c} \lim_{S \to \infty}$ or $\lim_{S \to \infty} \lim_{T \to T_c}$, respectively.

In particular, given a certain value of $\tau > 1$, upon fixing S and letting Σ gradually grow (corresponding to narrow criticality), we expect to see a crossover from a regime $\Sigma \ll S$ where $\langle H \rangle_S$ increases (as obtained by Eq. (3.21) letting $S \to \Sigma$) to another regime, when $\Sigma \gg S$, where $\langle H \rangle_S$ saturates to the value of Eq. (3.21). In order to make a semi-quantitative comparison with the behavior of a physical model, the two-dimensional Ising model, we should proceed as follows. First we should chose for the bare the form of $f(s/\Sigma(T))$ typical of the Ising model near criticality, and then plot $\langle H \rangle_S$ against an axis T such that $\Sigma \sim |T - T_c|^{-D\nu}$, where D is the fractal dimension of the geometric domains and ν the critical exponent of the $2d$ Ising model.

3.4 Comments

We conclude with some comments on the relevance of the picture drawn in this chapter with respect to the heterogeneity in interacting classical spin models. In the model solved in the sections above, domains are chosen from the bare probability distribution and the sample is kept when the area filling constraint is obeyed, i.e., the sum of the all sizes is exactly the area S. It is, in a sense, a mean-field approach as this is the only constraint imposed to the set of chosen domains. In a real system, e.g., geometric domains in the 2d Ising model, the equilibrium dynamics impose

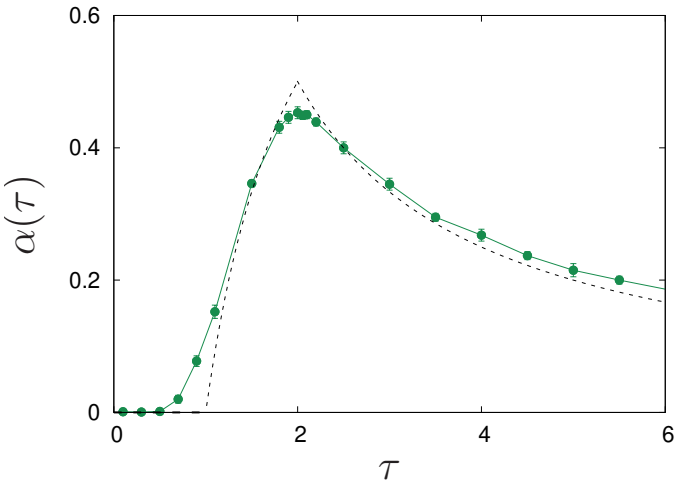

Figure 3.5: Behavior of the exponent $\alpha(\tau)$ as a function of τ. [4]

correlations between these domains. Since every domain is surrounded by others, any surface change on a given domain also changes the area of the circumscribing ones. For very large systems, the heterogeneity is maximum at T_c and the exponent is $\tau = 379/187 \simeq 2.027$ [121, 122], slightly larger than 2. There are, however, other ways to chose domains for the Ising model other then the geometrical ones. The Fortuin-Kasteleyn domains (or Coniglio-Klein droplets [123]), for example, are smaller than the geometric ones and consider that within the same domain the spins are not only parallel but effectively correlated. In this case, $\tau = 31/15 \simeq 2.067$, slightly larger than the value for geometric domains. Another possibility is to consider the area inside every hull, the external perimeter perimeter of a geometrical domain, despite the internal spins being all parallel or not. Although the number of these domains is exactly the same as the geometric domains as each hull is associated with a single domain, they do not need to obey the area constraint and, indeed, their total area is larger than S. Interestingly, their Fisher exponent is not only smaller, but is exactly 2. We thus think that the fewer constraints the domains are demanded to obey, the closer to $\tau = 2$ the Fisher exponent of their size distribution will be, maximizing the heterogeneity.

Part II

Potts model

Chapter 4

Metastable phases

In the first section of this chapter we briefly overview the problem of metastability in the two dimensional Potts model when it undergoes a temperature triggered first order transition, i.e. for $q > 4$. In the second one we study the metastable equilibrium properties of the model with heat-bath transition rates using a novel expansion, based on the work in Ref. [3].

4.1 Introduction: Metastability in the Potts model

The first order transition of the ferromagnetic two dimensional Potts model with $q > 4$ is accompanied by metastability properties. Indeed when a control parameter is

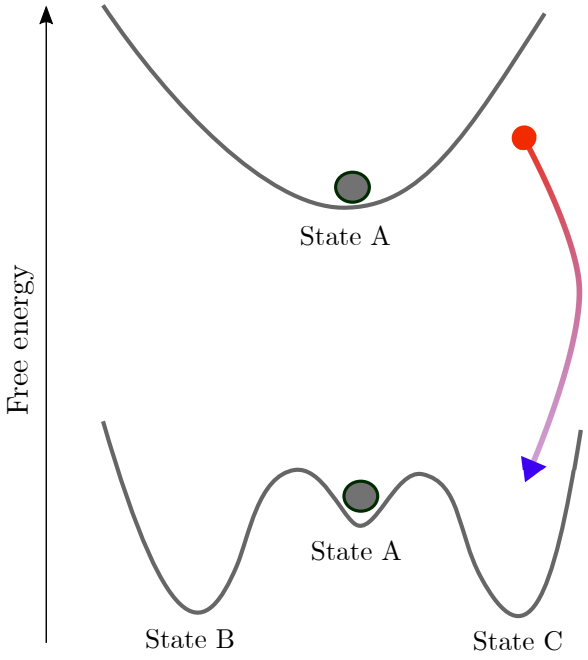

Figure 4.1: Pictorial representation of the free energy profile of the ferromagnetic two dimensional Potts model with $q > 4$ before and after a temperature quench. See main text for details.

changed in such a way that a thermodynamical system undergoes a first-order phase transitions one can usually observe hysteresis and metastability. These phenomena

are widespread in nature [124] and, particularly, in many areas of physics [125–127], among which the glass transition problem [124, 128]. Besides, metastability plays a prominent role also in biological systems such as, for instance, proteins and nucleic acids [129, 130]. To develope an intuitive idea of the phenomenon in the context of the Potts model consider the pictorial representation of the free energy landscapes given in Fig. 4.1. The above profile corresponds to the model in contact with a thermal bath at an uppercritical temperature, while the one below to a temperature lower then the critical one. In the first case there is only one minimum, State A, corresponding to a disordered phase. In the second, State A has become a relative minimum and there is a number $q > 4$ of degenerate absolute minima associated to ordered phases, here compactified in just two of them (State B and State C) to allow visualization. If the system (the gray ball) is prepared in equilibrium in the disordered phase, and then a quench to a sub-critical temperature is performed, before the (possibly long and complicated) relaxation process towards a new equilibrium it may remain trapped in the (now) metastable State A.

There are several considerations to be made with respect the simple picture given above. In general, quantifying metastability and the dynamic escape from it through nucleation is a hard and longstanding problem [61–63, 131]. Most dynamic studies of the model focused on the analysis of the coarsening dynamics after deep quenches at moderate subcritical temperatures [34, 59, 132, 133] so as to avoid getting stuck in long-lived metastable configurations [**?**, 22, 34, 54, 154, 158]. Referring to the intuitive representation of the problem in Fig. 4.1 the lower the quenching temperatures the lower the depth of the free energy basin corresponding to State A. The study of metastability and thermally assisted nucleation close to the critical temperature in this rather simple model has not been so much developed in the literature. Numerical evidence for thermodynamic metastability in finite but large size systems with $q > 4$ was provided in various papers. In particular, the analysis of the short-time dynamics [134] and Binder cumulant [135] was recently used with this purpose. However, Meunier and Morel [136] argued that thermodynamic metastability should disappear in the infinite system size limit and other authors [137] provided arguments supporting this claim. Extracting the infinite size limit behavior, and the eventual disappearance of metastability from numerical studies is, however, a dauntingly hard task. In this chapter we address metastability in the stochastic bidimensional Potts model with $q > 4$ from a novel perspective, that is, by solving the microscopic dynamics in the large q limit, based on the work in Ref. [3]. We focus on the (thermodynamic) characterization of the metastable state, leaving some questions related to its escape, and the consequent nonequilibrium dynamics, to be addressed in the next chapter.

4.2 Summary of the results

Classical spin models coupled to heat baths evolve in time stochastically according to some microscopic updates that have to be provided to make their definition complete. The microscopic rules of the Markov Chain that models the evolution of the system, from one microstate to the next, can be freely choose, conditioned to respect detailed balance. This last requirement indeed guarantees the stationary state of the dynamics to be an equilibrium one. As we argue below, the dynamics are faster, and also easier to understand analytically, when the heat bath microscopic updates are used. This is the rule that we adopt. The choice of initial conditions and working temperature decides the kind of metastability one accesses with the dynamic protocol. More precisely, for sub-critical quenches, in which we follow the evolution of a disordered initial state under conditions in which the system should order ferromagnetically, the metastable state is disordered. Instead, in the

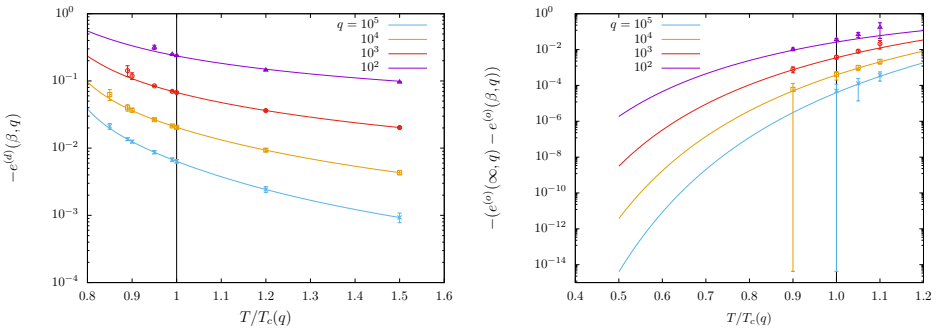

Figure 4.2: Energy density of the disordered (left panel) and ordered (right panel) metastable state *vs* T/T_c for several values of q (increasing from bottom to top), evaluated analitically (colored solid lines). Values from simulations are also presented with data points. They are time averages of the energy density. The error bars correspond to a standard deviation. The critical temperature is indicated with a vertical black line. See Fig. 4.7, Fig. 4.10 and text below for details.

opposite quench, in which we prepare the system in a ferromagnetic state and we heat it above the critical point, the metastable state is ferromagnetically ordered. We consider both kinds of instantaneous temperature quenches.

The main result of this chapter is the identification of the (few) relevant microscopic transition paths in the large q limit, the consequent derivation of the free-energy densities of the two phases and from this various thermodynamic observables that allow us to quantify the metastable state in full detail. Figure 4.2 displays the energy density of the metastable states. We also identify the spinodal temperatures for the disordered and for the ordered phase, respectively $T_c/2$ and $2T_c$ for $q \to \infty$.

4.3 Properties of the metastable phases in the large q limit

In this section we develope the method, based on an expansion in the large q limit, which allows us to describe in detail the metastable states of the model.

4.3.1 The dynamics

In this subsection we define the Heat Bath microscopic rule, we enumerate all possible updates of a chosen spin according to its surrounding configurations, and we derive the transition probability for each of them.

As we mentioned in the introduction, the usual microscopic dynamics used in Monte Carlo simulations of spin models are the Metropolis ones, in which one tries to change the spin to a new value (chosen at random among the remaining $q-1$ possibilities) and the move i) is accepted if the new local energy e_i' is lower than the previous local energy e_i or, otherwise, ii) it is accepted with probability $\exp(-\beta(e_i' - e_i))$. However, in the case of the Potts model, especially in its large q limit, another rule also respecting detailed balance, the so-called *heat bath* rule, is more efficient and allows for a partial analytic treatment, similarly to what found in other ferromagnetic models [138]. In short, with this rule the transition probabilities are proportional to $e^{-\beta e'}$. Specifically, the scheme works as follows. First, one considers the weight associated to each possible value that a spin, say φ_i, can take

depending on its local environment. As an example, assume that φ_i is surrounded, on the square lattice, by two spins taking the value 1, a spin with value 2 and another one with value 3. We attribute the weights $w_i(\varphi_i = 1) = e^{2\beta}$, corresponding to the fact that the spin i taking the value 1 yields a local energy of -2, $w_i(\varphi_i = 2) = e^{\beta} = w_i(\varphi_i = 3)$ because of the local energy being equal to -1 in these cases, and $w_i(\varphi_i = j) = 1$ for $3 < j \leq q$ for similar reasons. Next, we normalize the w_i and we define the probabilities

$$P_i(\varphi_i = k) = \frac{w_i(\varphi_i = k)}{\sum_{l=1}^{q} w_i(\varphi_i = l)} \ . \tag{4.1}$$

Having attributed probabilities to the state of the central spin, we can now evaluate the transition probabilities for its update. Imagine that the spin φ_i takes the value 1. Then, we choose a random number $r \in [0 : 1]$. If $r < P_i(1)$, the spin keeps its value $\varphi_i = 1$. Otherwise, if $r < P_i(1) + P_i(2)$, φ_i takes the new value $\varphi_i = 2$, or if $r < P_i(1) + P_i(2) + P_i(3)$, it is updated to $\varphi_i = 3$, and so on and so forth. Thus, we have the following transition probabilities for the spin $\varphi_i = 1$ surrounded by two spins 1, one spin 2 and one spin 3:

$$T_{1\to 1}^{\mathrm{HB}} = \frac{e^{2\beta}}{e^{2\beta} + 2e^{\beta} + q - 3} \ , \qquad T_{1\to 2}^{\mathrm{HB}} = T_{1\to 3}^{\mathrm{HB}} = \frac{e^{\beta}}{e^{2\beta} + 2e^{\beta} + q - 3} \ , \tag{4.2}$$

$$T_{1\to j}^{\mathrm{HB}} = \frac{1}{e^{2\beta} + 2e^{\beta} + q - 3} \ , \tag{4.3}$$

with j indicating any possible state with $j > 3$ (there are $q - 3$ such states). Notice that these probabilities do not depend on the initial state of the spin. Despite this, we prefer to use the notation above to make the comparison with the Metropolis probabilities (Eq. (4.4)). Proceeding in a similar way one can evaluate the transition probability of any spin, according to its state and the ones of its neighbors.

For the sake comparison, we recall the transition probabilities of the Metropolis rule:

$$\begin{aligned} T_{1\to 1}^{\mathrm{M}} &= 1 - \frac{1}{q-1}(2e^{-\beta} + (q-3)e^{-2\beta}), \\ T_{1\to 2}^{\mathrm{M}} &= T_{1\to 3}^{\mathrm{M}} = \frac{1}{q-1}e^{-\beta}, \\ T_{1\to j}^{\mathrm{M}} &= \frac{1}{q-1}e^{-2\beta}, \end{aligned} \tag{4.4}$$

for the same example considered above. In practice, we find that the heat-bath dynamics are much more efficient, in the sense that the approach to equilibrium is faster, in particular for large q. We only consider the heat-bath dynamics in the following. For any integer $q \geq 5$ we can classify all local configurations, seen as vertices with a central spin and its four nearest neighbors, and identify all possible updates. The method goes like this. Take one spin φ_i, count the number of neighboring spins with the same value as the selected central one, and call this number n_1. Next, count the number of neighbors with the most present spin value different from the central one and call this number n_2. Continue in this way and organize these numbers in decreasing order, that is, n_1, n_2, n_3, ... It is easy to see that, with this classification, there are only 11 local configurations (we do not distinguish which are the neighbors that take the same or different values as the central one) and they are represented in the figure below:

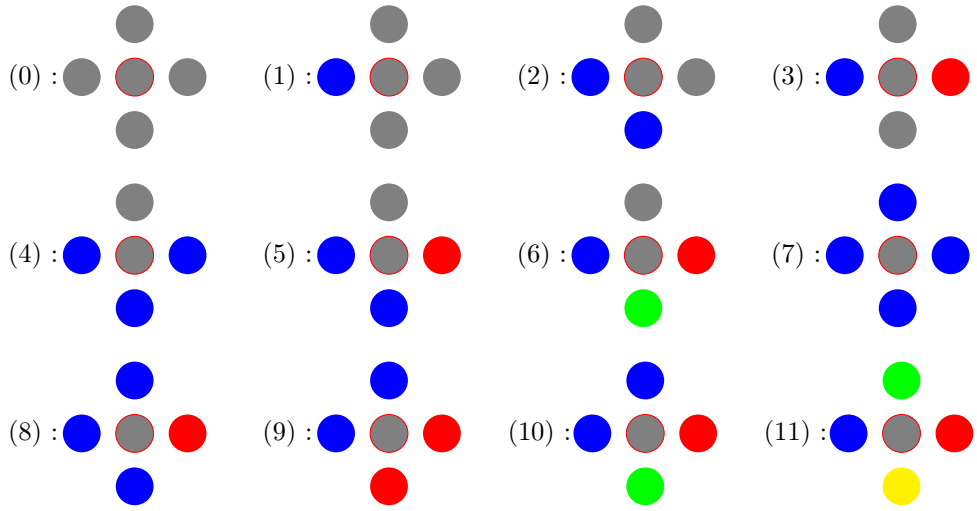

In the following we will use the name "sand" to refer to the configurations (11) in which all sites take different values. We now use a more detailed notation to identify each of these configurations writing explicitly the number of neighbors of each kind, that is to say, using $[n_1, n_2, \dots]$ where only the values $n_i \neq 0$ are kept. Proceeding in this way we have

$$
\begin{array}{rcl}
(0) & : & [4] \to (0)\ ,\ (7) \\
(1) & : & [3,1] \to (1)\ ,\ (4)\ ,\ (8) \\
(2) & : & [2,2] \to (2)\ ,\ (2)\ ,\ (9) \\
(3) & : & [2,1,1] \to (3)\ ,\ (5)\ ,\ (10) \\
(4) & : & [1,3] \to (4)\ ,\ (1)\ ,\ (8) \\
(5) & : & [1,2,1] \to (5)\ ,\ (3)\ ,\ (10) \\
(6) & : & [1,1,1,1] \to (6)\ ,\ (11) \\
(7) & : & [0,4] \to (7)\ ,\ (0) \\
(8) & : & [0,3,1] \to (8)\ ,\ (1)\ ,\ (4) \\
(9) & : & [0,2,2] \to (9)\ ,\ (2) \\
(10) & : & [0,2,1,1] \to (10)\ ,\ (3)\ ,\ (5) \\
(11) & : & [0,1,1,1,1] \to (11)\ ,\ (6)
\end{array}
$$

where the right arrows and the values after them indicate the transitions generated by the update of the central spin. For example, the first configuration, denoted by (0), can either keep the same value, thus the (0) on the right, or take another value, thus the configuration (7) : $[0,4]$. Again, this should be easy to grasp by looking at the sketch above. For each local situation, we can then read the rules for the heat-bath dynamics. The local configuration (0) remains the same with probability $\simeq e^{4\beta}$ and changes to any of the other $q-1$ possible values of the spin with probability $e^0 = 1$. Then, normalizing the probabilities, we obtain

$$
P_{0\to 0} = \frac{e^{4\beta}}{e^{4\beta} + q - 1}\ , \qquad P_{0\to 7} = \frac{q-1}{e^{4\beta} + q - 1}\ . \tag{4.5}
$$

In a similar way, we derive all other transition probabilities:

$$P_{1\to1} = \frac{e^{3\beta}}{e^{3\beta}+e^{\beta}+q-2}\,, \qquad P_{1\to4} = \frac{e^{\beta}}{e^{3\beta}+e^{\beta}+q-2}\,, \qquad P_{1\to8} = \frac{q-2}{e^{3\beta}+e^{\beta}+q-2}\,,$$
$$P_{2\to2} = \frac{2e^{2\beta}}{2e^{2\beta}+q-2}\,, \qquad P_{2\to9} = \frac{q-2}{2e^{2\beta}+q-2}\,,$$
$$P_{3\to3} = \frac{e^{2\beta}}{e^{2\beta}+2e^{\beta}+q-3}\,, \qquad P_{3\to5} = \frac{2e^{\beta}}{e^{2\beta}+2e^{\beta}+q-3}\,, \qquad P_{3\to10} = \frac{q-3}{e^{2\beta}+2e^{\beta}+q-3}\,,$$
$$P_{4\to4} = \frac{e^{\beta}}{e^{\beta}+e^{3\beta}+q-2}\,, \qquad P_{4\to1} = \frac{e^{3\beta}}{e^{\beta}+e^{3\beta}+q-2}\,, \qquad P_{4\to8} = \frac{q-2}{e^{\beta}+e^{3\beta}+q-2}\,,$$
$$P_{5\to5} = \frac{2e^{\beta}}{2e^{\beta}+e^{2\beta}+q-3}\,, \qquad P_{5\to3} = \frac{e^{2\beta}}{2e^{\beta}+e^{2\beta}+q-3}\,, \qquad P_{5\to10} = \frac{q-3}{2e^{\beta}+e^{2\beta}+q-3}\,,$$
$$P_{6\to6} = \frac{4e^{\beta}}{4e^{\beta}+q-4}\,, \qquad P_{6\to11} = \frac{q-4}{4e^{\beta}+q-4}\,,$$
$$P_{7\to7} = \frac{q-1}{e^{4\beta}+q-1}\,, \qquad P_{7\to0} = \frac{e^{4\beta}}{e^{4\beta}+q-1}\,,$$
$$P_{8\to8} = \frac{q-2}{e^{3\beta}+e^{\beta}+q-2}\,, \qquad P_{8\to1} = \frac{e^{3\beta}}{e^{3\beta}+e^{\beta}+q-2}\,, \qquad P_{8\to4} = \frac{e^{\beta}}{e^{3\beta}+e^{\beta}+q-2}\,,$$
$$P_{9\to9} = \frac{q-2}{2e^{2\beta}+q-2}\,, \qquad P_{9\to2} = \frac{2e^{2\beta}}{2e^{2\beta}+q-2}\,,$$
$$P_{10\to10} = \frac{q-3}{e^{2\beta}+2e^{\beta}+q-3}\,, \qquad P_{10\to3} = \frac{e^{2\beta}}{e^{2\beta}+2e^{\beta}+q-3}\,, \qquad P_{10\to5} = \frac{2e^{\beta}}{e^{2\beta}+2e^{\beta}+q-3}\,,$$
$$P_{11\to11} = \frac{q-4}{4e^{\beta}+q-4}\,, \qquad P_{11\to6} = \frac{4e^{\beta}}{4e^{\beta}+q-4}\,.$$

Note that for any spin in the bulk, that does not feel the boundary if there exists one, these expressions are independent of the system size. Their large q limit is established below, when we simultaneously decide the temperature range studied that itself also varies with q.

4.3.2 Disordered metastable phase

Let us focus now on the first dynamic protocol, a quench to a subcritical temperature $T < T_c(q)$ from a completely disordered state, *i.e.*, an equilibrium configuration at $T \to \infty$.

Consider a totally random configuration, a typical initial state at $t = 0$. The number of sites in the configurations labeled (a), with $a = 0, \ldots, 11$ as in the sketch with colored circles above, are $N_a(t=0) = N_a(0) = [(q-1)/q^4]\,\tilde{N}_a(0)\,N$ with

$$\begin{aligned}
&\tilde{N}_0(0) = 1/(q-1)\,, && \tilde{N}_1(0) = 4\,, && \tilde{N}_2(0) = 6\,,\\
&\tilde{N}_3(0) = 6(q-2)\,, && \tilde{N}_4(0) = 4\,, && \tilde{N}_5(0) = 12(q-2)\,,\\
&\tilde{N}_6(0) = 4(q-2)(q-3)\,, && \tilde{N}_7(0) = 1\,, && \tilde{N}_8(0) = 4(q-2)\,, \qquad (4.6)\\
&\tilde{N}_9(0) = 3(q-2)\,, && \tilde{N}_{10}(0) = 6(q-2)(q-3)\,,\\
&\tilde{N}_{11}(0) = (q-2)(q-3)(q-4)\,.
\end{aligned}$$

For large q, the state (11) largely dominates the disordered configuration since

$$N_{11}(0) \simeq N(q-1)(q-2)(q-3)(q-4)/q^4 \simeq N\,. \qquad (4.7)$$

The next configurations in the hierarchy are the (6) and (10) ones with

$$N_6(0) \simeq 4N/q\,, \qquad N_{10}(0) \simeq 6N/q\,. \qquad (4.8)$$

All the other states appear with a much lower probability, reduced by at least another power of q.

In the large q limit we can also write

$$e^{\beta} = e^{\beta_c T_c/T} = e^{T_c/T \ln(1+\sqrt{q})} = (1+\sqrt{q})^{T_c/T} \simeq q^{T_c/(2T)} \ . \tag{4.9}$$

Thus, during an update of the full lattice, the probability that a state (11) be replaced by a state (6) can be expressed as

$$P_{11\to 6} = \frac{4e^{\beta}}{4e^{\beta}+q-4} \simeq \frac{4q^{T_c/(2T)}}{4q^{T_c/(2T)}+q} = \frac{1}{1+\frac{1}{4}q^{1-T_c/(2T)}} \ , \tag{4.10}$$

showing that the temperature $T = T_c/2$ plays a special role and can be identified in this limit with the *metastable* temperature T_m we mentioned in the introduction. Indeed, for $q \gg 1$

$$P_{11\to 6} \to 1 \qquad \text{at} \qquad T < T_c/2 \ , \tag{4.11}$$

i.e., the state (11) is completely unstable and the system tends to reorganize really fast at these low temperatures. In the same large q limit, at the cross-over temperature,

$$P_{11\to 6} \to 4/5 \quad \text{and} \quad P_{6\to 11} = 1 - P_{11\to 6} \to 1/5 \qquad \text{at} \qquad T = T_c/2 \ , \tag{4.12}$$

meaning that the states labeled (11) are again unstable, even though in a weaker way. The system will still reorganize at $T_c/2$. Finally,

$$P_{11\to 6} \to 0 \qquad \text{at} \qquad T > T_c/2 \ , \tag{4.13}$$

and the system remains disordered in the large q limit, in the full temperature interval $(T_c/2, T_c]$.

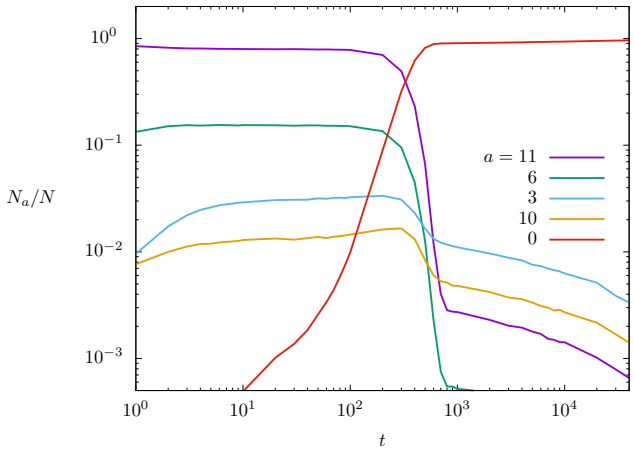

Figure 4.3: The time evolution of $N_a(t)/N$ for $a = 0, 3, 6, 10, 11$ at $T = 0.9\,T_c$ in a square lattice system with linear size $L = 10^3$ and $q = 10^3$. [3]

When q is large but finite the picture is qualitatively similar, although the change is no longer at $T = T_c/2$ and it is not as sharp. The system does not in general remain disordered after a quench at $T > T_c/2$ but it is only in this region that it can be found in a metastable state. To be more precise, let us consider a particular case. For a finite value of $q = 10^3$ and after a quench at $T = 0.9\,T_c$, we observe the

behavior shown in Figs. 4.3 and 4.4. i) During a first period, most of the spins are in the (11) state and there are only very small domains, the configurations look like sand. The density of vertices (11) is almost 1, see Fig. 4.3, and the left snapshot in Fig. 4.4 shows one such configuration. ii) At a later time, we see the appearance of the stable state (0) and some larger domains are formed, see the central snapshot in Fig. 4.4. For the chosen parameters q and T, the crossover occurs at a time $t \simeq 100$. iii) At even later times, most of the states are in the (0) state and large domains are formed, see the right panel in Fig. 4.4. This is the proper coarsening regime. Each of these three regimes is characterized by a different type of dynamical behavior. We call them i) metastable, ii) fast forming finite domains and iii) coarsening.

We found that the measurement of $N_a(t)/N$ is a very practical way of determining the type of dynamics. Next, we found that for a given value of q, the time t at which the change of behavior is observed depends strongly on the value of the temperature at which the system is quenched. In particular, if T moves close to T_c, the system seems to be blocked in a metastable state forever. For $T = 0.99\,T_c$ and $q = 10^3$, as we will see below, the system is not able to escape the metastable state.

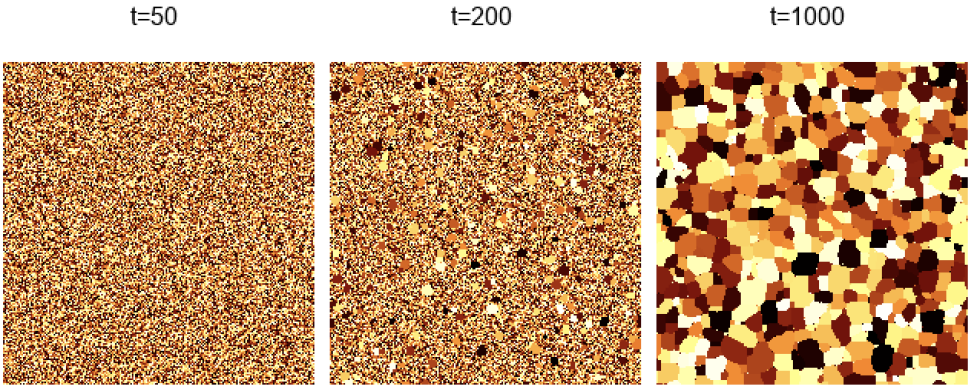

Figure 4.4: Snapshots at times $t = 50, 200, 1000$ for a square lattice system with linear size $L = 10^3$ and $q = 10^3$. Different colors are different spin values. [3]

Thus for a given value of q, after a quench to $T < T_c$, we observe metastable states up to a time which seems to diverge at some temperature value that we parameterize as $r_t(q) = T/T_c$. The quantity $r_t(q)$ does not seem to depend on the systems' linear size considered. We found numerically $r_t(q = 10^3) \simeq 0.98$, $r_t(q = 10^4) \simeq 0.94$, $r_t(q = 10^5) \simeq 0.92$, $r_t(q = 10^6) \simeq 0.90$ and $r_t(q = 10^9) \simeq 0.87$. Thus, as we increase q, the temperature above which we observe metastable states forever slowly decreases. Presumably, this quantity will go to 0.5 in the limit of infinite q.

For $T/T_c > r_t(q)$, we always observed metastable states. We will concentrate in the following in the study of these metastable states.

We illustrate the properties of these metastable states in Fig. 4.5, where we show the evolution of N_a/N as a function of time for $q = 10^3$ and $L = 10^3$ at $T/T_c = 0.99$. We only show the states which contribute the most. Already at times of the order of $t \simeq 10^1$ MCs after the quench, we found $N_0(t) = N_2(t) = N_4(t) = N_7(t) = N_8(t) = N_9(t) = 0$ while $0 \neq N_1(t) \simeq N_5(t) \simeq O(1) \ll N$ are not shown in the plot. The only values of order N at this time scale are N_3, N_6, N_{10} and N_{11}. Their expected values, according to the predictions based on the method we develop below, are $N_{11}/N \simeq 0.862$, $N_6/N \simeq 0.120$, $N_3/N \simeq 0.010$, $N_{10}/N \simeq 0.009$ and are shown with thin flat lines in the figure. The solid lines, instead, are the results of the

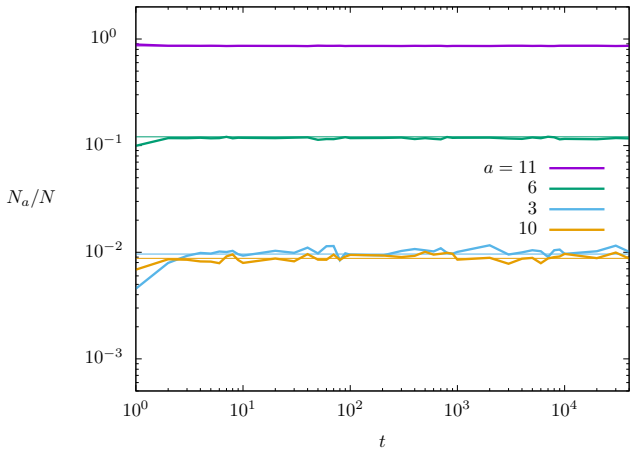

Figure 4.5: The time evolution of $N_a(t)/N$ for $a = 3, 6, 10, 11$ at $T = 0.99\,T_c$ in a square lattice system with linear size $L = 10^3$ and $q = 10^3$. The thick lines are data from a numerical simulation while the thin ones are analytical predictions based on the method we develop in this work. The curves demonstrate the hierarchy in Eq. (4.14). [3]

numerical simulations, and are in excellent agreement with the analytic predictions. Statistically, the configurations do not change after running the simulation much longer: the state made of "vertices" (3), (6), (10) and (11) according to the hierarchy

$$N_3(t) \simeq N_{10}(t) \ll N_6(t) \ll N_{11}(t) \tag{4.14}$$

with all of them being $\mathcal{O}(N)$, is metastable over very long time-scales.

In the following, we concentrate on cases in which T is close to T_c. Moreover, we use the hierarchy relation (4.14) to develop an expansion that is notably accurate even keeping only the dominant order. We rename N_a ($a = 0, ..., 11$) the *normalized* (by N) abundances that can also be interpreted as the probabilities that a randomly picked site be in the state (a). Exploiting the hierarchy relation (4.14), expected to apply to the metastable state, we consider the evolution of

$$N_{11} \simeq 1\,, \qquad N_6 \simeq p\,, \qquad N_{10} \simeq p^2 \qquad \text{and} \qquad N_3 \simeq p^2 \tag{4.15}$$

thus rescaled with the parameter $p \equiv P_{11\to 6}$ which, at $T \simeq T_c$, is proportional to $q^{-1/2}$:

$$p \equiv P_{11\to 6} \simeq q^{-1/2} \qquad \text{for} \qquad T \sim T_c\,. \tag{4.16}$$

In the large q limit, we will then use it as the small parameter in our expansion, that we will develop up to second order in powers of p.

Concretely, our aim now is to construct a master equation for the probabilities N_{11}, N_6, N_{10}, ..., and then find the stationary solution that determines the proportions of the vertices of each kind in the metastable states.

In order to do so, we first picture what kind of structures, *i.e.*, configurations of spins of the same color (spin value) in a background of "sand" (*i.e.* spins in the (11) state) have a probability to exist which is proportional to p^2 or greater. It turns out that spins in the states (6), (3) and (10), the only relevant ones in the large N limit according to the discussion in the previous Subsection, can only be found in the following structures

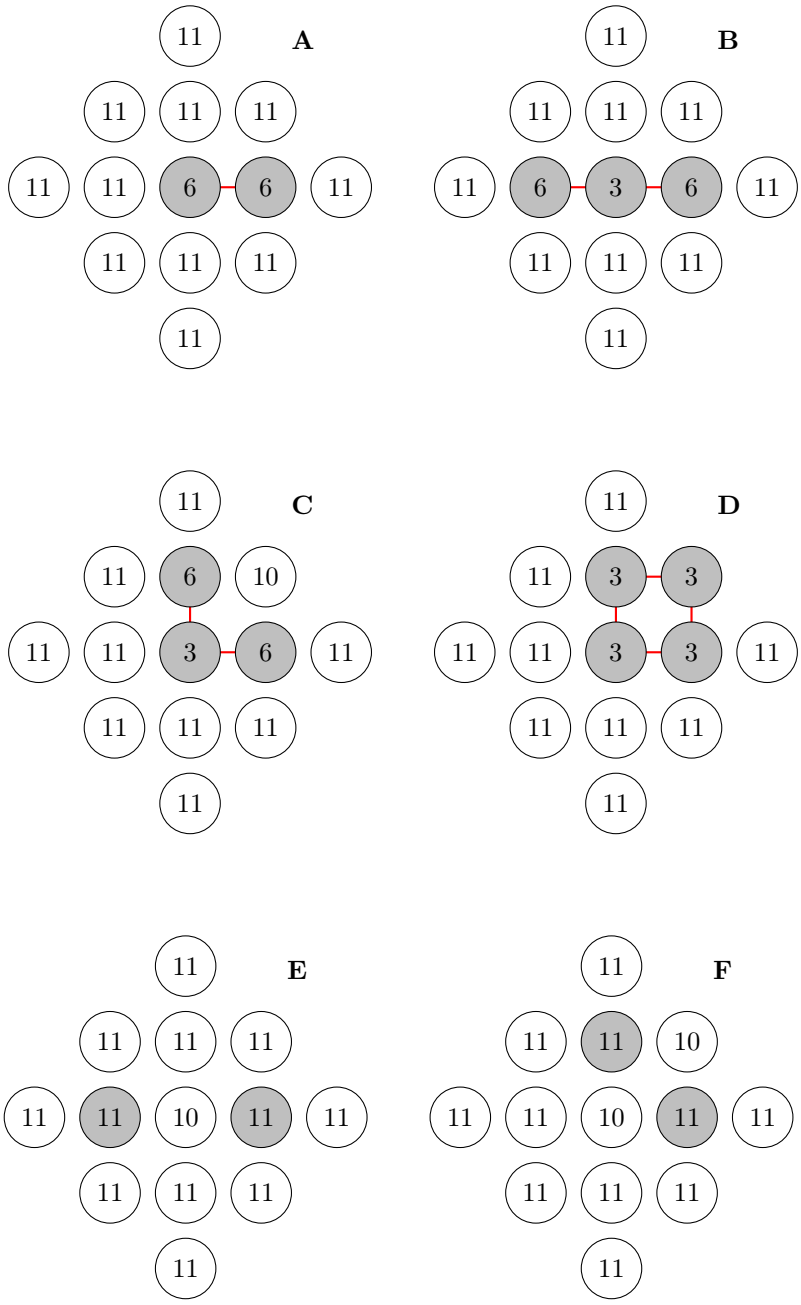

where the gray sites in a given diagram possess the same color, while the white sites have a different color with respect to the gray ones and also with respect to the nearest and next-to-nearest other white ones. The numbers indicate the kind of vertex, following the notation used in the previous Subsections. The red segments, which highlight the satisfied bonds, are useful to keep track of the energy contribution of the structures. It is possible to check that all the other possible structures are of order p^3 or higher and we will not take them into account.

Now, we identify the evolution that these structures can make in a single time step. As an example consider structure **B**. The following move

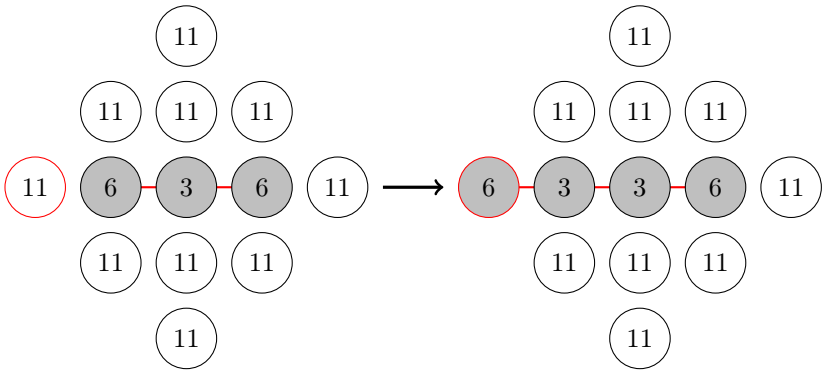

consists of a spin in state (11) turning into a state (6) and thus forming the structure on the right. The probability of this move is negligible because the probability to pick a (11) which is around the structure on the left (which contains (3)) is proportional to p^2 and the probability now for it to become a (6) is proportional to p. The result is therefore proportional to p^3 and hence negligible at the order we are keeping. This kind of analysis can be performed for all the cases and thus prove that the structures labeled **A** to **F** are at most of order p^2 and every other is negligible.

The next step is to list all the possible moves that are relevant for the second order of our expansion and understand what are the consequences of each of these moves. This will allow us to write down all the terms of the master equations for the probabilities N_{11}, N_6, N_3 and N_{10}. In practice we find that for (3) and (10) we need an equation for each of the configurations in which these states can be found so we define the following quantities

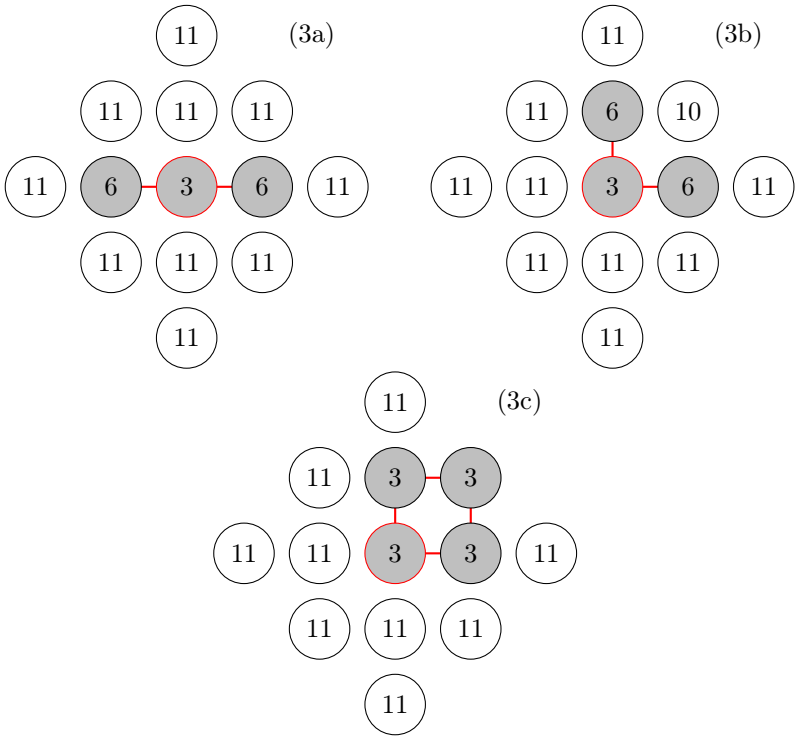

and

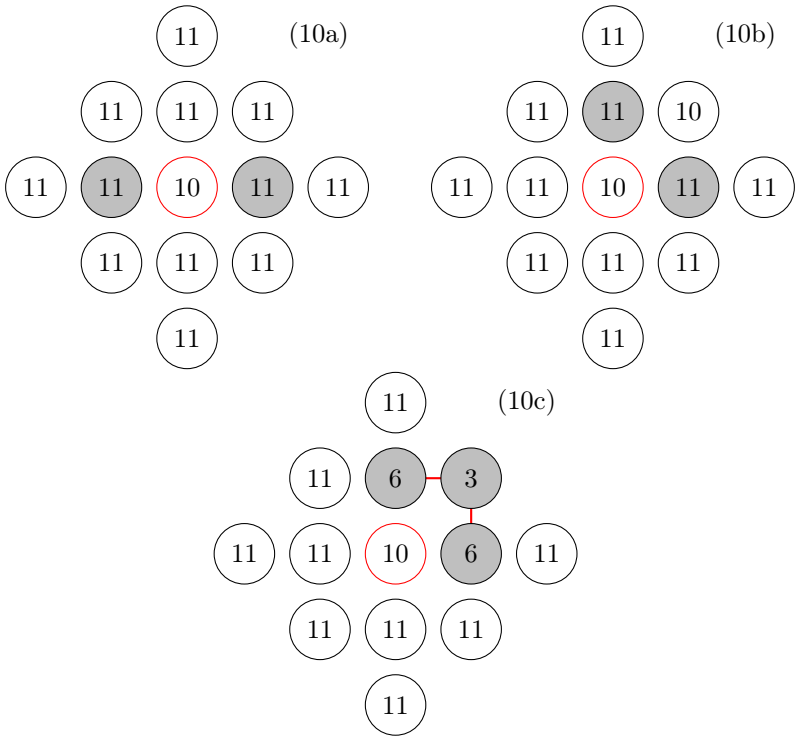

We can now express the probabilities for all the structures introduced above in terms of the probabilities of the various states

$$\begin{aligned} P(\mathbf{A}) &= (N_6 - 2N_{3a} - 2N_{3b})/2 \ , \\ P(\mathbf{B}) &= N_{3a} \ , \\ P(\mathbf{C}) &= N_{3b} = N_{10c} \ , \\ P(\mathbf{D}) &= N_{3c}/4 \ , \\ P(\mathbf{E}) &= N_{10a} \ , \\ P(\mathbf{F}) &= N_{10b}/2 \ , \end{aligned} \tag{4.17}$$

where the first one comes from the fact that for every two (6) which are not in the structure **B** or **C** (which contain two (6) each) we count a structure **A**. The derivation of $P(\mathbf{B}), \ldots, P(\mathbf{F})$ is straightforward. These expressions turn out to be useful to write down the probabilities of the moves, as we explain below.

Let us start with all the moves that a site which is in (11) can make. Pick a site in (11) which is not a neighbor of any structure and turn it into a (6). The probability for this move is

$$P_{11\to 6} = p, \tag{4.18}$$

where we mean the extended, temperature and q dependent, form as in Eq. 4.10, times the probability of picking such a (11) state. The latter equals $N_{11} - 3N_6$ because there are 3 sites in state N_{11} surrounding every (6) in structure **A**, and we are neglecting the other terms of $P(\mathbf{A})$ and the other structures because they will lead to contributions of higher orders. In this move we lose 2 (11) states and we gain 2 (6) states. In the following sketch we represent the move, we give its

probability P and we indicate below the sketch the loss and gain of vertices induced by the move.

$$P = p(N_{11} - 3N_6)$$

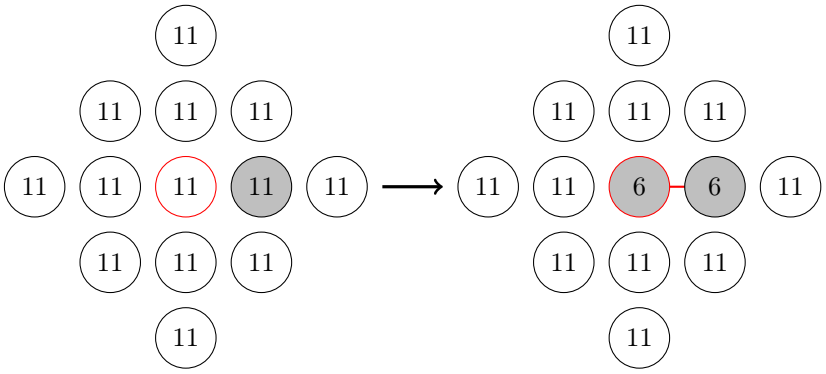

$$-2N_{11}, +2N_6$$

In a similar way, the probability of all the other 15 possible moves (to order p^2) are computed in Appendix B.

Collecting all the contributions for each of the probabilities N_a we can now build the master equations governing their evolution in this approximation

$$\dot{N}_{11} = -N_{11}\frac{12}{4e^\beta + q - 4} - 2N_{11}p + 2N_6 - \frac{7}{4}N_6 p - 2N_{3a} + 2N_{10b} + 2N_{10a} \quad (4.19)$$

$$+ 2[(N_{3b} + N_{3a})P_{3\to 10} - (N_{10b} + N_{10a})P_{10\to 3}] \quad (4.20)$$

$$\dot{N}_6 = 2N_{11}p - 2N_6 + \frac{1}{2}N_6 p + 4(N_{3a} + N_{3b}) + 2(N_{3c}P_{3\to 10} - N_{10c}P_{10\to 3}) \quad (4.21)$$

$$- 2[(N_{3b} + N_{3a})P_{3\to 10} - (N_{10b} + N_{10a})P_{10\to 3}] \quad (4.22)$$

$$\dot{N}_{3a} = \frac{1}{4}N_6 p - 2N_{3a} - (N_{3a}P_{3\to 10} - N_{10a}P_{10\to 3}) \quad (4.23)$$

$$\dot{N}_{3b} = \frac{1}{2}N_6 p - 2N_{3b} - (N_{3b}P_{3\to 10} - N_{10b}P_{10\to 3}) + (N_{3c}P_{3\to 10} - N_{10c}P_{10\to 3}) \quad (4.24)$$

$$\dot{N}_{3c} = -4(N_{3c}P_{3\to 10} - N_{10c}P_{10\to 3}) \quad (4.25)$$

$$\dot{N}_{10a} = N_{11}\frac{4}{4e^\beta + q - 4} - 2N_{10a} + (N_{3a}P_{3\to 10} - N_{10a}P_{10\to 3}) \quad (4.26)$$

$$\dot{N}_{10b} = N_{11}\frac{8}{4e^\beta + q - 4} - 2N_{10b} + 2(N_{3b}P_{3\to 10} - N_{10b}P_{10\to 3}) \quad (4.27)$$

$$\dot{N}_{10c} = \dot{N}_{3b} = \frac{1}{2}N_6 p - 2N_{3b} - (N_{3b}P_{3\to 10} - N_{10b}P_{10\to 3}) + (N_{3c}P_{3\to 10} - N_{10c}P_{10\to 3}). \quad (4.28)$$

We want to solve the equations at stationarity, to do so we write down the proba-

bilities in powers of p

$$\begin{aligned} N_{11} &= \alpha_0 + \alpha_1 p + \alpha_2 p^2 \\ N_6 &= \beta_1 p + \beta_2 p^2 \\ N_{3a} &= \gamma_{2a} p^2 \\ N_{3b} &= \gamma_{2b} p^2 \\ N_{3c} &= \gamma_{2c} p^2 \\ N_{10a} &= \delta_{2a} p^2 \\ N_{10b} &= \delta_{2b} p^2 \\ N_{10c} &= \delta_{2c} p^2. \end{aligned} \tag{4.29}$$

The normalization condition $N_{11} + N_6 + N_{3a} + N_{3b} + N_{3c} + N_{10a} + N_{10c} + N_{10b} = 1$ implies $\alpha_0 = 1$, $\beta_1 = -\alpha_1$, $\alpha_2 = -(\beta_2 + \gamma_{2a} + \gamma_{2b} + \gamma_{2c} + \delta_{2a} + \delta_{2b} + \delta_{2c})$. Plugging the expressions in (4.29) in the master equation we find from $\dot{N}_{3c} = 0$ that $\gamma_{2c} = \delta_{2c} P_{10\to 3}/P_{3\to 10}$, the first two equations contain first power terms of the form $2\alpha_1 p + 2p$, thus $\alpha_1 = -1$ and by construction $\delta_{2c} = \gamma_{2b}$. We are left with

$$\begin{aligned} \dot{N}_{11} &= -12xp^2 + 2p^2 + 2\beta_2 p^2 - \frac{7}{4}p^2 - 2\gamma_{2a}p^2 + 2\delta_{2b}p^2 + \delta_{2a}p^2 + \\ &\quad + 2p^2[(\gamma_{2b} + \gamma_{2a})P_{3\to 10} - (\delta_{2b} + \delta_{2a})P_{10\to 3}] \\ \dot{N}_6 &= -2p^2 - 2\beta_2 p^2 + \frac{1}{2}p^2 + 4p^2(\gamma_{2a} + \gamma_{2b}) \\ &\quad - 2p^2[(\gamma_{2b} + \gamma_{2a})P_{3\to 10} - (\delta_{2b} + \delta_{2a})P_{10\to 3}] \\ \dot{N}_{3a} &= \frac{1}{4}p^2 - 2\gamma_{2a}p^2 - p^2(\gamma_{2a}P_{3\to 10} - \delta_{2a}P_{10\to 3}) \\ \dot{N}_{3b} &= \frac{1}{2}p^2 - 2\gamma_{2b}p^2 - p^2(\gamma_{2b}P_{3\to 10} - \delta_{2b}P_{10\to 3}) \\ \dot{N}_{10a} &= 4xp^2 - 2\delta_{2a}p^2 + p^2(\gamma_{2a}P_{3\to 10} - \delta_{2a}P_{10\to 3}) \\ \dot{N}_{10b} &= 8xp^2 - 2\delta_{2b}p^2 + 2p^2(\gamma_{2a}P_{3\to 10} - \delta_{2a}P_{10\to 3}), \end{aligned} \tag{4.30}$$

where $x \equiv p^{-2}/(4e^{\beta} + q - 4)$.
From $\dot{N}_{10a} = 0$ we get

$$\delta_{2a} = \frac{4x + \gamma_{2a}P_{3\to 10}}{2 + P_{10\to 3}}, \tag{4.31}$$

from $\dot{N}_{3a} = 0$

$$\gamma_{2a} = \frac{1/2 + P_{10\to 3}/4 + 4xP_{10\to 3}}{4 + 2P_{10\to 3} + 2P_{3\to 10}}, \tag{4.32}$$

$\dot{N}_{10b} = 0$ gives

$$\delta_{2b} = \frac{4x + \gamma_{2b}P_{3\to 10}}{1 + P_{10\to 3}}, \tag{4.33}$$

$\dot{N}_{10b} = 0$

$$\gamma_{2b} = \frac{1/2 + P_{10\to 3}/2 + 4xP_{10\to 3}}{2 + 2P_{10\to 3} + P_{3\to 10}}, \tag{4.34}$$

and finally from $\dot{N}_6 = 0$

$$\beta_2 = -3/4 + 2(\gamma 21 + \gamma 22) - [(\gamma_{2a} + \gamma_{2b})P_{3\to 10} - (\delta_{2b} + \delta_{2a})P_{10\to 3}]. \tag{4.35}$$

Thus summarizing

$$
\begin{aligned}
\alpha_0 &= 1 \\
\alpha_1 &= -1 \\
\alpha_2 &= -(\beta_2 + \gamma_{2a} + \gamma_{2b} + \gamma_{2c} + \delta_{2a} + \delta_{2b} + \delta_{2c}) \\
\beta_1 &= -\alpha_1 \\
\beta_2 &= -3/4 + 2(\gamma 21 + \gamma 22) - [(\gamma_{2a} + \gamma_{2b})P_{3\to 10} - (\delta_{2b} + \delta_{2a})P_{10\to 3}] \\
\gamma_{2a} &= \frac{1/2 + P_{10\to 3}/4 + 4xP_{10\to 3}}{4 + 2P_{10\to 3} + 2P_{3\to 10}} \\
\gamma_{2b} &= \frac{1/2 + P_{10\to 3}/2 + 4xP_{10\to 3}}{2 + 2P_{10\to 3} + P_{3\to 10}} \\
\gamma_{2c} &= \delta_{2c}P_{10\to 3}/P_{3\to 10} \\
\delta_{2a} &= \frac{4x + \gamma_{2a}P_{3\to 10}}{2 + P_{10\to 3}} \\
\delta_{2b} &= \frac{4x + \gamma_{2b}P_{3\to 10}}{1 + P_{10\to 3}} \\
\delta_{2c} &= \gamma_{2b}.
\end{aligned}
\tag{4.36}
$$

In order to put the approach above to the numerical test, we collected the proportions N_a measured with the heat bath Monte Carlo simulations and we compared them to the values computed with the master equation analysis. Concretely, we used systems with $L = 10^3$, and $q = 10^4,\ 10^5$ and 10^6, at $T/T_c = 0.99$. The numerical and analytic data are displayed in Tab. 4.1. The number of digits shown correspond to results up to order p^2. The agreement between the values found with the two approaches is excellent.

q	10 000		100 000		1 000 000	
	numerical	analytic	numerical	analytic	numerical	analytic
N_{11}	0.95731	0.95729	0.986509	0.986509	0.9957020	0.9957023
N_6	0.04054	0.04064	0.013269	0.013272	0.0042752	0.0042751
N_{3a}	0.00021	0.00021	0.000022	0.000022	0.0000023	0.0000023
N_{3b}	0.00042	0.00041	0.000044	0.000044	0.0000046	0.0000046
N_{3c}	0.00048	0.00046	0.000050	0.000050	0.0000053	0.0000053
N_{10a}	0.00019	0.00019	0.000020	0.000020	0.0000020	0.0000020
N_{10b}	0.00044	0.00041	0.000045	0.000044	0.0000046	0.0000046
N_{10c}	0.00037	0.00038	0.000039	0.000039	0.0000040	0.0000040

Table 4.1: N_a for systems with $L = 10^3$ and $q = 10^4,\ 10^5,\ 10^6$ evolving at temperatures $T/T_c = 0.99$ after an instantaneous quench from infinite temperature. The first column show the numerical values at MC times such that the system is stationary in the metastable state, while the second ones give the asymptotic values calculated with the master equations approach. Only the relevant values (up to order p^2) are shown. The error bars on the numerical values are always smaller than one on the last shown digits.

In Tab. 4.2 we show data for a system with linear size $L = 10^3$ and $q = 10^6$, and we vary the temperature, moving progressively towards criticality at T_c. As explained below, for this value of q, we observe a divergence of the time required to reach a ferromagnetic state at $T/T_c \simeq 0.9$. The data in Tab. 4.2 show that the analytic approximation is very good (in the metastable state) even moderately away from T_c. However, the numerical measurements at $T/T_c = 0.88$ have been done at time $t = 10^3$, and at this time the agreement between numerical and analytical data is still good but not as good as for the higher temperatures. In particular, one

can notice a relatively important difference in N_{11} and N_{3c}. For longer measuring times, one would see this difference increase, showing that the system leaves the metastable state at $T/T_c = 0.88$. For the higher temperatures, there are no time-dependencies in the numerical results and for all purposes the metastable states remain for ever.

T/T_c	p		N_{11}	N_6	$10^3 N_{3a}$	$10^3 N_{3b}$	$10^3 N_{3c}$	$10^3 N_{10a}$	$10^3 N_{10c}$
0.88	0.01017	numeric	0.9895816	0.0101646	0.0130	0.0260	0.1772	0.0020	0.0039
		analytic	0.9895916	0.0101674	0.0129	0.0259	0.1705	0.0020	0.0039
0.92	0.00725	numeric	0.9926679	0.0072481	0.0066	0.0132	0.0444	0.0020	0.0039
		analytic	0.9926690	0.0072485	0.0066	0.0131	0.0438	0.0020	0.0040
0.98	0.00459	numeric	0.9953845	0.0045892	0.0026	0.0053	0.0070	0.0020	0.0040
		analytic	0.9953847	0.0045892	0.0026	0.0053	0.0070	0.0020	0.0040
0.99	0.00428	numeric	0.9957020	0.0042752	0.0023	0.0046	0.0053	0.0020	0.0040
		analytic	0.9957023	0.0042751	0.0023	0.0046	0.0053	0.0020	0.0040

Table 4.2: N_a for systems with linear size $L = 10^3$, $q = 10^6$ and various values of T/T_c (corresponding to different values of p ((second row)). For each temperature, the first line shows the numerical values at MC times such that the system is stationary in the metastable state, while the second ones give the asymptotic values calculated with the master equations approach. The error bars for the numerical values are of the order the last digit or smaller and they are not shown. We also have MC data for N_1, $10^3 N_1 = 0.0044$ at $T/T_c = 0.88$, $10^3 N_1 = 0.0005$ at $T/T_c = 0.92$, $10^3 N_1 = 0.0000$ at $T/T_c = 0.98$ and $T/T_c = 0.99$.

Once the proportions N_a are known it is possible to thermodynamically characterize the metastable states. For instance, we can evaluate the energy per spin of the disordered metastable state extended below the critical temperature, exploiting the stationary solutions obtained above. The only configurations that contribute to the energy are the (6) ones with one bond and the (3) ones with two bonds. Thus we have

$$e^{(d)}(\beta, q) = -\frac{1}{2}(N_6(\beta, q) + 2N_3(\beta, q)) \,, \tag{4.37}$$

where the 1/2 factor avoids double counting of the bonds on the lattice. Note that for quench inverse temperature $\beta < \beta_c$ the expression in Eq. (4.37) should provide the equilibrium value of the energy at β. In Fig. 4.6 we plot the energy density of the disordered state as predicted by Eq. (4.37) as a function of q at different ratios between the quench temperature and the critical one. The values of the energy density obtained with Monte Carlo simulations are also reported in the figure. The latter are time averages over single runs computed as long as the system stays in the metastable state (the error bars represent one standard deviation). A comparison with the exact mean field result for the energy at criticality [25] is reported. It is possible to appreciate that, for all temperatures, the energy decreases (in absolute value) approximately as $q^{-1/2}$, this is expected because the major contribution to Eq. (4.37) is given by the (6) term which scales indeed as $q^{-1/2}$ (see section above). Figure 4.7 shows instead the behavior of the energy density of the disordered state as a function of the final quench temperature. The results of the expansion are again tested against Monte Carlo numerical simulations showing really good agreement.

4.3.3 Ordered metastable phase

As we anticipated above, the upper-critical protocol, which deals with the persistence of the ordered phase after a quench to a temperature $T > T_c$ starting from a fully ordered configuration, is less interesting from a technical point of view. We

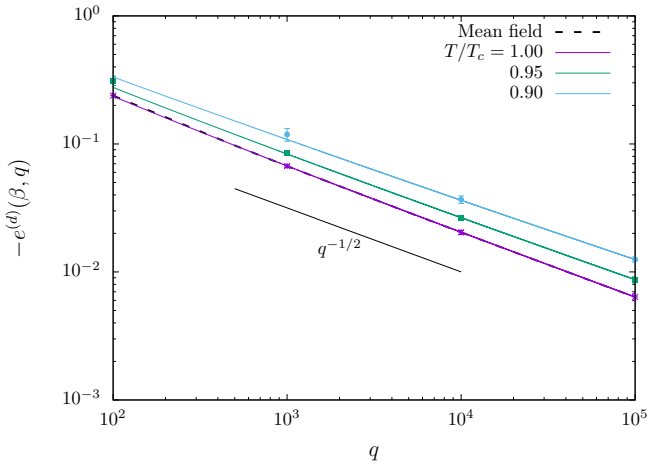

Figure 4.6: Theoretical predictions in Eq. (4.37) and simulations results for the energy density of a system with $L = 200$ when it is stuck in a paramagnetic metastable configuration, as a function of the number of states q, for several ratios of the quench temperature over the critical one. The numerical values are time averages over a single run. The error bars equal a standard deviation. The dashed tilted line correspond to the mean field exact result [25] at criticality. [3]

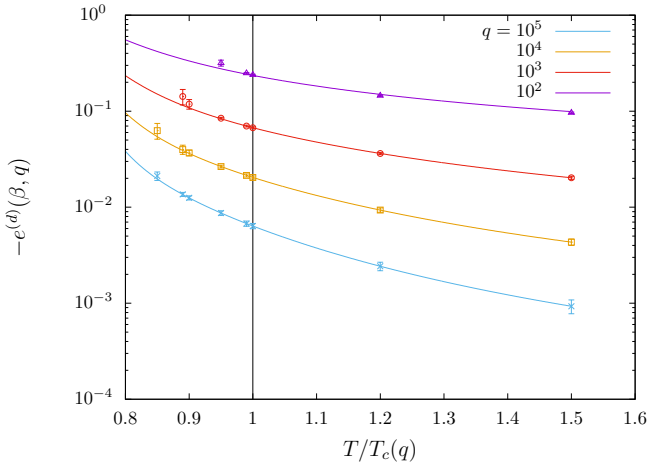

Figure 4.7: Energy density of the disordered metastable state *vs* T/T_c for several values of q (increasing from bottom to top), evaluated from Eq. (4.37) (colored solid lines). Values from simulations are also presented with data points. They are time averages of the energy density. The error bars correspond to a standard deviation. The critical temperature is indicated with a vertical black line. [3]

nonetheless perform a similar analysis (though less rich in terms of numerical evaluations) as for the disordered phase in order to complete the picture of metastability.

Let us take the initial configuration to be at zero temperature, that is to say, a completely ordered state. Thus, the system is in one of the q possible ground states and, consequently, all the N sites are in state (0).

Recalling that (see Eq. (4.9)) for large q we have $e^{\beta} \simeq q^{T_c/2T}$, during a lattice

update, the probability for a state (0) to turn into a state (7) can be written as

$$P_{0\to 7} = \frac{q-1}{q+e^{4\beta}-1} \simeq \frac{q}{q+q^{2T_c/T}} = \frac{1}{1+q^{2T_c/T-1}} \ . \tag{4.38}$$

Thus, in the upper critical regime, the crossover temperature that separates two very different behaviors in the $q \to \infty$ limit is $T = 2T_c$:

$$P_{0\to 7} \to 1 \qquad \text{at} \qquad T > 2T_c \ , \tag{4.39}$$

the (0) states turn into (7) states, and the system disorders really fast. At the crossover temperature

$$P_{0\to 7} \to 1/2 \qquad \text{at} \qquad T = 2T_c \ , \tag{4.40}$$

implying that states (7) can appear. Every (7) states will have as neighbors (1) states which (always in the limit $q \to \infty$) will become states (8) with probability $P_{1\to 8} \to 1$, and bring the system to a disordered configuration. Finally,

$$P_{0\to 7} \to 0 \qquad \text{at} \qquad T < 2T_c \ , \tag{4.41}$$

and the state (0) is completely stable in this temperature window close to T_c.

Going back to large but finite q, in Fig. 4.8, we show the evolution of N_a as a function of time for $a = 0, 1$ and 7, we only show the states which contribute the most.

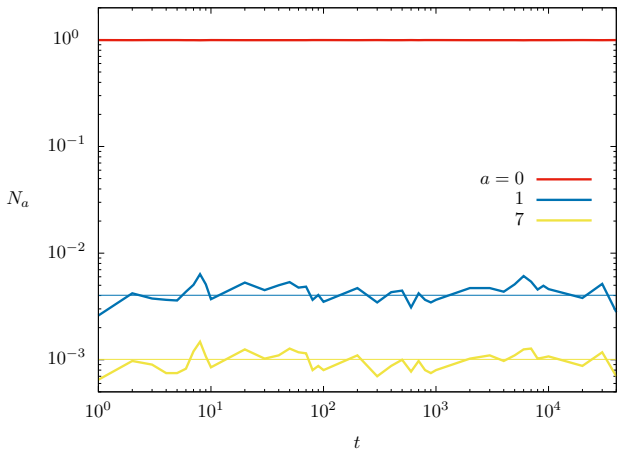

Figure 4.8: $N_a(t)$ for $a = 0, 1, 7$ evolving in time at $T = 1.01\,T_c$ in a square lattice system with linear size $L = 10^3$ and $q = 10^3$. In thin lines are reported the analytical predictions obtained from the master equations below, in thick lines data from a numerical simulation. Note that the (1) and (7) abundances are one the vertical translation of the other. This is due to the fact that, by construction, there are four (1) states for every (7) one (see below). [3]

Therefore, at upper critical temperatures, the following hierarchy holds

$$N_1 \simeq N_7 \ll N_0 \simeq 1 \ , \tag{4.42}$$

where the N_a are normalized by the number of spins in the sample, and all other states are negligible.

Using again the expansion parameter p with,

$$p^2 \simeq q^{-1} \simeq P_{0\to 7} \qquad \text{at} \qquad T \sim T_c \ , \tag{4.43}$$

we consider the evolution of $N_0 \simeq 1, N_7 \simeq p^2$ and $N_1 \simeq p^2$. Again we stop at second order in p.

It is straightforward to verify that the only structure that can appear in the sea of aligned spins (*i.e.*, in the (0) state), with a probability proportional to p^2 or greater, is a (7) state surrounded by (1) states

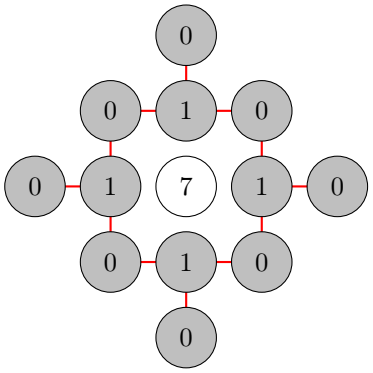

Indeed there are only two ways to build different structures from the one above. The first one is that a (1), which has a probability proportional to p^2 to be picked, turns into a (4) or into an (8), respectively with probabilities $P_{1\to4} \sim p^2$ and $P_{1\to4} \sim p$. The other possibility is that a (0) close to a 1, which again has probability proportional to p^2 to be picked, turns into a (7), with probability $P_{0\to7} \sim p^2$. The overall probabilities therefore are such that both scenarios are negligible in our approximation.

The only moves that should be taken into account to build a master equation for the ordered case are the switching of a (0) (surrounded by other (0) states) into a (7) and *vice versa*. In particular, we have that the probability of picking such a (0) is $N_0 - 8N_7$, because there are 8 (0) states next to a (1) surrounding each (7), but to the second order in p we only retain N_0, and the probability for it to turn into a (7) creating in doing so also 4 (1) states is $P_{0\to7}$

$$P = N_0 P_{0\to7}$$

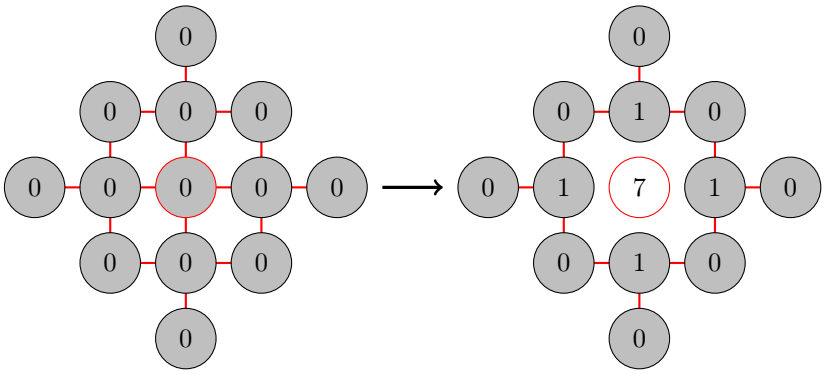

$$-5N_0, +N_7, +4N_1$$

The inverse move, consistently, with probability $N_7 P_{7\to0}$ causes the destruction of 4 (1) states and of 1 (7) state creating 5 (0) states

$$P = N_7 P_{7\to0}$$

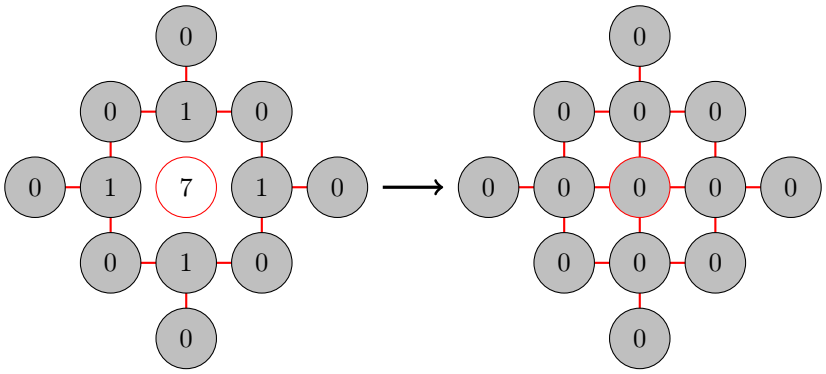

$$-N_7, -4N_1, +5N_0,$$

The master equations are therefore

$$\begin{aligned} \dot{N}_0 &= -5N_0P_{0\to 7} + 5N_7P_{7\to 0} \\ \dot{N}_7 &= -N_7P_{7\to 0} + N_0P_{0\to 7} \\ \dot{N}_1 &= -4N_7P_{7\to 0} + 4N_0P_{0\to 7} \quad . \end{aligned} \tag{4.44}$$

To solve them we write down the probabilities in powers of p

$$\begin{aligned} N_0 &= \alpha_0 + \alpha_1 p + \alpha_2 p^2 \\ N_7 &= \beta_2 p^2 \\ N_1 &= \gamma_2 p^2. \end{aligned} \tag{4.45}$$

By construction we have $N_1 = 4N_7$ and so $\gamma_2 = 4\beta_2$, moreover the normalization condition $N_0 + N_7 + N_4 = 1$ impose $\alpha_0 = 1$, $\alpha_1 = 0$ and $\alpha_2 = -5\beta_2$. Finally, looking for the stationary solution of either one of the three differential equations above, we find $\beta_2 = 1/P_{7\to 0}$. Summarizing

$$\begin{aligned} \alpha_0 &= 1 \\ \alpha_1 &= 0 \\ \alpha_2 &= -5/P_{7\to 0} \\ \beta_2 &= 1/P_{7\to 0} \\ \gamma_2 &= 4/P_{7\to 0} \ . \end{aligned} \tag{4.46}$$

We can put the results from the previous section to the numerical test analyzing, as for the disordered case, an interesting observable: the energy density of the metastable state. In this case the spin which falls in the (0) configuration contributes with four bonds, while the ones in (4) with three bonds. The ordered energy density thus reads

$$e^{(o)}(\beta, q) = -\frac{1}{2}(4N_0(\beta, q) + 3N_4(\beta, q)) \ . \tag{4.47}$$

This energy scales as q^{-1} at fixed temperature, consistently with the fact that the major contribution comes from (0). The agreement with the mean field results [25] and the outcome of the simulations analyses as in the disordered case is really good as can be checked by inspecting Fig. 4.9. The dependence of the energy density of the ordered state, as evaluated from Eq. (4.47), on temperature is portrayed in Fig. 4.10, where the comparison to the results of numerical evaluations shows again a perfect agreement.

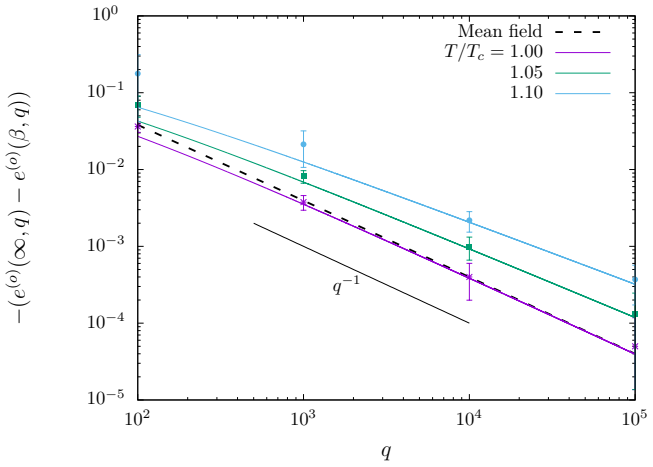

Figure 4.9: Energy density of the ordered state as predicted by Eq. (4.47) and simulation data, for $L = 200$, as a function of the number of states q, for several ratios of the quench temperature. The numerical values are averages in time of the energy for a single realization, the error bars correspond to a standard deviation. Exact mean field predictions at criticality [25] are reported as well (black dashed line). [3]

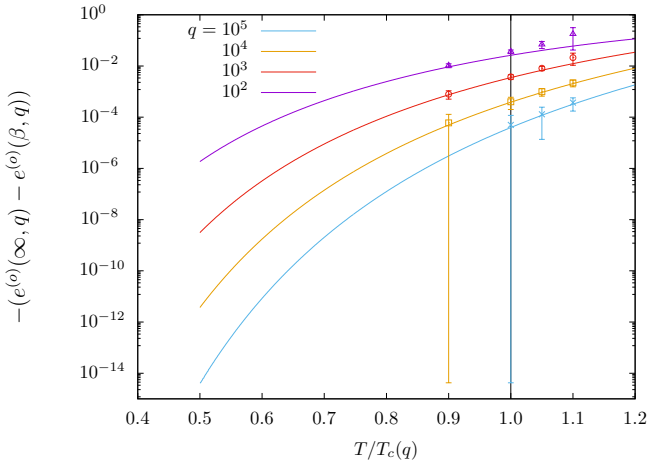

Figure 4.10: Ordered energy *vs* T/T_c for several values of q, evaluated from Eq. (4.37). Values from simulations for $L = 200$ are also present and are time averages for a single realization of the energy of the system as long as it stays in the metastable state, the error bars correspond to a standard deviation. [3]

4.4 Comments

The problem of metastability in the Potts model still poses unsolved questions. In this chapter we discussed a large q expansion of the heat bath microscopic dynamics, developed in Ref. [3], that allowed us to deduce, analytically, the metastability properties of the finite but large size model, in a rather wide range of temperatures around criticality (namely, from $T_c/2$ to $2T_c$). Although in the strictly infinite size limit the spinodals are expected to approach the critical point [136], we observe that the lifetime of the metastable state goes beyond reasonable times for relatively small

system sizes. Our expansion allows us to capture the properties of these metastable states with amazing numerical accuracy.

Chapter 5

Multinucletion and coarsening dynamics

This chapter, based on the work in Ref. [5], is organized as follows. In the first section we introduce the general problem of the escape from metastable states through nucleation, specializing in the particular case of the Potts model. Below we provide a general description of the whole dynamical process, from the instant of the quench, to the escape from metastability and further on with particular emphasis on the multinucleation process.

5.1 Introduction: Escape from metastable states

We address here some issues related to the phenomenology of the escape, and consequent relaxation dynamics, from a metastable state of the Potts model in the same scenario of the chapter above. Exploiting again the pictorial representation used to describe metastability, the problem at hand can be stated as follows: how the system escape State A (see Fig. 5.1) and relaxes towards equilibrium?

The simplest example of metastability and escape from it is perhaps a uniaxial ferromagnet in an external field, whose paradigmatic modelization is the Ising model. If the field is reversed, provided it is sufficiently small, if the temperature is subcritical the magnetization remains at the pre-reversal value for a certain time, the lifetime of the metastable state, before flipping to the new equilibrium value. The phenomenon can be ascribed to the competition between surface tension and bulk energy and is accounted for, at least at a simple semi-quantitative level, by classical nucleation theory [124, 139, 140]: a *nucleus* of the equilibrium phase in a metastable see is unstable unless its size exceeds a critical value. If it is not the case it disappears. Then, in this picture, the lifetime of the metastable state is the time needed to nucleate, by thermal fluctuations, critical nuclei. Elaborating on such ideas, more refined theories of nucleation [141–151] have been developed which are able to describe the phenomenon with good accuracy.

In the previous example, the metastable state and the equilibrium one are associated to the two ergodic components which characterize the system at low temperatures. However, the situation is much less understood in systems where there are more ergodic components, State B and State C in our simplified scheme. More precisely upon quenching from $T > T_c$ to $T \lesssim T_c$ a finite-size systems remains for some time in the disordered state before starting the evolution towards the final equilibrium state. In this case the metastable state is the (single) ergodic component at $T > T_c$ while the target equilibrium state is one of the q symmetry-related ergodic components at $T < T_c$. Hence, at variance with the above discussed case

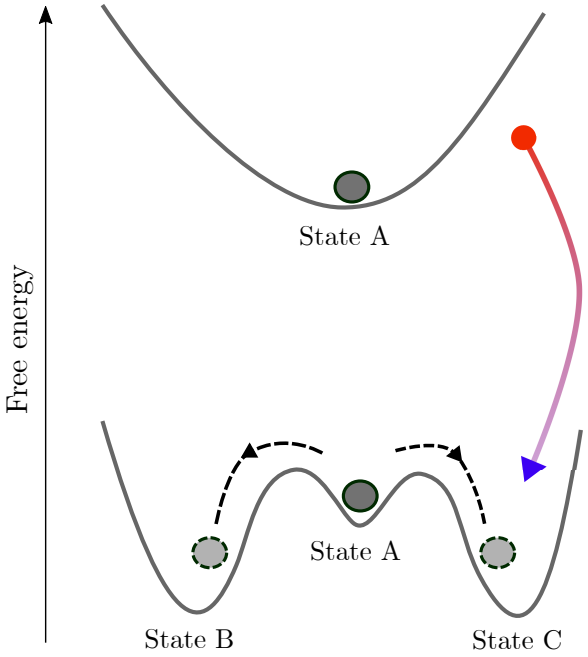

Figure 5.1: Pictorial representation of the first order transition of the two dimensional Potts model with $q > 4$. See chapter 4 (Fig. 4.1) and main text for details.

of the field-driven transition in the Ising model, here nucleation occurs towards a q-degenerate final state, and one speaks of multinucleation. Another important difference is that the transition is temperature driven.

To determine the lifetime of the metastable state, its dependence on the system size, the dynamic escape from it, and the nature of the nucleation process is a difficult and much debated issue [61–63,137,152]. In particular, as we already mentioned in the above chapter, it was argued [137] that both the lifetime of the metastable state and temperature range below T_c where it is observed shrink when the system size increases. This intriguing feature has no analog in the discontinuous transition of the Ising model. In [3] a rather precise description of the metastable state was given, both from the microscopic and thermodynamic point of view. However, a similar characterization of the escape kinetics is still missing for finite q. Specifically, while the nature of the metastable state can be well described in such analytical framework, its lifetime (for finite q) couldn't yet be determined and its very existence in the thermodynamic limit cannot be proved. Related to that, the issue of the order in which the two limits of large q and large system size remains to be clarified.

In this chapter, based on Ref. [5], we study the process whereby the metastable state is run away and how the target equilibrium state is approached in the Potts model with $q \geq 4$. We do this by numerical simulations for different values of q and of the system size L.

5.2 Summary of the results

The main result of this chapter is the characterization of the multinucleation process. We show that, for a given system size, the number k of phases that nucleate is a

logarithmically increasing function of L

$$k(q, T_f, L) = \left\{ \mathcal{P}(q) \ln \left[\frac{L}{A(q, T_f)} \right] \right\}_{\in [1,q]}, \tag{5.1}$$

where the notation $\{Z\}_{\in[1,q]} = \max\{1, \min\{q, Z\}\}$ accounts for the constraint $k \in [1, q]$, T_f is the temperature of the bath after the quench and $\mathcal{P}(q)$ and $A(q, T_f)$ are quantities discussed in the body of the chapter (See Eq. 5.16). We also find that k is a decreasing function of q (given some constraints), a fact which is consistent with the large-q results in [3]. Phases which do not nucleate disappear from the system immediately after the metastable state is escaped. Those which nucleate start competing, resulting in a coarsening process which leads, at some point, to the progressive elimination of the less represented colors until symmetry is definitively broken, one single color survives and equilibrium is attained.

5.3 Multinucleation in the Potts model

We consider a protocol in which the system, initially prepared in an infinite temperature equilibrium state, is suddenly quenched at time $t = 0$ to a low temperature $T_f < T_c$. As already mentioned the dynamical evolution has been studied in previous works [54, 59, 60, 112, 132, 153, 154] mainly focusing on the coarsening regime. Here we are more interested in metastability and nucleation, which are clearly observed when $T_f \lesssim T_c$. We use to simulate the dynamics in this case a Monte Carlo algorithm with Metropolis transition rates, defined in Eq. (1.10), associated with moves which changes a microstate φ_a to φ_b which differs only for the flip of one spin. For convenience we recall here the form of the rates

$$T_{a\to b} = \min\Big\{1, e^{-\beta_f(\mathcal{H}[\varphi^b]-\mathcal{H}[\varphi^a])}\Big\}, \tag{5.2}$$

along with the hamiltonian of the model

$$\mathcal{H}[\varphi] = -J \sum_{\langle i,j \rangle} \delta_{\varphi_i, \varphi_j}. \tag{5.3}$$

After the quench the system relaxes to a low energy state and the energy density $e(t) = \langle \mathcal{H}[\varphi](t) \rangle / L^2$ evolves towards the final equilibrium value $e(\infty)$. Here and in the following the non equilibrium average $\langle \dots \rangle$ is taken over thermal histories and initial conditions. In order to quantify the relaxation, therefore, we consider the energy density excess

$$\Delta e(t) = e(t) - e(\infty). \tag{5.4}$$

In a state with well formed domains, connected regions with the same spin state, the excess energy is stored on domain walls, hence $\Delta e(t)$ is proportional to the density of interfacial spins. Since for non fractal aggregates this quantity is, in turn, inversely proportional to the typical size of the domains, from $\Delta e(t)$ one can infer such characteristic length as

$$R^e(t) = \Delta e(t)^{-1}. \tag{5.5}$$

5.3.1 The correlation functions

A fundamental quantity, usually considered in coarsening processes, is the equal time spin-spin correlation function. Specifically, we define the quantity

$$C_{ij}(r,t) = \left. \frac{\sum_{p=1}^{q} [\langle \delta_{\varphi_i(t),p} \delta_{\varphi_j(t),p} \rangle - \langle \delta_{\varphi_i(t),p} \rangle \langle \delta_{\varphi_j(t),p} \rangle]}{\left(\sum_{p=1}^{q} [\langle \delta^2_{\varphi_i(t),p} \rangle - \langle \delta_{\varphi_i(t),p} \rangle^2] \right)^{1/2} \left(\sum_{p=1}^{q} [\langle \delta^2_{\varphi_j(t),p} \rangle - \langle \delta_{\varphi_j(t),p} \rangle^2] \right)^{1/2}} \right|_{|\vec{r}_i - \vec{r}_j| = r} . \tag{5.6}$$

Notice that, due to isotropy and homogeneity, $C_{ij}(r,t)$ only depends on the distance $r = |\vec{r}|$, where $\vec{r}$ is the vector joining i and j, and should be independent of i and j. Hence, below we just use $C(r,t)$ and, enforcing this symmetry, we rather compute the spatial average of the quantity in Eq. (5.6), namely $L^{-2} \sum_{ij} C_{ij}(r,t)$. In this way the statistic is improved. It is clear that on the one hand at $r = 0$, (namely $i = j$) it is $C(r = 0, t) = 1$; and on the other hand, at very large distance, $C(r \to \infty, t) = 0$ because of the expected factorization of the first term in the numerator. Defining

$$\sigma_p^2(t) = \langle \delta^2_{\varphi_i(t),p} \rangle - \langle \delta_{\varphi_i(t),p} \rangle^2, \tag{5.7}$$

Eq. (5.6) can be re-written as

$$C(r,t) = \frac{\sum_{p=1}^{q} \sigma_p^2(t) C_p(r,t)}{\sum_{p=1}^{q} \sigma_p^2(t)}, \tag{5.8}$$

where

$$C_p(r,t) = \frac{\langle \delta_{\varphi_i(t),p} \delta_{\varphi_j(t),p} \rangle - \langle \delta_{\varphi_i(t),p} \rangle \langle \delta_{\varphi_j(t),p} \rangle}{\sigma_p^2(t)} \tag{5.9}$$

is the correlation function restricted to the color p. Equation (5.8) transparently expresses the fact that the unrestricted correlation is the weighted average of the restricted ones, the weights being the variances of the Boolean variables associated to φ_i, see Eq. (5.7).

When dynamical scaling holds, $C(r,t)$ takes the following form

$$C(r,t) = g\left[\frac{r}{R(t)}\right], \tag{5.10}$$

where g is a scaling function and $R(t)$ a characteristic size with the meaning of typical domains' linear dimension. From the correlation function one can extract such a size in different ways. For instance, one can use the momenta as

$$R(t) = \left[\frac{\sum_r r^m C(r,t)}{\sum_r C(r,t)}\right]^{\frac{1}{m}}. \tag{5.11}$$

In case of dynamical scaling, determinations with different values of m provide proportional results (however large m values are numerically problematic since the noisy large-r tails of $C(r,t)$ are heavily weighted). Similarly, one can use the half-height width to define $R(t)$ as

$$C(R(t),t) = \frac{1}{2}. \tag{5.12}$$

In the following we will use this determination which is easier. Analogously, the typical size of domains of a specific color $R_p(t)$ can be defined replacing C with C_p in Eq. (5.12):

$$C_p(R_p(t),t) = \frac{1}{2}. \tag{5.13}$$

Let us mention that Eq. (5.13) cannot be used to determine R_p in two situations: i) The corresponding color is not present in the system. In this case $C_p \equiv 0$, Eq. (5.13) loses its meaning, and R_p could be taken to be identically zero. ii) The color has invaded the whole system. Also in this situation one has $C_p \equiv 0$, because of the subtraction term in Eq. (5.9). Clearly, in this case Eq. (5.13) cannot be used to determine the size of the domain of color p. Hence it must be kept in mind that finding a small value of R_p does not necessarily mean that the corresponding color is present only in small domains, but it could as well be that it has flooded the system. Which case applies must be ascertained differently, for instance, by visual inspection of the configurations. This is important in for discussion below. The labeling of the q possible values of the spins is implemented in the following in a dynamical way: at any time we order the color according to their abundances, from the most to the least represented, and label them with p increasing from 1 to q. This method is useful, particularly in the late stage of the dynamics where, as we show below, a clear hierarchy of abundances sets in.

5.3.2 The dynamical process

Here we discuss the results of the numerical simulations of the Potts model introduced above. We mainly consider the three values $q = 9$, 24, 100, as a paradigm of small, intermediate and large q behaviors. These systems are quenched to final temperatures close to the critical one, $T_c(q)$, in order to appreciate the metastable state and its lifetime. In most of our simulations we set $T_f = 0.9912 \cdot T_c$ for $q = 9$, $T_f = 0.98 \cdot T_c$ for $q = 24$, and $T_f = 0.95 \cdot T_c$ for $q = 100$. This choice is motivated by the requirement to have a comparable nucleation time $\tau(q, T_f)$ (see discussion below and Fig. 5.2) for the three reference values of q. Notice that fixing $\tau(q, T_f)$ does not correspond to fixing $(T_f - T_c)/T_c$.

A first qualitative description of the kinetic process after a quench can be done considering the behavior of $R^e(t)$, the typical length scale extracted from the analysis of the excess energy as in Eq. (5.5), which is shown in Fig. 5.2. With some quantitative differences, the same kind of pattern is observed for any value of q (see also [155] where this quantity for more q values was shown). After a short transient, one can clearly identify three extended regimes. The first is associated to R^e growing slowly or staying approximately constant, $R^e(t) \simeq R_m$. This plateau, which is flatter and longer as $T_f \to T_c$ at fixed q or as $q \to \infty$ at fixed $(T_f - T_c)/T_c$, is a clear manifestation of metastability. In this time lag the kinetics is useless because the system is confined in a local free energy minimum and the trapping barrier is not yet jumped over. In order to do that, critical nuclei, namely ordered domains of a sufficient large size, must develop. However this is an activated process which requires a certain time $\tau(q, T_f)$, the nucleation time. At times $t \ll \tau(q, T_f)$ the system is still in a rather disordered state, visually not too different from the initial one, as it can be seen from the snapshots taken at $t = 800$ shown in Fig. 5.3. Some small domains can be spotted but they are too small to start nucleation.

Actually, this metastable state is *similar* to the equilibrium state at T_c, in a sense we specify below. We illustrate this point by means of the correlation function defined in Eq. (5.6). In Fig. 5.4 this quantity is plotted against r during the evolution after a quench. Let us focus, to start with, on the left panel, where curves for a quench to $T_f = 0.99 \cdot T_c$ (continuous lines) are compared to those for a quench to $T_f = T_c$ (dashed ones). In the latter case one sees that, as time goes on, the correlation extends to larger values of r until, starting from $t_{eq}(T_c) \simeq 10^3$ the curves start to superimpose, signaling that equilibrium has been reached. At short times, a similar pattern is displayed by the curves of the subcritical quench (continuous ones) which stay close to the ones previously discussed. At longer times, for $t > t_{eq}(T_c)$, the correlations move to the right further than those of the quench to T_c

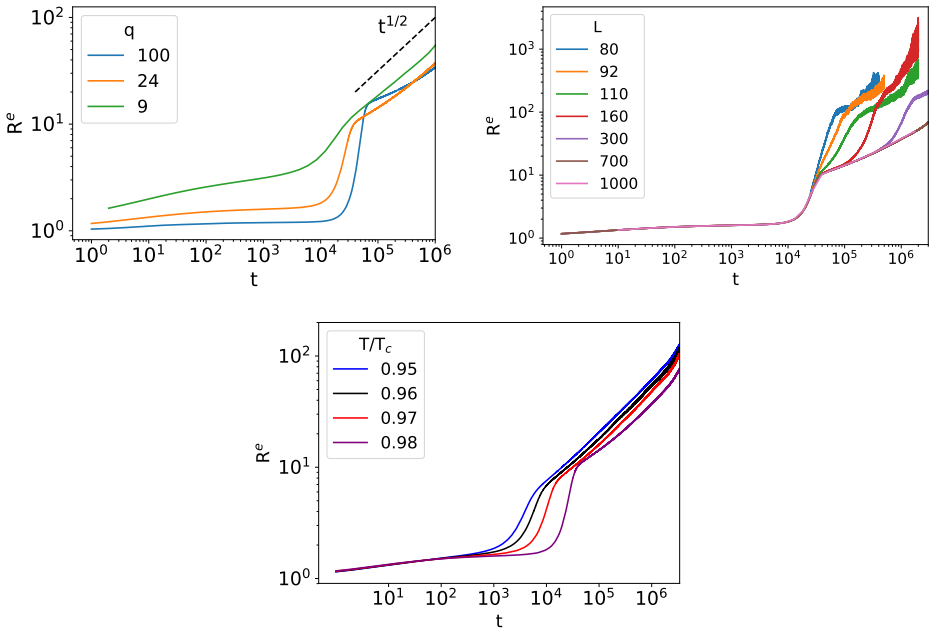

Figure 5.2: Upper-left panel: the time evolution of $R^e(t)$ for $q = 9, 24, 100$ (see the key). The system size is $L = 700$. The dashed segment shows the behavior $t^{1/2}$. Upper-right panel: as in the right panel for $q = 24$ and different system sizes $L = 80, 92, 110, 160, 300, 700, 1000$. Lower panel: the dependence on T of the case with $q = 24$ and $L = 700$ is shown. [5]

and tend to accumulate on a curve somewhat broader than the equilibration one at T_c. This occurs roughly in the range of times $t \in [10^3, 10^4]$ which corresponds to the lifetime of the metastable state. In this time range the correlation is almost time-independent at short r, whereas some evolution can be spotted at large r. This signals that the metastable state is not really stable, and that a prodrome of its failure, which can be interpreted as the build up of critical nuclei, is occurring at large distances. Finally, roughly for $t > 10^4$, a quick growth of correlations is observed, unveiling that metastability is over and that the next stage, where coarsening takes place, has been entered. In this case, the classification of the behavior of the correlation into three stages (initial evolution, stasis, late evolution) is not sharp because, as we discuss below, T_f is relatively far from T_c.

Let us now have a look at the right panel. Here the subcritical quench is so close to T_c that the departure from the metastable state cannot be observed within the simulated times. Besides that, one sees a pattern similar to the one observed in the left panel, with the notable difference that the correlations in the metastable state are almost indistinguishable from the ones of equilibrium at T_c. This clarifies our statement that the metastable state is *similar* to the equilibrium one at T_c: the more the system is quenched near to T_c (from below), the longer the metastable state lives and the closer to equilibrium at T_c it is. More precisely, indicating with $\mathcal{S}_{T_f}(t)$ a one-time observable measured in a system quenched to $T_f \lesssim T_c$, one has $\lim_{T_f \to T_c^-} \mathcal{S}_{T_f}(t) = \mathcal{S}_{eq,T_c}$, where the latter is the measurement of $\mathcal{S}$ made in equilibrium at T_c. Clearly, this cannot be true for any function $\mathcal{S}$ of the state of the system, particularly if it is weighting hugely the large distance features, but the statement is expected to be correct for most quantities of physical interest.

The nucleation time $\tau(q, T_f)$ can be roughly identified as the time when the

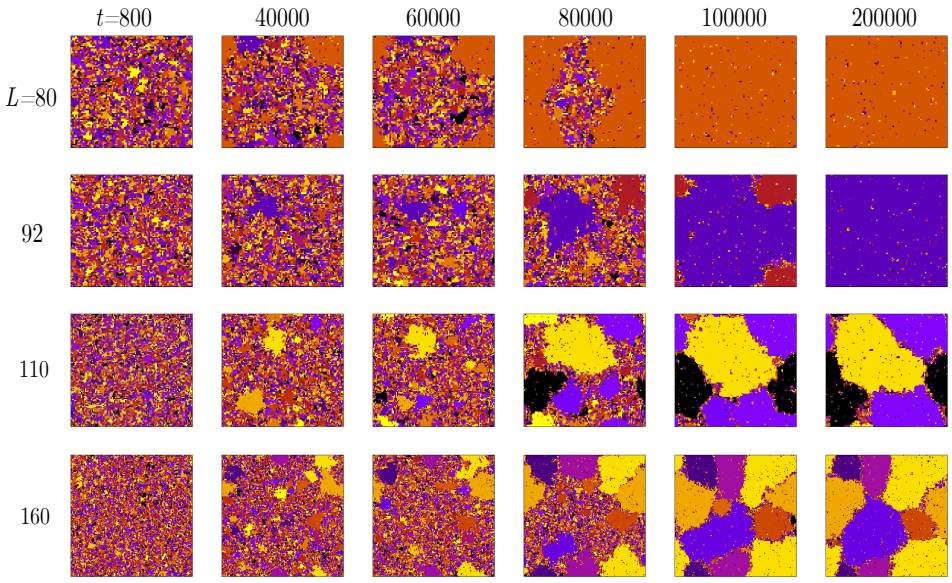

Figure 5.3: Snapshots of a typical evolution of the $q = 24$ Potts model quenched to $T_f = 0.98\ T_c$ for different lattice sizes. It is possible to appreciate that the number of phases that nucleate increase with the size of the system. [5]

plateau is over and $R^e(t)$ jumps rather abruptly to a higher value, see Fig. 5.2. This is a violent process corresponding to the fast invasion of available space by the super-critical nuclei, as it can be seen from the snapshots in Fig. 5.3 corresponding to $t = 4 \cdot 10^4$ and $t = 6 \cdot 10^4$. It was shown in [155] that $R^e(t)$ increases in an exponential way in this time domain. This violent relaxation becomes sharper upon increasing q. This can be understood recalling that the metastable state is similar to the equilibrium one at T_c, in the sense specified above, arguing then that the size R_{nucl} of critical nuclei at the beginning of the nucleation process is comparable to the equilibrium coherence length at T_c. This quantity decrease from ∞ to 0 as q goes from $q = 4$ to $q = \infty$. [156]. Clearly, the smaller R_{nucl} is, the larger the nuclei size must grow to take them in contact, yielding a more pronounced step in the shape of $R^e(t)$.

The duration $\tau(q, T_f)$ of the metastable state increases as $T \to T_c^-$, as it can be seen in the lower panel of Fig. 5.2. In the same picture we can also observe that the plateau value R_m is rather T_f-independent while, instead, there is a clear dependence on q, as it can be appreciated in the left panel. In [155] it was found that this value is well approximated by $R_m \propto [\ln(q-4)]^{-1}$ for small q ($q \lesssim 50$) and then, increasing further q, it saturates to a value of order one. This can be understood as follows: In [3], as shown in the previous chapter, the large-q behavior of the energy density e_m in the metastable state was computed. This quantity goes to zero as $e_m \simeq -a(T)q^{-1/2}$, where $a(T) > 0$ is a temperature dependent factor. For large q the equilibrium quantity $e(\infty) < 0$ becomes independent on q [157], hence we have that $e_m = e_m - e(\infty)$ approaches a large-q value from below. Given the choice of temperatures made in the upper-left panel of Fig. 5.2 (as to have $\tau(q, T_f)$ fixed) it is clear that, working instead at a constant T_f or even at a finite fraction of T_c, i.e. $T_f = x \cdot T_c$, the lifetime of metastability increases with q. Similarly, we have also observed that the temperature range where metastability occurs widens for larger q. Specifically, indicating with T_ℓ the lower temperature T_f where metastability is still observed we find that $(T_c - T_\ell)/T_c$ increase with q.

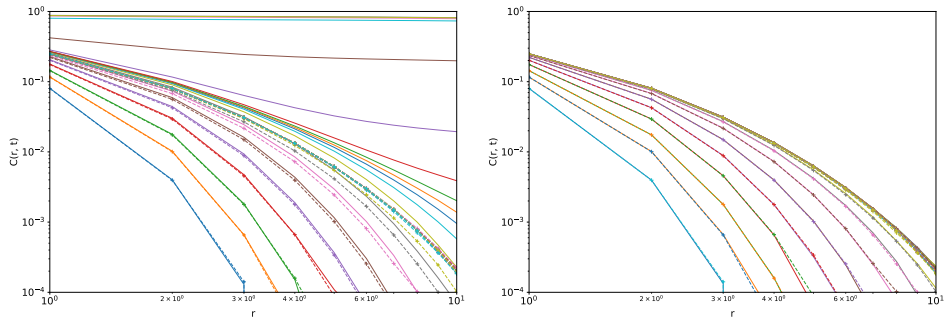

Figure 5.4: The correlation function $C(r,t)$ is plotted against r for a quench of the model with $q = 24$ from infinite temperature to $T_f = 0.99 \cdot T_c$ (continuous lines, left panel) or $T_f = 0.999 \cdot T_c$ (continuous lines, right panel). The dashed lines refer to a quench to $T_f = T_c$. Different curves correspond to different times exponentially spaced (from bottom to top t =2, 4, 7, 15, 31, 64, 137, 291, 618, 1316, 2802, 5968, 12709, 27066, 57642, 122762, 261451, 556822, 1185886, 2525627). [5]

The fast process associated to the steep increase of $R^e(t)$ ends at a time t_{coal} when nuclei of different color come in contact, a configuration that can be observed in Fig. 5.3 at times $t = 8 \cdot 10^4$ and/or $t = 10^5$ (except for the smallest size $L = 80$ where one single color nucleates, see discussion in Sec. 5.3.3). At this point a coarsening phenomenon sets in produced by the competition among domains, as shown in Fig. 5.3 and reported in [54, 57, 59, 133, 153, 158] and, for the closely related *vector Potts* (or clock) model in [159]. In this kind of evolution one expects dynamical scaling and $R^e(t) \sim t^{1/2}$, which is indeed roughly observed in Fig. 5.2 at very long times (for $q = 100$ this behavior is likely to be observed on times longer than the simulated ones).

Before closing this section let us comment on the fact that the data for R^e are free from finite-size effects until domains coarsen up to a length comparable to the system size, which occurs at a time $t_{fs}(L)$. This can be seen in the upper-right panel of Fig. 5.2 where one sees that the curves depart from the one corresponding to the larger system size ($L = 1000$) when $R^e(t) \simeq 0.1 \cdot L$. For instance, this occurs at a time $t_{fs}(L = 300)$ of order $6 \cdot 10^5$, and around $t_{fs}(L = 160) \simeq 10^5$. However, the fact that this particular quantity (R^e) does not feel the size of the system before $t_{fs}(L)$ does not mean that the dynamics is globally free from finite-size effects in this time domain. Actually, in Fig. 5.3 one clearly sees that the configurations of the model at a given time look very different in systems of different sizes. The next section is devoted to the discussion of this feature.

5.3.3 Multinucleation

We briefly mentioned above that, at variance with the Ising field-driven first order transition, here the role of the system size is relevant for the metastable state because $\tau(q, T_f)$ and the pseudo-spinodal temperature seem to depend on it. In the previous section we have already anticipated that also the nature of the dynamic escape from the metastable state changes significantly with the system size. A visual inspection of Fig. 5.3, where the same quench of the $q = 24$ model is operated on systems of different sizes, clearly displays this fact. Specifically, in this figure one observes that, when a relatively small size is considered ($L = 80$, upper row) one sees that a single critical droplet forms and grows, invading the whole system (last two snapshots). This is what we call mono-nucleation, or 1-nucleation. We have

checked that such phenomenon is observed rather independently of the thermal realization of the process. Notice that the winning color (orange) did not seem to be the favored one before its outburst (one would have rather predicted the violet or yellow color were better candidates), a fact that shows the rapidity of critical nucleation.

In the second row the behavior of a slightly larger size ($L = 92$) is shown. This small size increase is sufficient to modify qualitatively the situation, in that there are two nucleating colors, the red and the violet ones. Then, in this case, we have bi-nucleation, or 2-nucleation. Again, this feature is rather independent of the thermal realization. After nucleation, surface tension closes the domain of the minority color (last snapshot), symmetry is definitely broken and equilibrium is attained.

Increasing further the system size as in the two rows below, the fate of a system changes again and one observes 3-nucleation and 6-nucleation. Notice that, after nucleation, the competition among domains of different colors leads to a progressive elimination of their number. Increasing further L (not shown) one can observe k-nucleation with k up to q ($q = 24$ in this example).

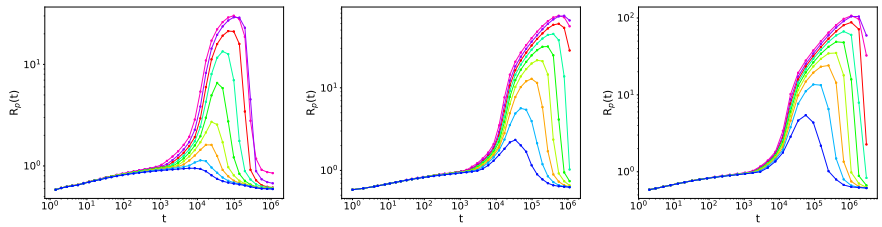

Figure 5.5: The typical lengths $R_p(t)$ of the various colors are plotted against time (on a log-log scale) for the model with $q = 9$ quenched to $T_f = 0.9912 \cdot T_c$. The system size is $L = 300$ (left panel), $L = 700$ (middle panel) and $L = 1000$ (right panel). Each data is averaged over 500 non-equilibrium realizations. Colors are ordered from the most represented (denoted #1) to the least represented one. [5]

In order to discuss the multinucleation process and its dependence on the system size at a more quantitative level we consider the typical lengths of the various colors, $R_p(t)$, which are shown for three different system sizes in Fig. 5.5. From this figure one clearly sees that R_p for the various colors initially grow, up to a characteristic time when $R_p(t)$ reaches a maximum R_p^* and then it shrinks. This means that domains of the corresponding color grow, reach a maximum size, and then collapse and disappear. For the winning color, denoted by #1 in Fig. 5.5, the interpretation is different, since the final decrease of R_1 must be associated to the invasion of the whole space, according to what discussed in case ii) at the end of Subsec. 5.3.1.

From the comparison between the three different system sizes represented in Fig. 5.5, one can make some observations. First, it is clear that for small sizes some colors do not nucleate, whereas they do in larger systems. For instance, color #9, represented in blue, does not show the exponential increase typical of nucleation for system size $L = 300$ and R_9 does not go beyond ~ 1, whereas it does grow significantly in the larger systems with $L = 700$ and $L = 1000$. This indicates that R_p is a quantity one can look at to establish the number of nucleating colors. Secondly, from Fig. 5.5 one sees that both the peak time and its height $R_p^*(q, T_f, L)$ are increased in a larger system. Exploiting these two observations we developed a method to determine the number of nucleating phases as a function of L and q, that we now describe. First, we measure $R_p^*(q, T_f, L)$ for all p's and different system sizes. This information is summarized for $q = 24$ in the inset of the upper-right

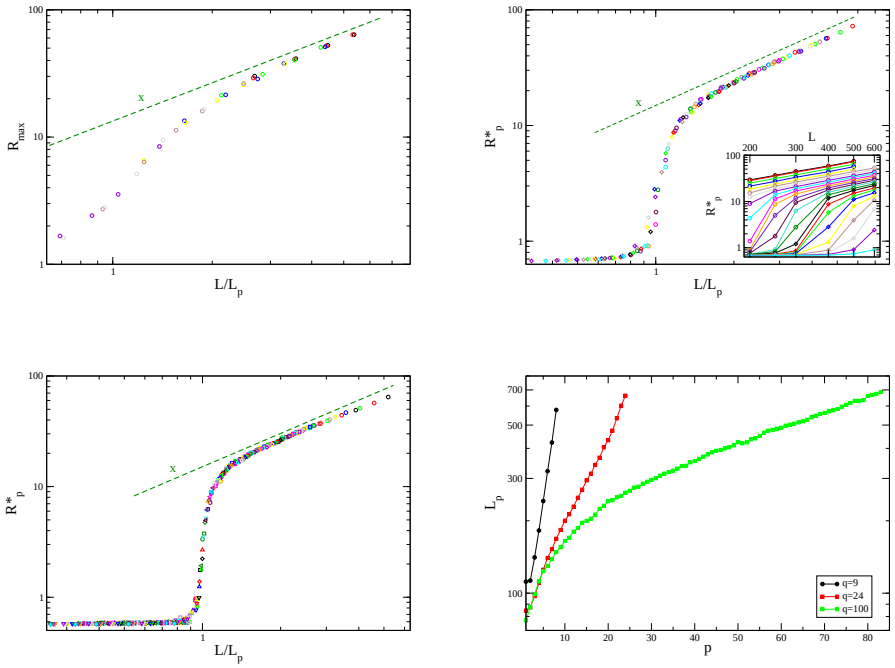

Figure 5.6: $R_p^*(q, T_f, L)$ is plotted in log-log scales against the rescaled size $L/L_p(q, T_f)$ (see text) for $q = 9$ (upper left panel), $q = 24$ (upper right) and $q = 100$ (lower left). The dashed green lines are the linear behavior $y \sim x$. The inset in the upper right panel contains the unscaled data ($R_p^*(q, T_f, L)$ vs L) for $q = 24$ and various values of p, (from the most abundant phase on the top, to the less abundant on the bottom). In the lower right panel the dependence of L_p on the color p is plotted for the three values of q, in a semilog plot. [5]

panel of Fig. 5.6. The upper panels and the lower-left one of the figure, which refer to different values of q, show that the data very clearly obey a scaling form

$$R_p^*(q, T_f, L) = f_q \left[\frac{L}{L_p(q, T_f)} \right], \tag{5.14}$$

where $L_p(q, T_f)$ is a fitting parameter which is plotted in the inset of the lower panel of Fig. 5.6. A similar pattern is found for other values of q, not reported in the figure. The scaling function $f_q(x)$ stays small for $x \ll 1$, it suddenly increases around $x = 1$ (the larger the q, the steeper the growth) and it then behaves as $f_q(x) \sim x$ for large x. This latter trend indicates that, for each color such that the representative point lies in this sector, the maximum size of the domains is triggered linearly by the system size, as it usually happens for a finite size effect in a standard (e.g. binary) coarsening system (see also the discussion at the end of this section). Hence one can argue that $L > L_p(q, T_f)$ is the condition for the p-th color to enter the coarsening stage. This is further discussed below. We observe also that the small-x value of $f_q(x)$ decreases with increasing q. This is because, as pointed out above, the size of the pre-nucleation domains gets smaller upon increasing q. Notice that imposing collapse of the curves according to Eq. (5.14) only fixes $L_p(q, T_f)$ up to an arbitrary constant. We fix it by asking that the steep part of $f_q(x)$ be centered at $x = 1$.

Looking at the plot of $L_p(q, T_f)$ in the lower right panel of Fig. 5.6, one finds an exponential dependence

$$L_p(q, T_f) = A(q, T_f) e^{p/\mathcal{P}(q)}. \tag{5.15}$$

This law describes well all the data for $q = 9, 24$, and the large p region for $q = 100$ (with fitting parameters $A(q, T_f) = 59.43$, 82.97, 200.00 and $\mathcal{P}(q) = 3.546$, 11.848, 67.568 for $q = 9, 24, 100$, respectively). Furthermore, we found an analogous behavior for other values value of q not portrayed in Fig. 5.5. Repeating the procedure above for different temperatures we find that $\mathcal{P}$ is, within errors, independent of T. This is shown in Fig. 5.7 where, in the left panel, it is seen that for a fixed $q = 24$, $P(q)$ stays constant within errors upon changing T_f. Similar results are found for other values of q. This explains the parameter dependencies written in Eq. (5.15). As shown in Fig. 5.7 (left panel) $\mathcal{P}(q)$ turns out to increase in a roughly linear way with q. Moving to $A(q, T_f)$, its dependence on T_f (at fixed q) can be appreciated in Fig. 5.7 (right panel), where one finds that $A(q, T_f)$ increases with T_f. On the other hand, with the choice of T_f made in our simulations, which as discussed earlier correspond to fix the lifetime $\tau(q, T_f)$ of the metastable state, one finds that also $A(q, T_f)$ increases with q, similarly to $\mathcal{P}$. This is shown in the right panel of Fig. 5.7.

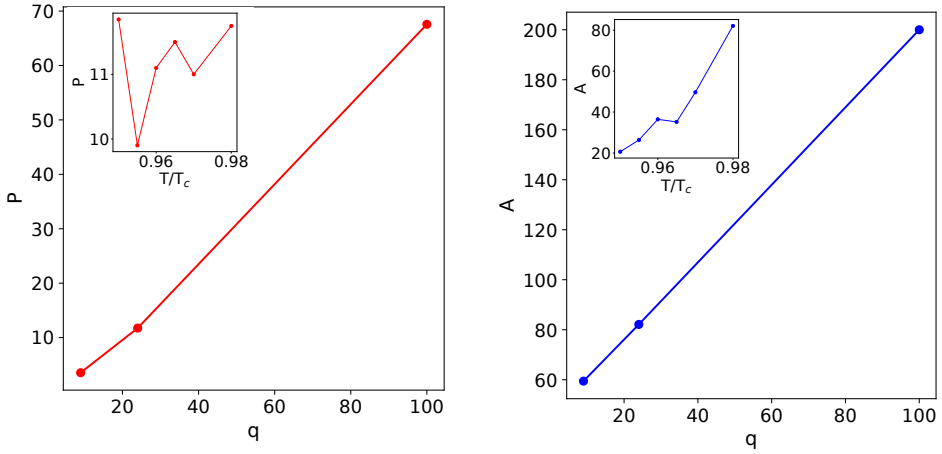

Figure 5.7: Left panel: dependence of $\mathcal{P}$ on q by keeping T_f at a q-dependent value such that the lifetime $\tau(q, T_f)$ of the metastable state is kept constant. In the inset the dependence of $\mathcal{P}$ on T is displayed, showing that it is not significative (notice the narrow interval on the y-axis). Right panel: dependence of A on q by keeping T_f at a q-dependent value such that the lifetime $\tau(q, T_f)$ of the metastable state is kept constant. In the inset the dependence of A on T is shown. [5]

Notice that, for large $\mathcal{P}(q)$, meaning for sufficiently large q, after Eq. (5.15) one has $A(q, T_f) \simeq L_1(q, T_f)$, the typical size associated to the prevailing color. Since for $L/L_p(q, T_f)$ the behavior $f_q(x) \propto x$ is associated to the coarsening phenomenon, one can interpret $A(q, T_f) \simeq L_1(q, T_f)$ as the smallest system size in order to have coarsening. This means that such a size must host the largest domain present at t_{coal} when coarsening starts. Hence we conclude that $A(q, T_f)$ has the physical meaning of the typical size of the largest droplets in the system at the time t_{coal}. This can be appreciated in Fig. 5.8 where a ruler of length $L_p(q, T_f)$ is plotted on top of the configurations of the model at $t = t_{coal}$. We remark though that this interpretation is sound for those values of q such that the exponential fit is good

even for small p. For $q = 100$, for example, the fit deviate for small p (see Fig. 5.6) and further investigation is needed to clarify these cases.

Coming to the issue of multinucleation, repeating the argument above for $L_1(q, T_f)$, we can say that the p-th color has nucleated if $L > L_p$. Using Eq. (5.15) we arrive at the conclusion that, given a system size L, one has k-nucleation with

$$k(q, T_f, L) = \left\{ \mathcal{P}(q) \ln \left[\frac{L}{A(q, T_f)} \right] \right\}_{\in [1,q]}, \tag{5.16}$$

where the notation $\{Z\}_{\in[1,q]} = \max\{1, \min\{q, Z\}\}$ simply accounts for the constraint $k \in [1, q]$. Using the values of $\mathcal{P}(q)$ and $A(q, T_f)$ in this equation, in fact, one can correctly predict the number of nucleating colors observed in the various cases of Fig. 5.3. This result shows that, for a given q, the number of nucleating phases grows only logarithmically with the system size. When the thermodynamic limit is taken from the onset, all phases nucleate. Conversely, for a given finite size L, increasing T_f towards T_c with fixed q reduces the number of nucleating phases to one, because $A(q, T_f)$ increases. Also, if the size of the system is large enough, i.e. $L \gg A(q, T_f)$, increasing q reduces the number of nucleating phases. This however is true only for such large values of L, because when L is comparable with $A(q, T_f)$ *probably* an interplay takes place between the growth (with q) of $\mathcal{P}(q)$ and that of $A(q, T_f)$, that can produce different results. Let us also notice that Eq. (5.16) informs us on the number of nucleating phases, but does not predict the time needed to nucleate. Clearly if this time grows to infinity, nucleation is not observed at all. This happens in the large-q limit [3].

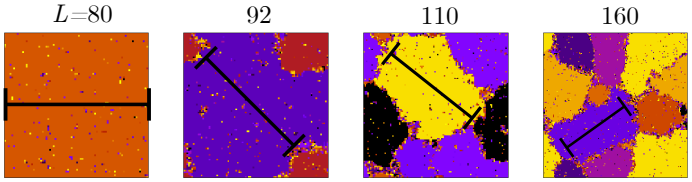

Figure 5.8: Snapshot at $t = 10^5$ for the $q = 24$ Potts model quenched to $T = 0.98 \cdot T_c$. This is approximately the time t_{coal} when coarsening starts (see Fig. 5.3). The black ruler is the length $A(q, T)$ (see Eqs. (5.15) and (5.16)). [5]

The discussion above shows that the multi-nucleation dynamics of the two dimensional Potts model is interested by peculiar finite size effects, rather different from the usual ones observed in the phase-ordering of binary systems. In the latter, there are only two competing colours and the growth of the domains does not feel the finiteness of the system until some time $t_{end}(L)$, when the domains' size becomes comparable to L. At this point the coarsening process is interrupted and the system enters a final stage whereby equilibrium is approached. For times $t \ll t_{end}$ any (intensive) measurement does not depend on the value of L. In the Potts model, one observes an analogous behaviour when observing a quantity like R^e, as we discussed at the end of Sec. 5.3.2. This also true also per the size R_1, R_2 of the two winning colours. However, the number k of coarsening phases depends on L up to a value of L as large as L_q, given in Eq. (5.15). Notice that this characteristic size diverges both as $T \to T_c$ for a given q and as $q \to \infty$ for a given T, as discussed above. Worst, the sizes R_n ($n \in [1, q-2]$) of the domains of the minority colours, do depend on L even if measured at times $t \ll t_{end}$ and even if $L > L_q$ (see Fig. 5.6). This strange size dependence is perhaps at the origin of many controversies on the size dependence of the metastable dynamics.

One might wonder how it may be possible that the unrestricted quantity R^e be size-independent whereas the restricted ones R_p do depend on L, given that R^e is morally the average of the R_ps. This occurs because R^e only fixes the average size of domains but not their color, and it is schematically illustrated in Fig. 5.9. The configuration on the left shows a portion of a system of size $L = L_1$ at a time t where six phases are present. On the right, instead, the same portion of an analogous system with a different size $L = L_2 < L_1$ is represented at the same time t. It can be seen that, although two phases (the green one and the brown one) are absent in the smaller lattice (hence the number of colors is L dependent), the size of the domains does not change (hence is L independent).

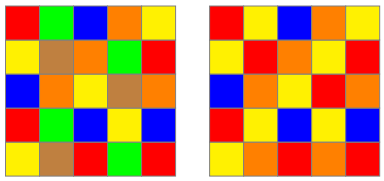

Figure 5.9: Two pictorial configurations of the bidimensional Potts model. The system on the right has a size L_2 and the picture represents the whole lattice, the one on the left has a larger size $L_1 > L_2$ but in the picture only a part of size L_2 of it is shown. The two systems are characterised by the same size of domains, but in the right one the green and the brown phases have vanished. [5]

5.4 Comments

The main result of this chapter, which is contained in Eq. (5.16), is that the number of nucleating phases of the two-dimensional Potts model increases logarithmically with the system size. The logarithmic behavior itself informs us that this feature cannot be related to the trivial geometrical fact that a larger system can *accommodate* a larger number of developing colors. If this were the origin, looking at the snapshots in Fig. 5.3 one should see, in systems of different sizes, an equal number of nucleating phases in portions of equal area. This is not observed. For instance, comparing the systems of relative double size $L = 80$ (first line) and $L = 160$ (last row), at time $t = 80000$, one sees that there is only one nucleating color (orange, besides a remnant of the disordered phase) in the smallest system, whereas there are typically more than one color in a portion of area 80×80 of the system with $L = 160$. This raises an important question which, by the way, concerns also the observed size dependence of the metastable state recalled in the introduction: how can a system with a very short coherence length (of the order of the nuclei size, as it can also be appreciated from the correlation function of Fig. 5.4) feel the boundary effects? Rephrased differently, if nucleation is a local process, since correlations are short, how could it be influenced by a global property such as the total size?

Here we provide a possible, although at the moment completely speculative, answer. In a series of papers [105, 160–162] it has been shown that in a rather broad class of $2d$ binary systems the fate of the system, namely which of the two colors will eventually invade the sample, is decided at a very early stage when a percolation cluster grows as large as the whole system. Since percolation is an uncorrelated phenomenon, this occurs when spatial correlations are still minimal and the ferromagnetic domains are yet microscopic. However, such tenuous invisible structure determines the phase that will eventually (at much longer times) win the

competition simply by touching the boundaries. Therefore, it may be conjectured that something similar – in a way to be better investigated – happens also in the present case with q colors. Namely, a large but slender structure (not necessarily with a percolation topology as in the case with $q = 2$), which cannot be easily associated to the pattern of the nucleating domains, can invade the sample till its boundaries, and determine the fate of the colors. This seems to agree with the observation, made regarding Fig. 5.4, that within the metastable state $C(r, t)$ does not vary at small r, whereas it does so at large distances. Which are the geometrical features to look for to identify such large scale structure, if any, is still an open question.

Appendix A

In this Appendix we derive the expressions for the evolution at long times of qualities of interest for the problem of the COP dynamics of fluctuations of the order parameter sample variance in the Gaussian model (see Chapter 2). For the average of s, in the large-volume limit we have, from Eq. (2.34)

$$\begin{aligned}\langle s(t)\rangle &= \tfrac{\Omega_d}{(2\pi)^d}\int_0^\Lambda dk\,\tfrac{k^{d-1}}{\beta_k(t)\omega_k}\\ &= \tfrac{\Omega_d}{(2\pi)^d}\int_0^\Lambda dk\tfrac{k^{d-1}((\beta_i^{-1}-\beta_f^{-1})e^{-2k^2(k^2+r)t}+\beta_f^{-1})}{k^2+r}.\end{aligned} \tag{A.1}$$

The final equilibrium value, obtained for $t\to\infty$ in the previous expression, reads

$$\langle s\rangle^{(eq,\beta_f)} = \frac{\Omega_d}{(2\pi)^d}\int_0^\Lambda dk\,\frac{k^{d-1}}{\beta_f(k^2+r)}. \tag{A.2}$$

The difference $\langle s(t)\rangle - \langle s\rangle^{(eq,\beta_f)}$ is therefore given by

$$\langle s(t)\rangle - \langle s\rangle^{(eq,\beta_f)} = \frac{\Omega_d(\beta_i^{-1}-\beta_f^{-1})}{(2\pi)^d}\int_0^\Lambda dk\,\frac{k^{d-1}e^{-2k^2(k^2+r)t}}{k^2+r}. \tag{A.3}$$

Changing variable $x = t^{\frac{1}{2}}k$ leads to

$$\langle s(t)\rangle - \langle s\rangle^{(eq,\beta_f)} = \frac{\Omega_d(\beta_i^{-1}-\beta_f^{-1})t^{-d/2}}{(2\pi)^d}\int_0^{\Lambda\sqrt{t}} dx\,\frac{x^{-d/2}e^{-2x^2(x^2/t+r)}}{x^2/t+r}. \tag{A.4}$$

For large t, due to the fact that only small x contribute, the integral can be written as

$$\langle s(t)\rangle - \langle s\rangle^{(eq,\beta_f)} \simeq \frac{\Omega_d(\beta_i^{-1}-\beta_f^{-1})t^{-d/2}}{r(2\pi)^d}\int_0^\infty dx\,x^{-d/2}e^{-2x^2r}. \tag{A.5}$$

Accordingly, one recovers Eq. (2.35), with

$$\begin{aligned}A &= \tfrac{\Omega_d(\beta_i^{-1}-\beta_f^{-1})}{r(2\pi)^d}\int_0^\infty dx\,x^{-d/2}e^{-2x^2r}\\ &= \tfrac{\Omega_d(\beta_i^{-1}-\beta_f^{-1})\Gamma(d/2)}{r(2\pi)^d(2r)^{d/2+1}},\end{aligned} \tag{A.6}$$

where Γ is the Gamma function. In order to assess the accuracy of this approximation for large t we evaluated numerically $\langle s(t)\rangle$ in the case $d=3$, finding almost perfect correspondence.

For the evolution of the critical point s_c at long times we have, again in the large-volume limit, starting from Eq. (2.30)

$$s_c(t) - s_c^{(eq,\beta_f)} = \frac{\Omega_d}{(2\pi)^d}\int_0^\Lambda dk\,k^{d-1}\Big[\frac{1}{(k^2+r)\beta_k(t)-r\beta_i} - \frac{1}{(k^2+r)\beta_f - r\beta_i}\Big], \tag{A.7}$$

where $\beta_k(t)$ is defined in (2.18). Changing variables $x = t^{\frac{1}{2}}k$ one has

$$s_c(t) - s_c^{(eq,\beta_f)} = \frac{\Omega_d t^{-d/2}}{(2\pi)^d} \int_0^{\Lambda\sqrt{t}} dx\, x^{d-1} \Big[\frac{1}{\frac{x^2/t+r}{(\beta_i^{-1}-\beta_f^{-1})e^{-2x^2(x^2/t+r)}+\beta_f^{-1}} - r\beta_i} - \frac{1}{(x^2/t+r)\beta_f - r\beta_i} \Big]. \tag{A.8}$$

For large t we end up with

$$s_c(t) - s_c^{(eq,\beta_f)} \simeq \frac{\Omega_d t^{-d/2}}{(2\pi)^d} \int_0^{\infty} dx\, x^{d-1} \Big[\frac{1}{\frac{r}{(\beta_i^{-1}-\beta_f^{-1})e^{-2x^2 r}+\beta_f^{-1}} - r\beta_i} - \frac{1}{r(\beta_f - \beta_i)} \Big], \tag{A.9}$$

namely Eq. (2.37). The value of the coefficient a introduced therein is

$$\begin{aligned} a &= \tfrac{\Omega_d}{(2\pi)^d} \textstyle\int_0^{\infty} dx\, x^{d-1} \Big[\frac{1}{\frac{r}{(\beta_i^{-1}-\beta_f^{-1})e^{-2x^2 r}+\beta_f^{-1}} - r\beta_i} - \frac{1}{r(\beta_f-\beta_i)} \Big] \\ &= \tfrac{\Omega_d \beta_f \Gamma(d/2)\zeta(d/2)}{(2\pi)^d (2r)^{d/2+1}\beta_i(\beta_f-\beta_i)}, \end{aligned} \tag{A.10}$$

where ζ is the Riemann zeta function. Numerical calculations, for the test case $d = 3$, confirm Eq. (A.9) with excellent accuracy.

Finally we determine the dynamics of the condensing mode $s_0(s,t)$ in the condensation-developing region. We recall that $s_0(s,t)$ is defined in Eq. (2.32), where $z^*(s,t)$ is defined via Eq. (2.28)

$$s = \Omega_d \int_0^{\Lambda} \frac{dk}{(2\pi)^d} \frac{k^{d-1}}{\beta_k(t)\omega_k - 2z^*}, \tag{A.11}$$

with ω_k defined after Eq. (2.8). In order to determine the behavior of $s_0(s,t)$ as time goes by, we must first determine that of $z^*(s,t)$. Taking the time derivative of Eq. (A.11) one has

$$0 = \int_0^{\Lambda} dk k^{d-1} \frac{[\tilde{\omega}_k \omega_k \beta_k^2(t)(\beta_i^{-1} - \beta_f^{-1})e^{-2\tilde{\omega}_k t} - \dot{z}^*(s,t)]}{[\beta_k(t)\omega_k - 2z^*(s,t)]^2}, \tag{A.12}$$

where $\dot{z}^*$ stands for the time derivative of z^*, while $\beta_k(t)$ is given in Eq. (2.18) and $\tilde{\omega}_k$ is defined after Eq. (2.14). Accordingly,

$$\dot{z}^* = \frac{\int_0^{\Lambda} dk \frac{k^{d-1}\tilde{\omega}_k\omega_k\beta_k^2(t)(\beta_i^{-1}-\beta_f^{-1})e^{-2\tilde{\omega}_k t}}{[\beta_k(t)\omega_k - 2z^*(s,t)]^2}}{\int_0^{\Lambda} dk \frac{k^{d-1}}{[\beta_k(t)\omega_k - 2z^*(s,t)]^2}}. \tag{A.13}$$

In order to proceed, we distinguish between values of s inside the CD region, i.e., $s_c^{(eq,\beta_f)} < s < s_c^{(eq,\beta_i)}$ and the limiting value $s = s_c^{(eq,\beta_f)}$. In the former case, s_0 will diverge in a finite time so in the integrals in Eq. (A.13) we can consider the limit of small k, which also correspond to the portion of the domain where the variation in time is more important. Accordingly, from Eq. (A.13) one finds

$$\dot{z}^* = \frac{\int_0^{\Lambda} dk \frac{\frac{k^{d+1}r^2(\beta_i^{-1}-\beta_f^{-1})}{(\beta_i^{-1})^2}}{\left(\frac{r}{\beta_i^{-1}} - 2z^*\right)^2}}{\int_0^{\Lambda} dk \frac{k^{d-1}}{\left(\frac{r}{\beta_i^{-1}} - 2z^*\right)^2}} = \frac{\int_0^{\Lambda} dk\, \frac{k^{d+1}r^2(\beta_i^{-1}-\beta_f^{-1})}{(\beta_i^{-1})^2}}{\int_0^{\Lambda} dk\, k^{d-1}} = \text{const.} \tag{A.14}$$

Thus z^* is linear in t, implying

$$s_0(s,t) \simeq (t^*(s) - t)^{-1}, \qquad \forall s \in (s_c^{(eq,\beta_f)}, s_c^{(eq,\beta_i)}). \tag{A.15}$$

In the other case, $s = s_c^{(eq,\beta_f)}$ is at the border of the CD region and we can consider the limit of long times in Eq. (A.13). The integrand in the denominator, then, can be approximated by its leading behavior for small $k \ll r^{1/2}$, i.e., as a constant

$$\beta_k(t)\omega_k - 2z^*(s_c^{(eq,\beta_f)}, t) \simeq \beta_f r - 2z^*(s_c^{(eq,\beta_f)}, \infty). \tag{A.16}$$

Accordingly, Eq. (A.13) in the same limit renders

$$\dot{z}^* \simeq \frac{d}{\Lambda^d} \int_0^\Lambda dk \frac{k^{d-1}k^2r^2(\beta_i^{-1} - \beta_f^{-1})e^{-2k^2rt}}{[(\beta_i^{-1} - \beta_f^{-1})e^{-2k^2rt} + \beta_f^{-1}]^2}, \tag{A.17}$$

where we used that $\tilde{\omega}_k \simeq k^2 r$ and $\omega_k \simeq r$. The change of variables $x = t^{\frac{1}{2}}k$ gives

$$\dot{z}^* \simeq \frac{t^{\frac{d+2}{2}}d}{\Lambda^d} \int_0^{\Lambda\sqrt{t}} dk \frac{x^{d+1}r^2(\beta_i^{-1} - \beta_f^{-1})e^{-2x^2r}}{[(\beta_i^{-1} - \beta_f^{-1})e^{-2x^2r} + \beta_f^{-1}]^2}. \tag{A.18}$$

In the long-time limit the integral is well approximated by the one in which the upper extreme of integration is set to infinity, and therefore $\dot{z}^* \simeq t^{-d/2+1}$. Accordingly

$$z^*(s_c^{(eq,\beta_f)}, t) \simeq z^*(s_c^{(eq,\beta_f)}, \infty) + Ct^{-d/2}, \tag{A.19}$$

where the asymptotic value equals $\beta_0\omega_0/2$ and C is a proportionality constant. We conclude that

$$s_0(s_c^{(eq,\beta_f)}, t) \simeq t^{d/2}, \tag{A.20}$$

namely Eq. (2.39). We confirmed numerically the validity of this result in the specific case $d = 3$.

Appendix B

In this appendix we consider all the moves that should be taken into account to build the master equation (**??**) which is at the core of Chapter 4.

Consider starting from a state (11) next to a structure **A**, turn it into a state (6), and make then a structure **B** be born. The probability of picking the starting site is N_6 because there are 2 (11) in such position for every structure **A** (again we are keeping only the terms which at the end will contribute up to the second order) and the probability to switch to (6) exactly in the needed direction is $p/4$. The probability of the move is thus $pN_6/4$ and we end up with with 1 (11) less and 1 (3a) more.

$$P = pN_6/4$$

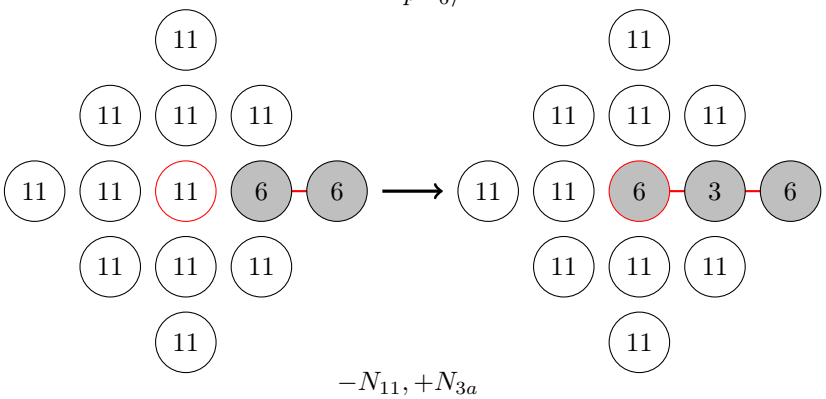

$$-N_{11}, +N_{3a}$$

The same move but with as a consequence a formation of a structure **C** has *mutatis mutandis* probability $pN_6/2$, and we lose 2 states (11) and gain 1 (3b) and 1 (10c):

$$P = pN_6/2$$

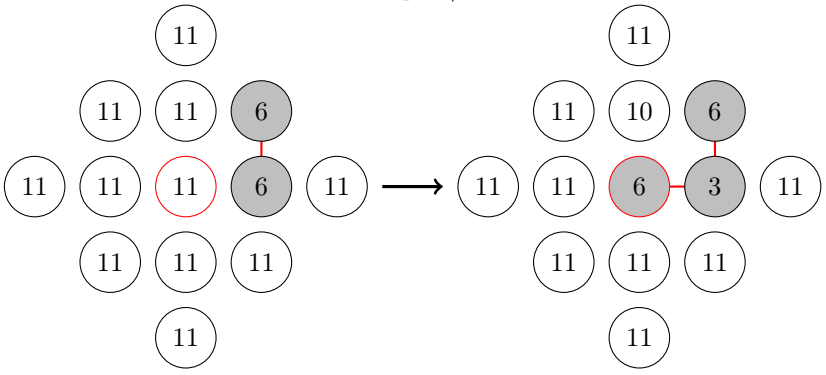

$$-2N_{11}, +N_{3b}, +N_{10c}$$

A site in a state (11) that is far from any structures and flips to another q value but remains in the state (11) can, with probability $N_{11}4/(4e^{\beta}+q-4)$ assume the same color of one of its next to nearest neighbors thus forming an **E** or, again with probability, $N_{11}4/(4e^{\beta}+q-4)$ form an **F** structure. We have, respectively,

$$P = N_{11}(4/(4e^{\beta}+q-4))$$

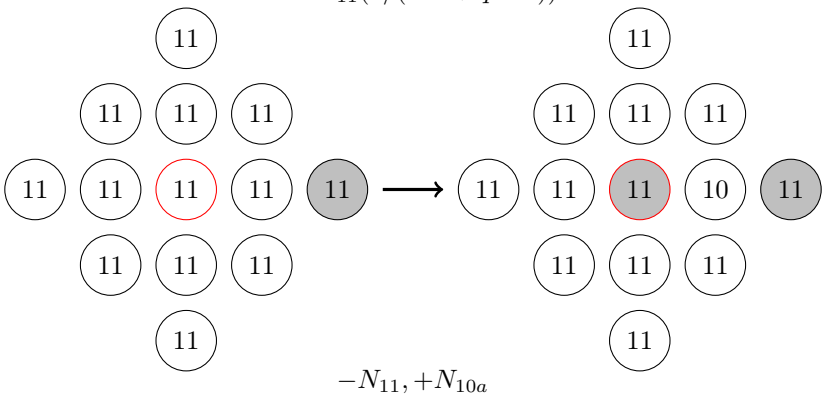

$$-N_{11}, +N_{10a}$$

and

$$P = N_{11}(4/(4e^{\beta}+q-4))$$

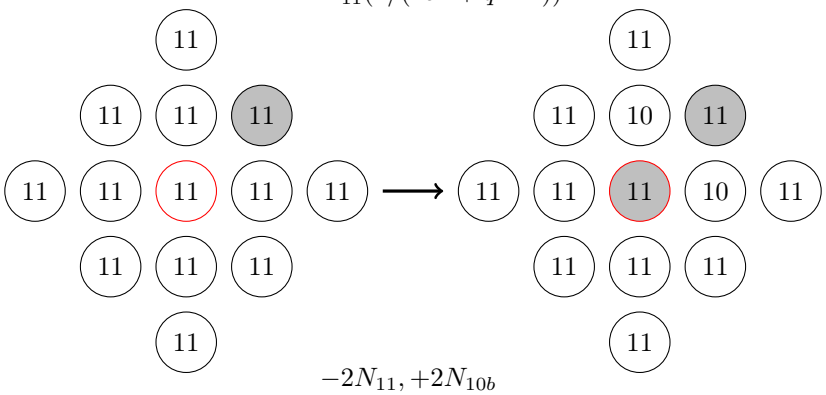

$$-2N_{11}, +2N_{10b}$$

Picking one of the two gray sites which are part of an **E** structure has probability $2P(\mathbf{E}) = 2N_{10a}$. The probability for it to change color but stay in a state (11) is $P_{11\to 11} = 1-p$. Thus, the following move

$$P = 2N_{10a}$$

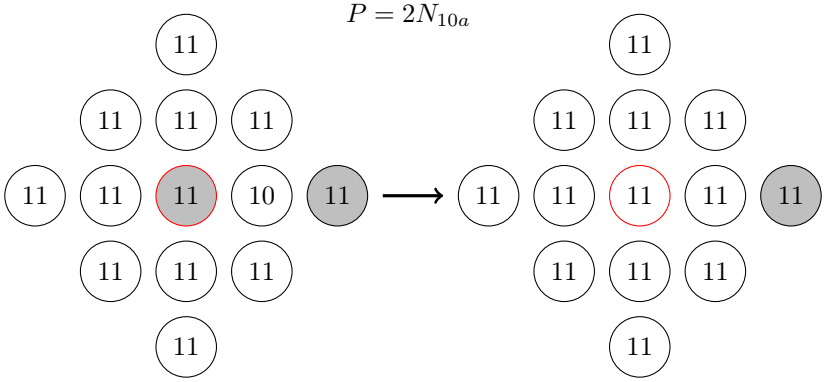

$$-N_{10a}, +N_{11}$$

occurs with probability $2N_{10a}$ and causes a loss of a (10a) and a gain of an (11)

Similarly, there are two gray (11) which are part of a structure **F**. Thus with probability N_{10b} the following move cause a loss of 2 (10b) and the gain of 2 (11)

$$P = N_{10b}$$

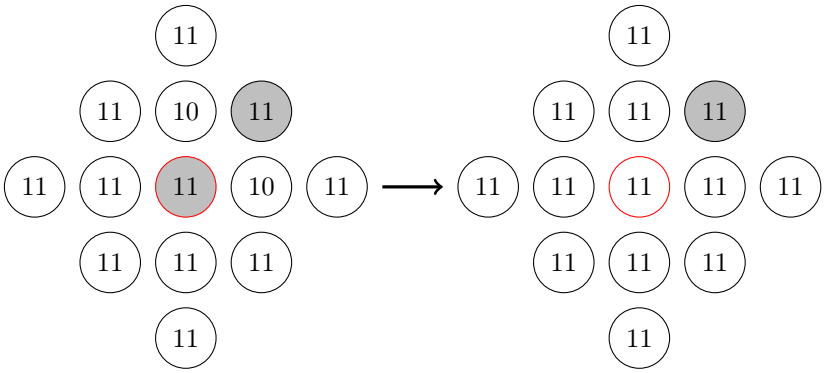

$$-2N_{10b}, +2N_{11}$$

Now we consider the cases when the starting state is a (6). The probability of picking a (6) which is part of a structure **A** is $2P(\mathbf{A}) = N_6 - 2N_{3a} - 2N_{3b}$ and it turns to a (11) with probability $1-p$. So, to the second order in p^2, with probability $N_6(1-p) - 2(N_{3a} + N_{3b})$, 2 (6) disappears and 2 (11) appears

$$P = N_6(1-p) - 2(N_{3a} + N_{3b})$$

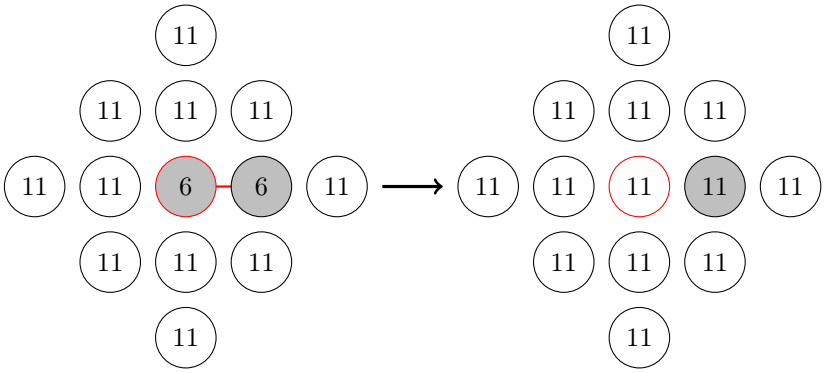

$$-2N_6, +2N_{11}$$

Considering instead picking one of the two (6) which are part of a structure **B** or **C**, the transition to a (11) leads respectively with probability $2N_{3a}$ to a loss of 1 (3a) and a gain of a (11)

$P = 2N_{3a}$

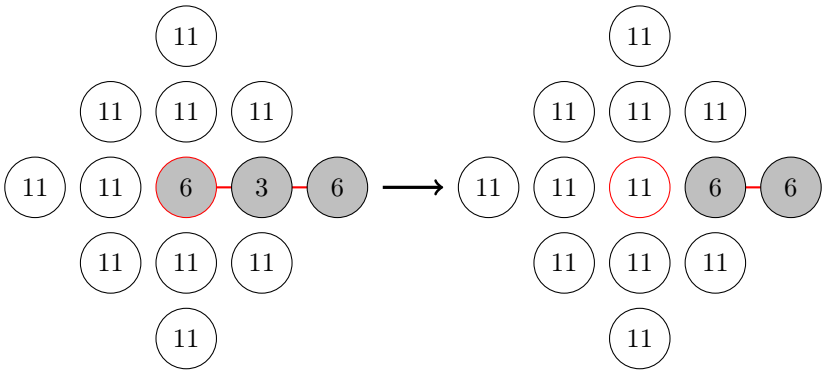

and with probability $2N_{3b}$ to the destruction of 1 (3b) and 1 (10c) and the creation of 2 (11)

$P = 2N_{3b}$

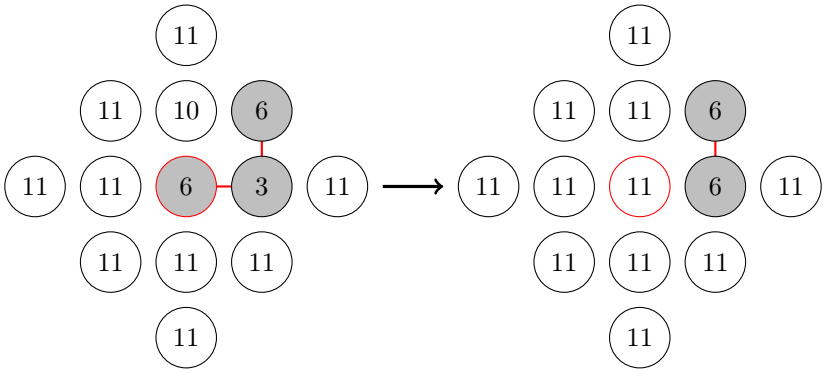

Now we consider all the moves involving as starting sites a (3) or a (10) of all the possible kinds. This states, which can be picked with probability proportional to p^2 can turn one into the other with probabilities $P_{3\to10} \sim 1/2$ and $P_{10\to3} \sim 1/2$ for $T \simeq T_c$. Consider picking a (3a), this happens with probability N_{3a}, if it turns into a (10) (it happens with probability $P_{3\to10}$) it cause the loss of 1 (3a) and 2 (6) and the gain of 1 (10a) and 2 (11)

$$P = N_{3a} P_{3 \to 10}$$

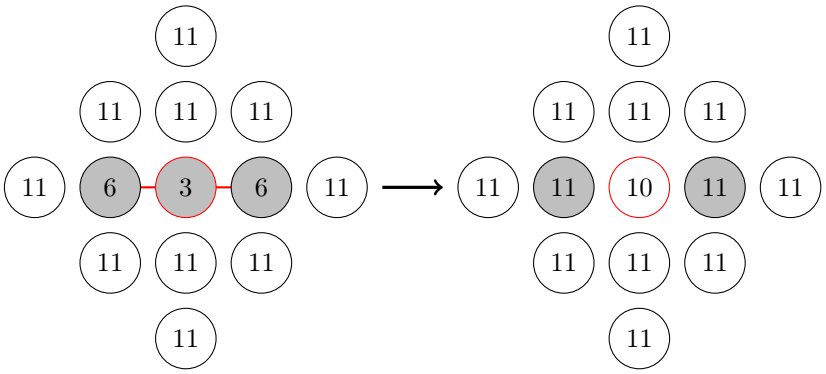

$$-N_{3a}, -2N_6, +N_{10a}, +2N_{11}$$

The inverse is

$$P = N_{10a} P_{10 \to 3}$$

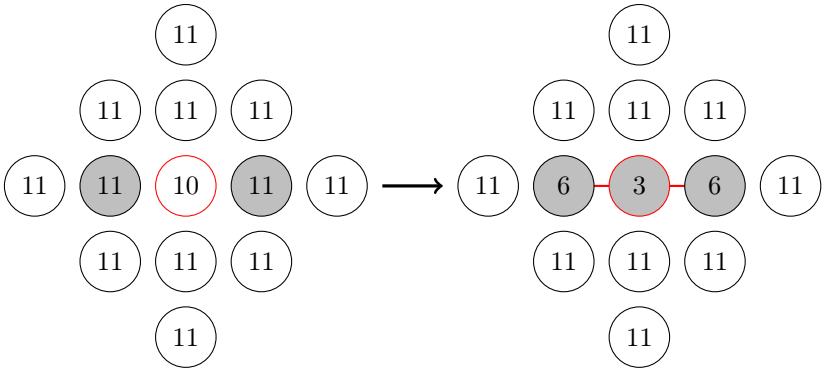

$$-N_{10a}, -2N_{11}, +N_{3a}, +2N_6$$

If we pick a (3b), the probability of the move is $N_{3b} P_{3 \to 10}$ and cause the destruction of 1 (3b), 1 (10c) and 2 (6) while creates 2 (10b) and 2 (11). We have

$$P = N_{3b} P_{3 \to 10}$$

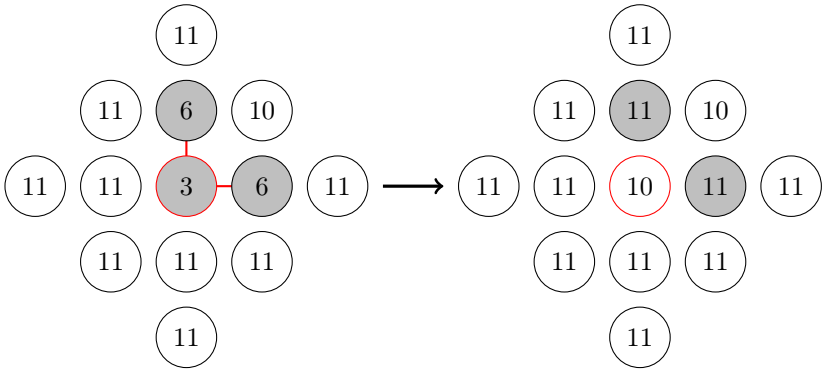

$$-N_{3b}, -N_{10c}, -2N_6, +2N_{10b}, +2N_{11}$$

and the opposite move with

$$P = N_{10b} P_{10\to 3}$$

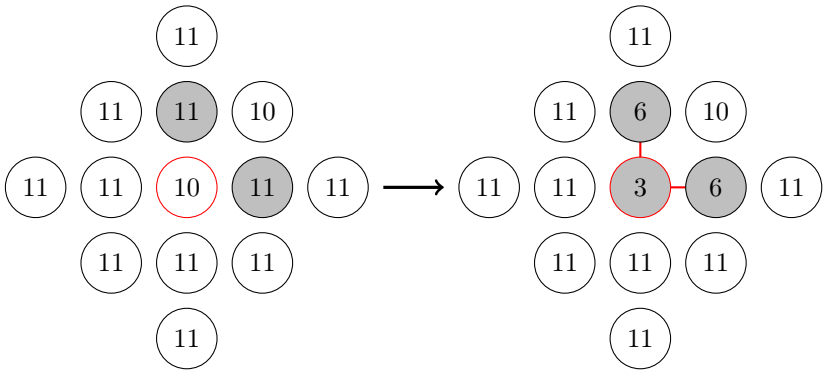

$$-2N_{10b}, -2N_{11}, +N_{3b}, +N_{10c}, +2N_6$$

Finally, with probability $N_{3c} P_{3\to 10}$, 4 (3c) are destroyed and 1 (3b), 1 (10c) and 2 (6) are created by

$$P = N_{3c} P_{3\to 10}$$

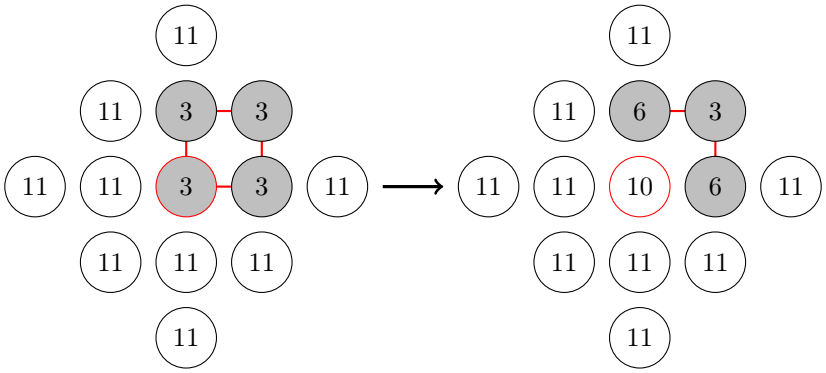

$$-4N_{3c}, +N_{3b}, +N_{10c}, +2N_6$$

the opposite of which happens with probability

$$P = N_{10c} P_{10\to 3}$$

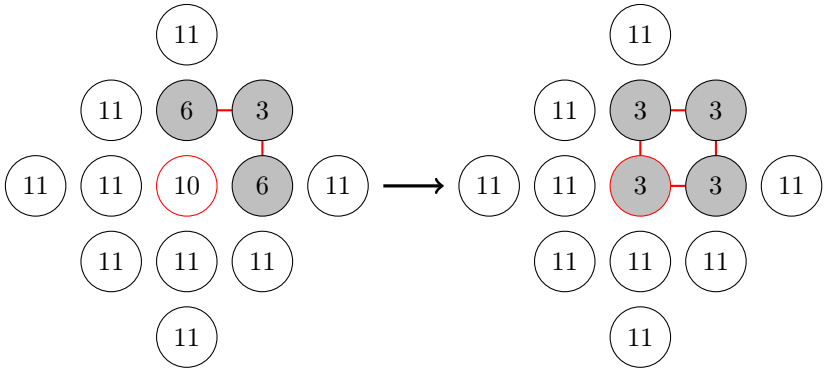

$$-N_{10c}, -N_{3b}, -2N_6, +4N_{3c}$$

Bibliography

[1] F. Corberi, O. Mazzarisi, and A. Gambassi. Dynamics of fluctuations in the Gaussian model with conserved dynamics. *Journal of Statistical Mechanics: Theory and Experiment*, 2019(10), 2019.

[2] F. Corberi, O. Mazzarisi, and A. Gambassi. Dynamics of uctuations in the Gaussian model with dissipative Langevin Dynamics. In *Journal of Physics: Conference Series*, volume 1548, 2020.

[3] O. Mazzarisi, F. Corberi, L. F. Cugliandolo, and M. Picco. Metastability in the Potts model: Exact results in the large q limit. *Journal of Statistical Mechanics: Theory and Experiment*, 2020(6), 2020.

[4] A. de Azevedo-Lopes, J. J. Arenzon, F. Corberi, and O. Mazzarisi. How heterogeneous a statistical system can be? *In preparation.*

[5] F. Corberi, L. F. Cugliandolo, M. Esposito, O. Mazzarisi, and M. Picco. How many phases nucleate in the bidimensional Potts model? *In preparation.*

[6] I. Newton. *Philosophiae naturalis principia mathematica.* 1687.

[7] V. I. Arnold. *Mathematical Methods of Classical Mechanics.* 1978.

[8] L. Boltzmann. *Vorlesungen über Gastheorie,.* J.A. Barth, Leipzig, 1896.

[9] E. Fermi, P. Pasta, S. Ulam, and M. Tsingou. Studies of the nonlinear problems. 1955.

[10] G. Morandi, E. Ercolessi, and F. Napoli. *Statistical Mechanics.* World Scientific, 2001.

[11] G. Gallavotti. Ergodicity: a historical perspective. Equilibrium and Nonequilibrium. *European Physical Journal H*, 2016.

[12] L. Sklar. Physics and Chance: Philosophical Issues in the Foundations of Statistical Mechanics. *The Philosophical Review*, 1995.

[13] N. Goldenfeld. *Lectures on Phase Transitions and the Renormalization Group.* Addison-Wesley, Reading, 1992.

[14] K. Binder and W. Kob. *Glassy materials and disordered solids: An introduction to their statistical mechanics.* 2005.

[15] B. Schmittmann and R. K.P. Zia. Statistical mechanics of driven diffusive systems, jan 1995.

[16] U. C. Täuber, M. Howard, and B. P. Vollmayr-Lee. Applications of field-theoretic renormalization group methods to reaction-diffusion problems, apr 2005.

[17] S. Ramaswamy. The mechanics and statistics of active matter. *Annual Review of Condensed Matter Physics*, 1:323–345, jul 2010.

[18] A. J. Bray. Theory of phase-ordering kinetics. *Adv. Phys.*, 43(3):357, 1994.

[19] L. F. Cugliandolo. Out-of-equilibrium dynamics of classical and quantum complex systems. *Comptes Rendus Physique*, 14(8):685–699, oct 2013.

[20] Van N.G. Kampen. *Stochastic Processes in Physics and Chemistry*. 2007.

[21] N. Metropolis, A. W. Rosenbluth, M. N. Rosenbluth, A. H. Teller, and E. Teller. Equation of state calculations by fast computing machines. *The Journal of Chemical Physics*, 1953.

[22] I. M. Lifshitz. Kinetics of Ordering During Second-Order Phase Transitions. *J. Exptl. Theoret. Phys. (U.S.S.R.)*, 1962.

[23] S. M. Allen and J. W. Cahn. A microscopic theory for antiphase boundary motion and its application to antiphase domain coarsening. *Acta Metallurgica*, 1979.

[24] R. J. Baxter. Exactly Solved Models in Statistical Mechanics. 1985.

[25] F. Y. Wu. The Potts model. *Reviews of Modern Physics*, 54(1):235–268, jan 1982.

[26] E. Ising. Beitrag zur Theorie des Ferromagnetismus. *Zeitschrift für Physik*, 1925.

[27] B. Derrida. Random-energy model: An exactly solvable model of disordered systems. *Physical Review B*, 1981.

[28] L. Onsager. Crystal statistics. I. A two-dimensional model with an order-disorder transition. *Physical Review*, 1944.

[29] R. B. Potts. Some generalized order-disorder transformations. *Mathematical Proceedings of the Cambridge Philosophical Society*, 1952.

[30] J. Ashkin and E. Teller. Statistics of two-dimensional lattices with four components. *Physical Review*, 1943.

[31] R. J. Baxter. Potts model at the critical temperature, 1973.

[32] D. Weairet and N. Rivier. Soap, cells and statistics-random patterns in two dimensions. *Contemporary Physics*, 1984.

[33] J. Stavans. Evolution of two-dimensional cellular structures: The soap froth. *Physica A: Statistical Mechanics and its Applications*, 1993.

[34] J. A. Glazier, M. P. Anderson, and G. S. Grest. Coarsening in the two-dimensional soap froth and the large- Q potts model: A detailed comparison. *Philosophical Magazine B: Physics of Condensed Matter; Statistical Mechanics, Electronic, Optical and Magnetic Properties*, 1990.

[35] A. D. Sokal. Chromatic polynomials, Potts models and all that. *Physica A: Statistical Mechanics and its Applications*, 2000.

[36] J. Salas and A. D. Sokal. Transfer matrices and partition-function zeros for antiferromagnetic potts models. I. General theory and square-lattice chromatic polynomial. *Journal of Statistical Physics*, 2001.

[37] M. Blatt, S. Wiseman, and E. Domany. Superparamagnetic clustering of data. *Physical Review Letters*, 1996.

[38] J. Reichardt and S. Bornholdt. Detecting fuzzy community structures in complex networks with a potts model. *Physical Review Letters*, 2004.

[39] P. Ronhovde, D. Hu, and Z. Nussinov. Global disorder transition in the community structure of large-q Potts systems. *EPL*, 2012.

[40] V. Dotsenko, M. Picco, and P. Pujol. Renormalisation-group calculation of correlation functions for the 2D random bond Ising and Potts models. *Nuclear Physics, Section B*, 1995.

[41] Vik S. Dotsenko, Vl S. Dotsenko, M. Picco, and P. Pujol. Renormalization group solution for the two-dimensional random bond potts model with broken replica symmetry. *EPL*, 1995.

[42] T. R. Kirkpatrick and D. Thirumalai. Mean-field soft-spin Potts glass model: Statics and dynamics. *Physical Review B*, 1988.

[43] D. Thirumalai and T. R. Kirkpatrick. Mean-field Potts glass model: Initial-condition effects on dynamics and properties of metastable states. *Physical Review B*, 1988.

[44] T. R. Kirkpatrick, D. Thirumalai, and P. G. Wolynes. Scaling concepts for the dynamics of viscous liquids near an ideal glassy state. *Physical Review A*, 1989.

[45] L. Berthier and G. Biroli. Theoretical perspective on the glass transition and amorphous materials. *Reviews of Modern Physics*, 2011.

[46] T. R. Kirkpatrick and D. Thirumalai. Colloquium: Random first order transition theory concepts in biology and physics. *Reviews of Modern Physics*, 2015.

[47] L. Mittag and M. J. Stephen. Mean-field theory of the many component Potts model. *Journal of Physics A: General Physics*, 1974.

[48] A. Baracca, M. Bellesi, R. Livi, R. Rechtman, and S. Ruffo. On the mean field solution of the potts model. *Physics Letters A*, 1983.

[49] K. Binder. Static and dynamic critical phenomena of the two-dimensional q-state Potts model. *Journal of Statistical Physics*, 1981.

[50] K. Nam, B. Kim, and S. J. Lee. Nonequilibrium critical relaxation of the order parameter and energy in the two-dimensional ferromagnetic Potts model. *Physical Review E - Statistical, Nonlinear, and Soft Matter Physics*, 2008.

[51] X. Huang, S. Gong, F. Zhong, and S. Fan. Finite-time scaling via linear driving: Application to the two-dimensional Potts model. *Physical Review E - Statistical, Nonlinear, and Soft Matter Physics*, 2010.

[52] C. D. Li, D. R. Tan, and F. J. Jiang. Applications of neural networks to the studies of phase transitions of two-dimensional Potts models. *Annals of Physics*, 2018.

[53] S. Iino, S. Morita, N. Kawashima, and A. W. Sandvik. Detecting Signals of Weakly First-order Phase Transitions in Two-dimensional Potts Models. *Journal of the Physical Society of Japan*, 2019.

[54] E. E. Ferrero and S. A. Cannas. Long-term ordering kinetics of the two-dimensional q -state Potts model. *Physical Review E - Statistical, Nonlinear, and Soft Matter Physics*, 76(3):31108, sep 2007.

[55] M. J. De Oliveira, A. Petri, and T. Tomé. Crystal vs. glass formation in lattice models with many coexisting ordered phases. In *Physica A: Statistical Mechanics and its Applications*, volume 342, pages 97–103. North-Holland, oct 2004.

[56] M. J. De Oliveira, A. Petri, and T. Tomé. Glassy states in lattice models with many coexisting crystalline phases. *Europhysics Letters*, 65(1):20–26, jan 2004.

[57] M. Ibáñez De Berganza, V. Loreto, and A. Petri. Phase ordering and symmetries of the Potts model. *Philosophical Magazine*, 87(3-5):779–786, jan 2007.

[58] F. Chippari, M. Picco, and L. F. Cugliandolo. Low-temperature universal dynamics of the bidimensional Potts model in the large q limit. *In preparation*, 2021.

[59] M. P. O. Loureiro, J. J. Arenzon, L. F. Cugliandolo, and A. Sicilia. Curvature-driven coarsening in the two-dimensional potts model. *Physical Review E - Statistical, Nonlinear, and Soft Matter Physics*, 81(2):21129, feb 2010.

[60] M. P. O. Loureiro, J. J. Arenzon, and L. F. Cugliandolo. Geometrical properties of the Potts model during the coarsening regime. *Physical Review E - Statistical, Nonlinear, and Soft Matter Physics*, 85(2):21135, feb 2012.

[61] K. Binder. Theory of first-order phase transitions. *Reports on Progress in Physics*, 1987.

[62] D. W. Oxtoby. Homogeneous nucleation: Theory and experiment. *Journal of Physics: Condensed Matter*, 1992.

[63] K. F. Kelton and A. L. Greer. *Nucleation in condensed matter: applications in materials and biology (Chapter 15)*. 2010.

[64] P. Fornasini. *The Uncertainty in Physical Measurements*. 2008.

[65] P. Donnelly and R. S. Ellis. Entropy, Large Deviations, and Statistical Mechanics. *Journal of the American Statistical Association*, 1987.

[66] H. Touchette. The large deviation approach to statistical mechanics. *Physics Reports*, 478(1-3):1–69, 2009.

[67] H. Hinrichsen. Non-equilibrium critical phenomena and phase transitions into absorbing states. *Advances in Physics*, 49(7):815–958, 2000.

[68] J. S. Langer. *Solids far from Equilibrium*, pages 297–363. Cambridge: Cambridge University Press, 1992.

[69] H. Touchette and E. G. D. Cohen. Anomalous fluctuation properties. *Physical Review E - Statistical, Nonlinear, and Soft Matter Physics*, 80(1):11114, jul 2009.

[70] H. Cramér. *Colloque Consacré à la Théorie Des Probabilités. Vol.3.* Paris: Hermann, 1938.

[71] H. Cramér. No Title. *Usp. Mat. Nauk*, 10:166, 1944.

[72] F. Corberi and A. Sarracino. Probability distributions with singularities. *Entropy*, 21(3):312, 2019.

[73] J. Szavits-Nossan, M. R. Evans, and S. N. Majumdar. Constraint-driven condensation in large fluctuations of linear statistics. *Physical Review Letters*, 112(2):20602, jan 2014.

[74] T. Agranov and G. Bunin. Extinctions of coupled populations, and rare-event dynamics under non-Gaussian noise. Technical report, 2020.

[75] Y. Baek and Y. Kafri. Singularities in large deviation functions. *Journal of Statistical Mechanics: Theory and Experiment*, 2015(8):P08026, aug 2015.

[76] M. Filiasi, G. Livan, M. Marsili, M. Peressi, E. Vesselli, and E. Zarinelli. On the concentration of large deviations for fat tailed distributions, with application to financial data. *Journal of Statistical Mechanics: Theory and Experiment*, 2014(9):P09030, sep 2014.

[77] R. J. Harris and H. Touchette. Current fluctuations in stochastic systems with long-range memory. *Journal of Physics A: Mathematical and Theoretical*, 42(34):342001, aug 2009.

[78] G. Gradenigo, A. Sarracino, A. Puglisi, and H. Touchette. Fluctuation relations without uniform large deviations. *Journal of Physics A: Mathematical and Theoretical*, 46(33):335002, 2013.

[79] A. Gambassi and A. Silva. Large deviations and universality in quantum quenches. *Physical Review Letters*, 109(25):250602, dec 2012.

[80] J. Goold, F. Plastina, A. Gambassi, and A. Silva. The Role of Quantum Work Statistics in Many-Body Physics. In "Binder Felix, , Luis A. Correa, Christian, Gogolin, Janet, Anders, Gerardo", and Adesso, editors, *Fundamental Theories of Physics*, volume 195, pages 317–336. Springer International Publishing, Cham, 2018.

[81] H. Touchette and E. G. D. Cohen. Fluctuation relation for a Lévy particle. *Physical Review E - Statistical, Nonlinear, and Soft Matter Physics*, 76(2):20101, aug 2007.

[82] F. Bouchet and H. Touchette. Non-classical large deviations for a noisy system with non-isolated attractors. *Journal of Statistical Mechanics: Theory and Experiment*, 2012(5):P05028, 2012.

[83] R. J. Harris, A. Rákos, and G. M. Schütz. Current fluctuations in the zero-range process with open boundaries. *Journal of Statistical Mechanics: Theory and Experiment*, 2005(8):55–78, aug 2005.

[84] P. Chleboun and S. Grosskinsky. Finite size effects and metastability in zero-range condensation. *Journal of Statistical Physics*, 140(5):846–872, 2010.

[85] P. Sasorov, B. Meerson, and S. Prolhac. Large deviations of surface height in the 1 + 1-dimensional Kardar-Parisi-Zhang equation: Exact long-time results for $\lambda h<0$. *Journal of Statistical Mechanics: Theory and Experiment*, 2017(6):63203, jun 2017.

[86] S. N. Majumdar and G. Schehr. Top eigenvalue of a random matrix: Large deviations and third order phase transition. *Journal of Statistical Mechanics: Theory and Experiment*, 2014(1):P01012, 2014.

[87] F. Corberi. Development and regression of a large fluctuation. *Physical Review E*, 95(3):32136, mar 2017.

[88] F. Corberi, L. F. Cugliandolo, and H. Yoshino. No Title. In L Berthier, G Biroli, J-P Bouchaud, L Cipelletti, and W van Saarloos, editors, *Dynamical heterogeneities in glasses, colloids, and granular media*. Oxford University Press, Oxford, 2011.

[89] F. Corberi. Large deviations, condensation and giant response in a statistical system. *Journal of Physics A: Mathematical and Theoretical*, 48(46):465003, oct 2015.

[90] A. Vezzani, E. Barkai, and R. Burioni. Single-big-jump principle in physical modeling. *Physical Review E*, 100(1):012108, jul 2019.

[91] A. Vezzani, E. Barkai, and R. Burioni. Rare events in generalized Lévy Walks and the Big Jump principle. *Scientific Reports*, 2020.

[92] M. Zannetti, F. Corberi, and G. Gonnella. Condensation of fluctuations in and out of equilibrium. *Physical Review E - Statistical, Nonlinear, and Soft Matter Physics*, 90(1):12143, jul 2014.

[93] F. Corberi, G. Gonnella, and A. Piscitelli. Singular behavior of fluctuations in a relaxation process. *Journal of Non-Crystalline Solids*, 407:51–56, 2015.

[94] F. Corberi. Development and regression of a large fluctuation. *Physical Review E*, 95(3):32136, mar 2017.

[95] F. Cagnetta, F. Corberi, G. Gonnella, and A. Suma. Large Fluctuations and Dynamic Phase Transition in a System of Self-Propelled Particles. *Physical Review Letters*, 119(15):158002, oct 2017.

[96] F. Corberi, G. Gonnella, A. Piscitelli, and M. Zannetti. Heat exchanges in a quenched ferromagnet. *Journal of Physics A: Mathematical and Theoretical*, 46(4):42001, jan 2013.

[97] F. Corberi and L. F. Cugliandolo. Dynamic fluctuations in unfrustrated systems: Random walks, scalar fields and the Kosterlitz-Thouless phase. *Journal of Statistical Mechanics: Theory and Experiment*, 2012(11):P11019, nov 2012.

[98] P. M. Chaikin and T. C. Lubensky. *Principles of Condensed Matter Physics*. Cambridge University Press, Cambridge, 1995.

[99] P. C. Hohenberg and B. I. Halperin. Theory of dynamic critical phenomena. *Rev. Mod. Phys.*, 49:435, 1977.

[100] M. Zannetti, F. Corberi, and G. Gonnella. Condensation of fluctuations in and out of equilibrium. *Physical Review E - Statistical, Nonlinear, and Soft Matter Physics*, 90(1):12143, jul 2014.

[101] T. H. Berlin and M. Kac. The spherical model of a ferromagnet. *Physical Review*, 86(6):821–835, jun 1952.

[102] T. Nemoto, É. Fodor, M. E. Cates, R. L. Jack, and J. Tailleur. Optimizing active work: Dynamical phase transitions, collective motion, and jamming. *Physical Review E*, 99(2):22605, 2019.

[103] J. J. Arenzon, A. J. Bray, L. F. Cugliandolo, and A. Sicilia. Exact results for curvature-driven coarsening in two dimensions. *Physical Review Letters*, 2007.

[104] A. Sicilia, J. J. Arenzon, A. J. Bray, and L. F. Cugliandolo. Domain growth morphology in curvature-driven two-dimensional coarsening. *Physical Review E - Statistical, Nonlinear, and Soft Matter Physics*, 2007.

[105] T. Blanchard, F. Corberi, L. F. Cugliandolo, and M. Picco. How soon after a zero-temperature quench is the fate of the Ising model sealed? *EPL*, 2014.

[106] T. Blanchard, L. F. Cugliandolo, M. Picco, and A. Tartaglia. Critical percolation in the dynamics of the 2D ferromagnetic Ising model. *Journal of Statistical Mechanics: Theory and Experiment*, 2017.

[107] B. Derrida, P. M. C. De Oliveira, and D. Stauffer. Stable spins in the zero temperature spinodal decomposition of 2D Potts models. *Physica A: Statistical Mechanics and its Applications*, 1996.

[108] A. Lipowski. Anomalous phase-ordering kinetics in the Ising model. *Physica A: Statistical Mechanics and its Applications*, 1999.

[109] V. Spirin, P. L. Krapivsky, and S. Redner. Fate of zero-temperature Ising ferromagnets. *Physical Review E - Statistical Physics, Plasmas, Fluids, and Related Interdisciplinary Topics*, 2001.

[110] V. Spirin, P. L. Krapivsky, and S. Redner. Freezing in ising ferromagnets. *Physical Review E - Statistical, Nonlinear, and Soft Matter Physics*, 2002.

[111] K. Barros, P. L. Krapivsky, and S. Redner. Freezing into stripe states in two-dimensional ferromagnets and crossing probabilities in critical percolation. *Physical Review E - Statistical, Nonlinear, and Soft Matter Physics*, 2009.

[112] J. Olejarz, P. L. Krapivsky, and S. Redner. Fate of 2D kinetic ferromagnets and critical percolation crossing probabilities. *Physical Review Letters*, 2012.

[113] T. Blanchard and M. Picco. Frozen into stripes: Fate of the critical Ising model after a quench. *Physical Review E - Statistical, Nonlinear, and Soft Matter Physics*, 2013.

[114] H. K. Lee, B. J. Kim, and H. Park. Continuity of the explosive percolation transition. *Physical Review E - Statistical, Nonlinear, and Soft Matter Physics*, 2011.

[115] J. D. Noh, H. K. Lee, and H. Park. Scaling of cluster heterogeneity in percolation transitions. *Physical Review E - Statistical, Nonlinear, and Soft Matter Physics*, 2011.

[116] W. S. Jo, S. D. Yi, S. K. Baek, and B. J. Kim. Cluster-size heterogeneity in the two-dimensional Ising model. *Physical Review E - Statistical, Nonlinear, and Soft Matter Physics*, 2012.

[117] J. P. Lv, X. Yang, and Y. Deng. Scaling of cluster heterogeneity in the two-dimensional Potts model. *Physical Review E - Statistical, Nonlinear, and Soft Matter Physics*, 2012.

[118] A. R. De La Rocha, P. M. C. De Oliveira, and J. J. Arenzon. Domain-size heterogeneity in the Ising model: Geometrical and thermal transitions. *Physical Review E - Statistical, Nonlinear, and Soft Matter Physics*, 2015.

[119] A. De Azevedo-Lopes, A. R. De La Rocha, P. M. C. De Oliveira, and J. J. Arenzon. Dynamical cluster size heterogeneity. *Physical Review E*, 2020.

[120] D. Stauffer and A. Aharony. *Introduction To Percolation Theory*. 2018.

[121] A. L. Stella and C. Vanderzande. Scaling and fractal dimension of Ising clusters at the d=2 critical point. *Physical Review Letters*, 1989.

[122] W. Janke and A. M. J. Schakel. Fractal structure of spin clusters and domain walls in the two-dimensional Ising model. *Physical Review E - Statistical, Nonlinear, and Soft Matter Physics*, 2005.

[123] A. Coniglio and W. Klein. Clusters and Ising critical droplets: A renormalisation group approach. *Journal of Physics A: Mathematical and General*, 1980.

[124] P. G. Debenedetti. *Metastable Liquids*. 2020.

[125] D. Stauffer, P. A. Rikvold, and B. M. Gorman. Recent results on the decay of metastable phases. In *Annual Reviews of Computational Physics I*. 1995.

[126] C. C. A. Günther, P. A. Rikvold, and M. A. Novotny. Numerical transfer-matrix study of metastability in the d=2 Ising model. *Physical Review Letters*, 1993.

[127] C. C.A. Günther, P. A. Rikvold, and M. A. Novotny. Application of a constrained-transfer-matrix method to metastability in the d = 2 Ising ferromagnet. *Physica A: Statistical Mechanics and its Applications*, 1994.

[128] P. G. Debenedetti and F. H. Stillinger. Supercooled liquids and the glass transition, 2001.

[129] D. Thirumalai and G. Reddy. Are native proteins metastable? *Nature Chemistry*, 2011.

[130] J. Völker, H. H. Klump, and K. J. Breslauer. DNA energy landscapes via calorimetric detection of microstate ensembles of metastable macrostates and triplet repeat diseases. *Proceedings of the National Academy of Sciences of the United States of America*, 2008.

[131] M. Slemrod. Dynamics of first order phase transitions. In *Phase Transformations and Material Instabilities in Solids*. 1984.

[132] A. Petri, M. I. De Berganza, and V. Loreto. Ordering dynamics in the presence of multiple phases. In *Philosophical Magazine*, 2008.

[133] M. P. O. Loureiro, J. J. Arenzon, and L. F. Cugliandolo. Geometrical properties of the Potts model during the coarsening regime. *Physical Review E - Statistical, Nonlinear, and Soft Matter Physics*, 2012.

[134] E. S. Loscar, E. E. Ferrero, T. S. Grigera, and S. A. Cannas. Nonequilibrium characterization of spinodal points using short time dynamics. *Journal of Chemical Physics*, 2009.

[135] E. E. Ferrero, J. P. De Francesco, N. Wolovick, and S. A. Cannas. Q-state Potts model metastability study using optimized GPU-based Monte Carlo algorithms. *Computer Physics Communications*, 2012.

[136] J. L. Meunier and A. Morel. Condensation and metastability in the 2D Potts model. *European Physical Journal B*, 2000.

[137] M. Ibàñez Berganza, P. Coletti, and A. Petri. Anomalous metastability in a temperature-driven transition. *EPL*, 2014.

[138] R. Burioni, F. Corberi, and A. Vezzani. Complex phase ordering of the one-dimensional Heisenberg model with conserved order parameter. *Physical Review E - Statistical, Nonlinear, and Soft Matter Physics*, 2009.

[139] A. Laaksonen, V. Talanquer, and D. W. Oxtoby. Nucleation: Measurements, theory, and atmospheric applications. *Annual Review of Physical Chemistry*, 1995.

[140] P. M. Chaikin and T. C. Lubensky. *Principles of Condensed Matter Physics*. 1995.

[141] R. Becker and W. Döring. Kinetische Behandlung der Keimbildung in übersättigten Dämpfen. *Annalen der Physik*, 1935.

[142] J. J. Burton. Nucleation Theory. In *Statistical Mechanics*. 1977.

[143] O. Penrose and J. L. Lebowitz. Towards a Rigorous Molecular Theory of Metastability. In *Fluctuation Phenomena*. 1979.

[144] D. Capocaccia, M. Cassandro, and E. Olivieri. A study of metastability in the Ising model. *Communications in Mathematical Physics*, 1974.

[145] O. Penrose and J. L. Lebowitz. Rigorous treatment of metastable states in the van der Waals-Maxwell theory. *Journal of Statistical Physics*, 1971.

[146] F. H. Stillinger. Statistical mechanics of metastable matter: Superheated and stretched liquids. *Physical Review E*, 1995.

[147] D. S. Corti and P. G. Debenedetti. Metastability and Constraints: A Study of the Superheated Lennard-Jones Liquid in the Void-Constrained Ensemble. *Industrial and Engineering Chemistry Research*, 1995.

[148] J. S. Langer. Theory of the condensation point. *Annals of Physics*, 1967.

[149] J. S. Langer. Theory of nucleation rates. *Physical Review Letters*, 1968.

[150] N. J. Gunther, D. J. Wallace, and D. A. Nicole. Goldstone modes in vacuum decay and first-order phase transitions. *Journal of Physics A: Mathematical and General*, 1980.

[151] F. Schmitz, P. Virnau, and K. Binder. Monte Carlo tests of nucleation concepts in the lattice gas model. *Physical Review E - Statistical, Nonlinear, and Soft Matter Physics*, 2013.

[152] J. D. Gunton. The dynamics of random interfaces in phase transitions. *Journal of Statistical Physics*, 34(5-6):1019–1037, mar 1984.

[153] D. P. Sanders, H. Larralde, and F. Leyvraz. Competitive nucleation and the Ostwald rule in a generalized Potts model with multiple metastable phases. *Physical Review B - Condensed Matter and Materials Physics*, 75(13):132101, apr 2007.

[154] J. Denholm and S. Redner. Topology-controlled Potts coarsening. *Physical Review E*, 2019.

[155] F. Corberi, L. F. Cugliandolo, M. Esposito, and M. Picco. Multinucleation in the first-order phase transition of the 2d Potts model. In *Journal of Physics: Conference Series*, 2019.

[156] E. Buddenoir and S. Wallon. The correlation length of the Potts model at the first-order transition point. *Journal of Physics A: Mathematical and General*, 1993.

[157] F. Y. Wu. The infinite-state potts model and restricted multidimensional partitions of an integer. In *Mathematical and Computer Modelling*, 1997.

[158] J. Olejarz, P. L. Krapivsky, and S. Redner. Zero-temperature coarsening in the 2d Potts model. *Journal of Statistical Mechanics: Theory and Experiment*, 2013.

[159] F. Corberi, E. Lippiello, and M. Zannetti. Scaling and universality in the aging kinetics of the two-dimensional clock model. *Physical Review E - Statistical, Nonlinear, and Soft Matter Physics*, 2006.

[160] F. Corberi, L. F. Cugliandolo, F. Insalata, and M. Picco. Coarsening and percolation in a disordered ferromagnet. *Physical Review E*, 2017.

[161] F. Insalata, F. Corberi, L. F. Cugliandolo, and M. Picco. Coarsening and percolation in the Ising Model with quenched disorder. In *Journal of Physics: Conference Series*, 2018.

[162] F. Corberi, L. F. Cugliandolo, F. Insalata, and M. Picco. Fractal character of the phase ordering kinetics of a diluted ferromagnet. *Journal of Statistical Mechanics: Theory and Experiment*, 2019.